Credit Value Adjustment for Multi-Asset Options

Proefschrift

ter verkrijging van de graad van doctor
aan de Technische Universiteit Delft,
op gezag van de Rector Magnificus prof.ir. K.C.A.M. Luyben,
voorzitter van het College voor Promoties,
in het openbaar te verdedigen op dinsdag 4 november 2014 om 12:30 uur

door

Yanbin SHEN
Master of Economics in Finance
Nankai University, Tianjin, China

geboren te Huzhou, China

Dit proefschrift is goedgekeurd door de promotor:
Prof.dr.ir. C.W. Oosterlee

Copromotor: Dr. J.A.M. van der Weide

Samenstelling promotiecommissie:

Rector Magnificus,	voorzitter
Prof.dr.ir. C.W. Oosterlee,	Technische Universiteit Delft, promotor
Dr. J.A.M. van der Weide,	Technische Universiteit Delft, copromotor
Dr.ir. J.H.M. Anderluh,	Technische Universiteit Delft
Prof.dr. M.D. Pandey,	University of Waterloo, Canada
Prof.dr. R.J.A. Laeven,	University of Amsterdam
Prof.dr. F.H.J. Redig,	Technische Universiteit Delft
Prof.dr.ir. A.W. Heemink,	Technische Universiteit Delft
Prof.dr.ir. G. Jongbloed,	Technische Universiteit Delft, reservelid

Credit Value Adjustment for Multi-Asset Options.
Dissertation at Delft University of Technology.

ISBN 978-94-6186-360-7

Acknowledgments

This thesis concludes my Ph.D. research at the Delft University of Technology, from October 2009 to June 2014. I would like to express my thanks to those people who have contributed to the success of this thesis.

First I wish to thank my supervisor Dr. Hans van der Weide, for providing me a good opportunity to study financial mathematics as a PhD student in Netherlands. He helped me come up with research topics that I am interested in, and during the most difficult times, he gave me lots of support and freedom to move on. From his guidance and numerous discussion we have had, I have benefited greatly and gained ability of doing independent research. In particular I thank him for translating the summary of this thesis and propositions into Dutch.

I would like to thank prof. Kees Oosterlee, for reading the entire manuscript thoroughly and giving constructive suggestions and criticisms. I learned a lot from his research group of computational finance. It has been great pleasure to attend workshops and discuss problems in his group. I also thank him for putting his efforts and time on my promotion.

I am grateful to Dr. J.H.M Anderluh for his contributions to the chapter on exposures of multi-asset instruments. I am thankful to him for stimulating discussion which inspired me a lot. His insightful issues and criticisms push me further for a deeper understanding of problems and a better expression of ideas.

I would like to express my gratitude to all colleagues in the Probability and Statistics group of TU Delft, for the pleasant research atmosphere and all academic and social activities. Working as a Ph.D. student in TU Delft turns out to be challenging but also exciting, and without the support of the Probability and Statistics group, it is impossible for me to successfully finish it. Particularly, I have benefited greatly from the group's financial support which provided me great opportunities to attend international conferences in different countries.

My special words of thanks should also go to friends and colleagues from financial industries, particularly, Dr. Lech Grzelak and Dr. Bin Chen from Rabobank who were my office mates in the first two years of my Ph.D. life in

Delft, Dr. Bowen Zhang working in Royal Bank of Scotland, and Dr. Shashi Jain from ING bank. I also would like to thank Jasper Hommels from Rabobank International for his introduction of an project on counterparty credit risk, which helped me come up new ideas in my own research.

I dedicate this thesis to my parents for their endless love and support.

Summary

Credit Value Adjustment for Multi-Asset Options

Yanbin SHEN

As one of the influential models in finance and economics, the Black-Scholes-Merton model (1973) [7, 46] which was originally used for European stock options pricing, has been extended to value different kinds of derivatives with different underlying asset price processes. One fundamental assumption in the Black-Scholes-Merton model is that the two sides of a derivatives transaction will respect their payment obligations. However, it is now recognized that default risk of a counterparty is an important consideration in derivative valuation. The research on valuation of options with default risk started quite early (such as 'vulnerable options' in Johnson and Stulz (1987) [42]), a topic which seemed to be more popular in academics than in industry. With the financial (credit) crisis of 2007 came opportunities, for the exploration of different aspects of counterparty credit risk. One of the challenging problems is the quantification of counterparty credit risk.

Generally, the quantification of credit risk starts from three basic components,

1. the probability of counterparty's default (PD) within a fixed time horizon.

2. the credit exposure at default (EAD), the amount the bank may potentially lose if the counterparty defaults.

3. loss given default (LGD), the proportion of the exposure that will be lost if a default occurs, which is equal to one minus the recovery rate.

It has become standard that EAD is assumed to be deterministic. The LGD is random but often replaced by its expectation for simplification. And the default probability will be modelled stochastically. However, for derivative transactions, the market price (and EAD) may change dramatically because of the stochastic behavior of underlying asset prices. Then, methods for appropriate modeling and quantification of derivative transaction's credit exposure are required.

One of the main tasks in this thesis is to quantify future credit exposure for *over-the-counter* (OTC) exotic and multi-asset options. In principle, two basic steps are involved in quantifying counterparty credit exposure. First, simulation paths of underlying asset prices have to be generated according to the specified models for the underlying asset price processes. Second, on each simulated state (grid point), the value of a derivative transaction has to be calculated. Particularly, in the second step of instrument price computation, when the valuation does not admit a closed form formula, appropriate approximation methods have to be proposed. A typical example is the approximation of the continuation value in American option pricing problems by using least squares regression.

Our starting point is the one-dimensional Bermudan option, which is intermediate between a European option and an American option. As a classical option pricing problem, the main challenging problem in Bermudan options is to find an efficient approximation of the continuation value on early exercise opportunities. Different from option pricing, in exposure calculation, we need an accurate computation of option values at each time step, from which we can further estimate quantities such as *expected exposure* (EE) and *potential future exposure* (PFE). PFE for a given date is the maximum of exposure at that date with a high degree of statistical confidence. EE for a given date is the average of exposure at that date.

We show that in the one-dimensional case, the credit exposure of Bermudan options can be calculated efficiently based on Monte Carlo simulation combined with a Fourier inversion option pricing method which is named the Monte Carlo-COS method [58]. The underlying asset price process is assumed to be a Lévy process and can be simulated appropriately. An accurate continuation value on early exercise opportunities is obtained by using the Fourier COS method instead of a least squares regression approximation. We compare the exposure profiles (PFE and EE) under the real world measure $\mathbb{P}$ and risk neutral measure $\mathbb{Q}$.

We then extend the one-dimensional case into multi-asset instruments. When the dimension of the problem becomes higher, numerical integration methods become computationally expensive. Although the *standard regression method* (SRM) [31] has the advantage of fast computation for high-dimensional problems, the accuracy of exposure calculations is typically not very good. This can be seen from a comparison of one-dimensional Bermudan option exposure profiles generated by SRM and the Monte Carlo-COS method. To make an improvement, we investigate different regression based methods, including

the *standard regression bundling method* (SRBM) and the *stochastic grid bundling method* (SGBM) [39]. We analyze each method in terms of computation speed, accuracy and standard deviation of estimates.

Note that both PFE and EE are quantities calculated for measuring the counterparty credit risk based on the exposure empirical distribution under the real world measure $\mathbb{P}$. To price the counterparty credit risk, the risk neutral measure $\mathbb{Q}$ comes in. The market price of counterparty credit risk is termed as *credit value adjustment* (CVA). The second task of the thesis is to find efficient computation methods for CVA.

We again consider the simple (but not trivial) example of one-dimensional Bermudan (put) options, where the option is written on the counterparty's stock price. Since the counterparty is subject to default risk, the investor in the Bermudan option has to value the default risk which should be taken into account in the option price. This problem is reduced to calculating CVA of Bermudan options. Based on the risk neutral pricing technique, a risk neutral pricing formula of CVA can be derived. Particularly, a practical formula for CVA in which the credit exposure is assumed to be independent of default probability, is just based on the multiplication of expected exposure (EE) and default probability under measure $\mathbb{Q}$. This can be done straightforwardly because we have already developed an efficient calculation method (Monte Carlo-COS method) for EE in the one-dimensional case.

The problem can become more interesting if we use more realistic assumptions. While several contributions in the literature have tried to measure the dependence between the default probability and LGD process, the same argument can be applied to model the dependence between the default probability and credit exposure. The positive (negative) dependence between the credit exposure and default probability is termed as *wrong (right) way risk*. We use a hazard rate approach for wrong way risk modeling. More precisely, in the empirical analysis approach (EAA), the hazard rate is assumed to be a function of the counterparty's equity price. And in another hazard rate approach, which is termed as portfolio value approach (PVA), the hazard rate is assumed to be a function of the derivative transaction value. Based on the modeling of wrong way risk, to show the effect of wrong way risk on CVA computation, we compare the value of CVA when wrong way risk is taken into account (CVA_W) to the value of CVA when wrong way risk is not taken into account (CVA_I). The relationship between the wrong way risk and the early exercise feature embedded in Bermudan options is analyzed. Numerical experiments show that the effect of wrong way risk on CVA of Bermudan options depends on its early exercise features. With a high exercise intensity, which is caused by high volatility of the stock price process, high strike price, or large number of possible early exercise dates, CVA_W could be smaller in value than CVA_I. This result is different from the conclusion if one uses the α multiplier approach in

the Basel III accord to take into account the wrong way risk effect, where the value of α is greater than one.

We further consider two extensions of the one-dimensional problem above. First, the assumption of the option written on the counterparty's stock price is replaced by a more flexible one, i.e., the option is written on an underlying asset which is different from the counterparty's stock, while the (positive or negative) correlation between the two assets can be added. We investigate the relationship between the correlation and wrong (right) way risk. Second, we extend the one-dimensional underlying asset into the multi-asset case. We investigate different simulation based methods for the efficient CVA computation of multi-asset instruments. These methods include SRM, SRBM and SGBM which were already discussed for the efficient calculation of exposure profiles. We focus on the efficiency comparison of different methods, including the computation speed, accuracy, and standard deviation of estimates of option prices and CVA.

Samenvatting

Credit Value Adjustment for Multi-Asset Options

Yanbin SHEN

Een van de invloedrijke modellen in finance en economie is het Black-Scholes-Merton-model (1973) [7, 46] . Dit model, oorspronkelijk gebruikt voor het waarderen van Europese aandelenopties, is uitgebreid om verschillende soorten derivaten te kunnen waarderen met verschillende onderliggende processen als model voor de aandeelprijs. Een fundamentele aanname in het Black-Scholes-Merton-model is dat de twee partijen in een derivatentransactie altijd hun betalingsverplichtingen zullen nakomen. Het wordt echter nu algemeen ingezien dat het risico op wanbetaling (faillissement) door een tegenpartij een belangrijke rol speelt bij het waarderen van derivaten. Het onderzoek naar de waardering van opties met het risico op wanbetaling begon heel vroeg (zoals 'vulnerable options' in Johnson en Stulz (1987) [42]), maar dit onderwerp leek meer populair in academische kring dan in de financië industrie. Met de financiële (krediet) crisis van 2007 kwamen kansen, voor de exploratie van de verschillende aspecten van het tegenpartijkredietrisico. Een van de uitdagende problemen is het kwantificeren van kredietrisico van de tegenpartij.

In het algemeen gaat men bij de kwantificering van het kredietrisico uit van drie basiscomponenten,

1. de kans op wanbetaling (PD) van de tegenpartij binnen een bepaalde tijdshorizon.

2. de krediet exposure at default (EAD), het bedrag dat de bank mogelijk zou kunnen verliezen als de tegenpartij in gebreke blijft.

3. Loss Given Default (LGD), het deel van de exposure, dat verloren gaat bij faillissement. Dit verlies is gelijk aan één minus de recovery rate.

Het is standaard gebruik geworden om ter vereenvoudiging aan te nemen dat de EAD deterministisch is. De LGD is stochastisch, maar wordt vaak vervangen door zijn verwachte waarde. En de kans op wanbetaling zal stochastisch worden gemodelleerd. Echter, de marktprijs en de EAD voor derivatentransacties kunnen als gevolg van het stochastisch gedrag van de onderliggende aandeelprijzen grote schommelingen vertonen. Als dit het geval is, dan zijn methoden voor een geschikte modellering en kwantificatie van de krediet exposure van derivaten transacties vereist.

Een van de belangrijkste taken in dit proefschrift is om toekomstig krediet-exposure voor *over-the-counter* (OTC) exotische en multi-asset opties te kwantificeren. In principe zijn twee fundamentele stappen nodig voor het kwantificeren van tegenpartijkredietrisico. Ten eerste, simulatie van paden van onderliggende aandeelprijsprocessen volgens van tevoren opgegeven modellen. Ten tweede, een benadering van de waarde van het derivaat op elke gesimuleerde toestand (roosterpunt). Een karakteristiek voorbeeld is de benadering van de continueringswaarde van een Amerikaanse optie met behulp van de kleinste kwadraten regressie.

Ons uitgangspunt is een één-dimensionale Bermuda optie, die het midden houdt tussen een Europese optie en een Amerikaanse optie. Het prijzen van de optie is een klassiek probleem, waarvan de grootste uitdaging bij Bermuda opties bestaat uit het vinden van een efficiënte benadering van de continueringswaarde op de tijdstippen waarop vervroegd mag worden uitgeoefend. Anders dan bij het prijzen van opties is bij het berekenen van de exposure op iedere tijdstap een precieze berekening van de optiewaarden nodig. Hieruit kunnen verder grootheden zoals de *verwachte exposure* (EE) en *potentieel toekomstig risico* (PFE) geschat worden. Onder de PFE voor een bepaalde datum wordt hierbij de maximale exposure op die datum verstaan met een hoge mate van statistische betrouwbaarheid. EE voor een bepaalde datum is het gemiddelde van de exposure op die datum.

We laten zien dat in voor één-dimensionale Bermuda opties, het kredietrisico efficiënt berekend kan worden uit Monte Carlo simulatie in combinatie met een Fourier-inversie methode om optieprijzen te berekenen. We duiden deze methode aan als de Monte Carlo-COS methode [58]. Aangenomen wordt dat het onderliggende aandeelprijsproces een Lévy proces is dat geschikt is om te simuleren. Een nauwkeurige methode om de continueringswaarde te berekenen op uitoefentijdstippen wordt verkregen door de Fourier COS methode toe te passen in plaats van een kleinste kwadraten regressie. De exposure profielen (PFE en EE) onder de 'echte wereld' en de risico-neutrale kansmaat $\mathbb{P}$ en $\mathbb{Q}$ worden vergeleken.

We breiden vervolgens het één-dimensionale geval uit tot multi-aandeel-instrumenten. Wanneer de dimensie van het probleem groter wordt, worden numerieke integratie methoden kostbaar qua rekentijd. Hoewel de *standaard regressie methode* (SRM) [31] het voordeel heeft van snelle rekentijd in hoogdimensionale problemen is de nauwkeurigheid van exposure-berekeningen gewoonlijk niet hoog genoeg. Dit blijkt al uit een vergelijking van exposure profielen bij één-dimensionale Bermuda opties die gegenereerd zijn via SRM en de Monte Carlo-COS methode. Om een verbetering te maken, onderzoeken we verschillende op regressie gebaseerde methoden, met inbegrip van de *standaard regressie bundelingsmethode* (SRBM) en de *stochastisch grid bundelingsmethode* (SGBM) [39]. Wij analyseren elke methode in termen van rekensnelheid, nauwkeurigheid en de standaarddeviatie van de schattingen.

Merk op dat zowel de PFE als de EE maten zijn voor kredietrisico van de tegenpartij op basis van de empirische verdelingsfunctie van de exposure onder de 'echte wereld' kansmaat $\mathbb{P}$. Waardering van het kredietrisico van de tegenpartij gebeurt ten opzichte van de risico-neutrale kansmaat $\mathbb{Q}$. De marktprijs van het tegenpartijkredietrisico wordt aangeduid met *kredietwaardeverandering* (CVA). De tweede taak van het proefschrift is om efficiënte berekeningsmethoden voor de CVA vinden.

We beschouwen opnieuw het eenvoudige (maar niet triviale) voorbeeld van één-dimensionale Bermuda (put) opties, geschreven op de aandeelprijs van de tegenpartij. Omdat de tegenpartij is onderworpen aan het risico op faillissement, moet de investeerder in de Bermuda optie rekening houden met de waarde van dit risico bij het bepalen van de optieprijs. Dit probleem wordt gereduceerd tot het berekenen van de CVA van Bermuda opties. Op basis van de risico-neutrale waarderingstechnieken, kan een risico-neutrale prijsformule worden afgeleid voor de CVA. In het bijzonder, is een praktische formule voor de CVA, waarbij de krediet exposure onafhankelijk is verondersteld van de kans op faillissement, alleen gebaseerd op een vermenigvuldiging van de verwachte exposure (EE) met de kans op faillissement onder $\mathbb{Q}$. Omdat we in het één-dimensionale geval al een efficiënte methode (Monte-Carlo COS) voor de berekening van de EE hebben kan dit in dit geval eenvoudig gedaan worden.

Het probleem zal interessanter worden als we uitgaan van meer realistische veronderstellingen. Terwijl in verschillende bijdragen in de literatuur gepoogd is om de afhankelijkheid van de kans op faillissement en het LGD proces te meten, kan dezelfde redenering worden toegepast om de afhankelijkheid van de kans op faillissement en krediet exposure te modelleren. De positieve (negatieve) afhankelijkheid van krediet exposure en kans op faillissement wordt *wrong (right) way risico* genoemd. We maken gebruik van een hazard rate aanpak om wrong way risico te modelleren. Preciezer geformuleerd, in de empirische analyse benadering (EAA) nemen we aan dat de hazard rate een functie is van de aandeelprijs van de tegenpartij. En in een andere hazard rate benadering, de zogeheten portfolio waarde aanpak (PVA), wordt aangenomen dat de hazard rate een functie is van de transactiewaarde van het derivaat. Om het effect te bestuderen van wrong way risico op de CVA vergelijken we op basis van een model voor wrong way risico de CVA waarde *met* (CVA_W) en *zonder* wrong way risico (CVA_I). De relatie tussen wrong way risico en de vervroegde uitoefeningsfunctie ingebed in Bermudan opties wordt onderzocht. Numerieke experimenten tonen aan dat het effect van wrong way risico op de CVA van Bermuda opties afhangt van zijn vervroegde uitoefeningsmogelijkheden. Met een hoge uitoefenintensiteit, die kan worden veroorzaakt door een hoge volatiliteit van de koers van het aandeelproces, hoge uitoefenprijs, of groot aantal mogelijke uitoefendata, kan CVA_W ook kleiner in waarde zijn dan CVA_I. Dit resultaat verschilt van de conclusie is als de α multiplier benadering gebruikt met $\alpha > 1$, die wordt voorgesteld in het Basel III akkoord om wrong way risico mee te rekenen.

Verder beschouwen we twee uitbreidingen van het één-dimensionale probleem hierboven. Eerst wordt de aanname dat de optie is geschreven op de tegenpartij's aandelenkoers vervangen door een meer flexibeleaanname dat de optie geschreven is op een onderliggend aandeel dat verschillen kan van het aandeel van de tegenpartij, terwijl de (positieve of negatieve) correlatie tussen de twee aandelen kan worden toegevoegd. We onderzoeken de relatie tussen de correlatie en het wrong (right) way risico. Ten tweede breiden we het één-dimensionale geval uit tot het multi-aandeel geval. We onderzoeken verschillende op simulatie gebaseerde methoden voor een efficiënte CVA berekening van multi-aandeel-instrumenten. Deze methoden omvatten SRM, SRBM en SGBM die reeds werden besproken bij de efficiënte berekening van exposure profielen. Wij richten ons nu op het vergelijken van de efficiëntie van de verschillende methoden, met inbegrip van de rekensnelheid, nauwkeurigheid, en de standaarddeviatie van de schattingen van de optieprijzen en CVA.

Contents

Chapter 1

Introduction

1.1 Background

"During the financial crisis, however, roughly two-thirds of losses attributed to counterparty credit risk were due to CVA losses and only about one-third were due to actual defaults " is a statement from the Bank for International Settlements (BIS).

High-profile defaults that happened during the financial crisis of 2007 to 2009 (collapse of Bear Stearns, Lehman Brothers, Wachovia) have emphasized the importance for financial institutions to measure and manage counterparty credit risk. According to the Basel II and Basel III accords, counterparty credit risk is the risk that a counterparty in an over-the-counter (OTC) derivatives transaction will default before the expiration of the instrument and will not make current and future payments required by the contract. Only contracts privately negotiated between the counterparties, such as OTC derivatives, are subject to the counterparty credit risk. Derivatives traded on an exchange are normally considered to have no counterparty risk since the payments promised by the derivatives are guaranteed by the exchange.

Since OTC derivatives represent a large part of financial transactions worldwide, which includes a wide variety of asset classes, the management of counterparty credit risk in OTC derivatives market becomes crucial. The development of the OTC derivatives markets for different asset classes is shown in figure 1.1. Beginning from 1998, although the increase in notional amounts has stopped at the peak of the financial crisis, the overall growth is still impressive. In table 1.1, we can see clearly the gross notional values of different asset classes during June 2007 (the beginning of the crisis) and June 2010.

Counterparty credit risk is similar to other types of credit risk (such as lending risk) in the sense that the reason of economic loss is an obligor's default.

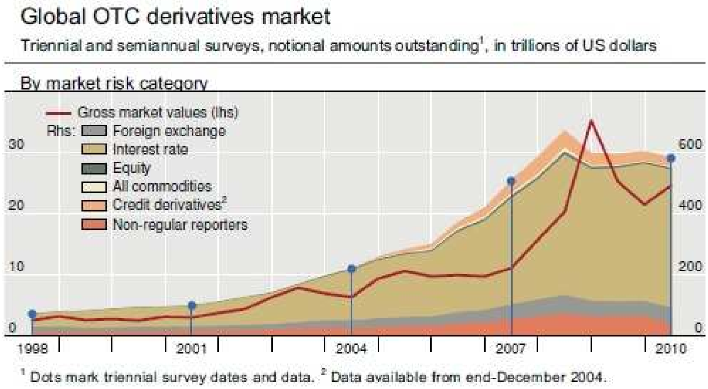

Figure 1.1: Notional amounts outstanding in OTC derivatives markets, in trillions USD, cited from R. Cont and T. Kokholm (2014) [25]. Original source: BIS.

However, counterparty credit risk has two unique features which are different from lending risk:

1. Uncertainty of credit exposure. Credit exposure of one counterparty to another is determined by the market value of all the contracts between these counterparties. One can obtain the current exposure from the current contract values, however, the future exposure is uncertain because the future contract values are not known at present.

2. Bilateral nature of credit exposure. Since both counterparties can default and the value of many financial contracts (such as swaps) can change signs, the direction of future credit exposure is uncertain. Counterparty A may be exposed to default of counterparty B under one set of future market scenarios, while counterparty B may be exposed to default of counterparty A under another set of scenarios.

Because of the uncertainty and bilateral nature of credit exposure, the quantification of counterparty credit risk becomes a challenging problem. The purpose of this thesis is to find efficient computation methods for the quantification of the counterparty credit risk, especially in the field of exotic and multi-asset derivatives.

Table 1.1: Gross notional values in OTC derivatives markets in billions as of June 2007 and June 2010, cited from Rama Cont and Thomas Kokholm (2014) [25]. Original source: BIS

Asset Class	2007	2010
Commodity	$8,255$	$3,273$
Equity Linked	$9,518$	$6,868$
Foreign Exchange	$57,604$	$62,933$
Interest Rate	$381,357$	$478,093$
Credit Derivatives	$51,095$	$31,416$
Other	78	72
total	$507,907$	$582,655$

1.2 CVA and wrong way risk

Some basic definitions and the risk-neutral pricing technique for the quantification of counterparty credit risk are introduced here and will be used in the rest of the thesis.

1.2.1 Credit exposure

The credit exposure on an OTC derivative position is the amount that would be lost on that position in the event of default by the counterparty, assuming no recovery. For example, assuming that there is no collateral or other offsetting positions with the counterparty, the credit exposure on a purchased equity option is its market value.

Depending on market conditions, some positions, such as swaps and forwards, can have negative market values. In that case, the exposure is zero because default by the counterparty would, under the standard settlement procedures of the International Swaps and Derivatives Association (ISDA), result in immediate settlement at market value and, thus, zero loss. In general, at a given time t, for an uncollateralized position with a market value of $V(t)$, the exposure is $\max(0, V(t))$, see figure 1.2. We can give the definition of credit exposure in the following way,

Definition 1. *The counterparty credit exposure of a derivative security, E_t, is defined as the non-negative part of the derivative security's value, $V(t)$, at time t,*

$$E_t = \max\big(V(t), 0\big) = V(t)^+, 0 \le t \le T$$

When there is collateral $C(t)$,

$$E_t = \max\big(V(t) - C(t), 0\big) = \big(V(t) - C(t)\big)^+, 0 \le t \le T$$

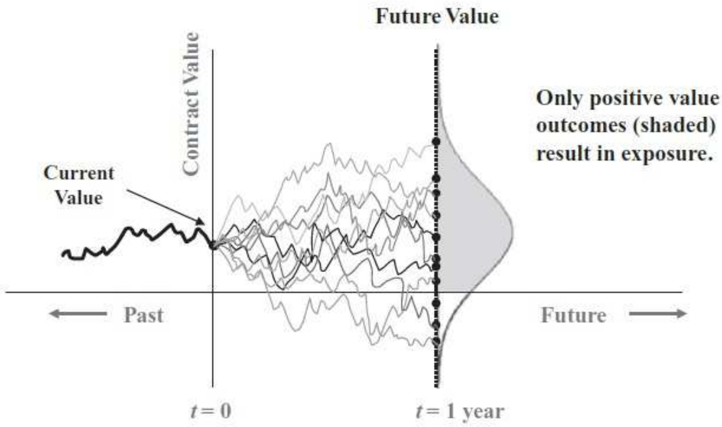

Figure 1.2: Portfolio Market Value and Counterparty Credit Exposure. Source: M. Pykhtin (2011) [48].

Because of the complexity of banks' portfolios, the probability distribution (or empirical distribution) of credit exposure at future time points is usually obtained by Monte Carlo simulation. Given the mathematical models (such as geometric Brownian motion dynamics) of the underlying market risk factors (e.g., stock price, interest rates, foreign exchange rates, etc.), the Monte Carlo modeling framework is widely used to calculate the credit exposure in practice. Typically, it has two major steps,

1. Scenario generation. Dynamics of market risk factors are specified by stochastic processes. These processes are calibrated either to historical or to market implied data. Future values of the market risk factors are simulated for a fixed set of future time points.

2. Portfolio valuation. For each simulation time point and for each realization of the underlying market risk factors, valuation is performed for the portfolio of interest.

1.2.2 Credit exposure profiles

The most complete characterization of future credit exposure is given by its probability distribution at each future time point. However, for many risk management applications, a single deterministic quantity characterizing exposure at a given time point is needed. For example, in deciding whether to have additional OTC positions with a given counterparty, a single number characterizing the exposure would be useful. A collection of such numbers obtained

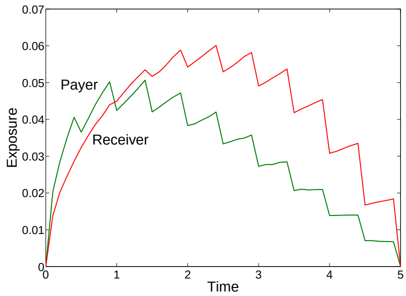

Figure 1.3: PFE (97.5%) for payer and receiver swap under the Hull-White interest rate model

by applying the same procedure to exposure distributions at all simulation time points is known as an exposure profile. Two types of exposure profiles are widely used in practice: potential future exposure (PFE) and expected exposure (EE).

A potential future exposure profile is obtained by calculating a high confidence level (e.g., 97.5 percent) quantile of exposure at each simulation time point,

Definition 2. *The potential future exposure (PFE) at time t is defined as*

$$PFE_{\alpha,t} = inf\{x : \mathbb{P}(E_t \leq x) \geq \alpha)\}, 0 \leq t \leq T,$$

where α is the given confidence level, and $\mathbb{P}$ is the real-world measure.

In figure 1.3, we give an example of PFE (97.5%) for a payer and a receiver swap under the Hull-White interest rate model.

An expected exposure profile is obtained by calculating the sample mean of the simulated exposure realizations at each simulation time point,

Definition 3. *The expected exposure (EE) at time t is defined as*

$$EE_t = \mathbb{E}^{\mathbb{P}}\left[E_t\right], 0 \leq t \leq T.$$

1.2.3 Market-implied default probabilities

To quantify the counterparty credit risk, besides the credit exposure component discussed above, another critical component is the default probability of the counterparty. The introduction of various methods to determine the default probability, such as historical estimation and equity-based approaches (i.e., Merton approach, KMV approach [1]), can be found in the literature, see Gregory (2009). To focus the discussion, we will only review the market-implied default probabilities method which will be used in our work.

Let $S_{ur}(t)$ denote the risk neutral survival function of the counterparty. If we use the concept of hazard rate λ_t to represent the survival function, then $S_{ur}(t)$ can be written as,

$$S_{ur}(t) = \mathbb{E}^{\mathbb{Q}}[\exp(-\int_0^t \lambda_u \mathrm{d}u)].$$

The default probability during a time interval, for example, $\big(t_{m-1}, t_m\big)$, reads,

$$S_{ur}(t_{m-1}) - S_{ur}(t_m) = \mathbb{E}^{\mathbb{Q}}[\exp(-\int_0^{t_{m-1}} \lambda_u \mathrm{d}u)] - \mathbb{E}^{\mathbb{Q}}[\exp(-\int_0^{t_m} \lambda_u \mathrm{d}u)].$$

If we use a one year average hazard rate to approximate λ_t, then λ_t can be estimated by a well known formula, i.e.,

$$\lambda_t \approx \frac{c(t)}{1-\delta},$$

with $c(t)$ the one year par credit spread, which is embedded in the one year CDS prices. The estimation results of λ_t are then used to calculate the counterparty's default probability during the time period of interest.

1.2.4 Pricing counterparty credit risk

Consider a simple case where only one side of the counterparties is defaultable. For example, we assume that the bank holding the portfolio has no default risk, while the bank's counterparty is subject to default risk. To price the portfolio, the bank should ask for a risk premium to be compensated for the counterparty's default risk. The market value of this risk premium is named unilateral credit value adjustment (CVA).

A risk neutral pricing framework is used for pricing counterparty credit risk. In the default event, the bank's loss due to the counterparty's default at time τ, discounted to time 0, can be written as,

$$1_{\{\tau \leq T\}}(1-\delta)D(0,\tau)E_{\tau}, \tag{1.1}$$

where $1_{\{\tau \leq T\}}$ is the default indicator function (takes value 1 when default occurs before maturity and a value of 0 otherwise.); δ is the fraction of the exposure that the bank recovers in the counterparty default event; $D(0,\tau)$ is the

[1] KMV Corp., now Moody's KMV, develops and distributes credit risk management products.

discount factor from τ to 0; T is the maturity of the transaction. Then the unilateral CVA is obtained by taking the risk neutral expectation of equation (1.1),

$$\mathrm{CVA}(0,T) = \mathbb{E}^{\mathbb{Q}}[1_{\{\tau \leq T\}}(1-\delta)D(0,\tau)E_\tau]$$

Generally, the risk neutral pricing formula of unilateral CVA is given by the following proposition,

Proposition 1.2.1. *(Risk neutral pricing formula of CVA) At valuation time s, provided the counterparty has not defaulted before s, i.e., at $\{\tau > s\}$, the risky value of the derivative security under counterparty credit risk, $\widetilde{V}(s)$, reads,*

$$\widetilde{V}(s) = V(s) - CVA(s,T),$$

where

$$CVA(s,T) = \mathbb{E}^{\mathbb{Q}}[1_{\{\tau \leq T\}}(1-\delta)D(s,\tau)E_\tau \mid \mathcal{F}_s].$$

Proof. The proof can be found in [9, 33]. □

If we take a set of discrete time grid points for $[0,T]$, $\pi = \{t_1, ..., t_M\}$, where $0 = t_0 \leq t_1 < ... < t_M = T$, $m = 1, ..., M$, then the discretization of the CVA formula reads,

$$\begin{aligned}
\mathrm{CVA}(0,T) &= \sum_{m=1}^{M} \mathbb{E}^{\mathbb{Q}}[(1-\delta)D(0,\tau)E_\tau 1_{t_{m-1}<\tau\leq t_m}] \\
&\approx \sum_{m=1}^{M} \mathbb{E}^{\mathbb{Q}}[(1-\delta)D(0,t_{m-1})E_{t_{m-1}} \mid t_{m-1} < \tau \leq t_m]\mathbb{Q}(t_{m-1} < \tau \leq t_m).
\end{aligned}$$

For ease of exposition, we assume the discount factor $D(0,t)$ to be deterministic and there is no dependence between δ (constant) and either the exposure or default event, then the discretization form reads,

$$\begin{aligned}
\mathrm{CVA}(0,T) &\approx (1-\delta)\sum_{m=1}^{M} D(0,t_{m-1})\mathbb{E}^{\mathbb{Q}}[E_{t_{m-1}} \mid t_{m-1} < \tau \leq t_m]\mathbb{Q}(t_{m-1} < \tau \leq t_m) \\
&= (1-\delta)\sum_{m=1}^{M} D(0,t_{m-1})EE^*_{t_{m-1},t_m}\big(S_{ur}(t_{m-1}) - S_{ur}(t_m)\big),
\end{aligned}$$

where $EE^*_{t_{m-1},t_m}$ denotes the expected exposure conditional on default, $\mathbb{E}^{\mathbb{Q}}[E_{t_{m-1}} \mid t_{m-1} < \tau \leq t_m]$. In practice, the dependence between exposure and default is often ignored, then CVA can be calculated approximately as,

$$\mathrm{CVA}(0,T) \approx (1-\delta)\sum_{m=1}^{M} D(0,t_{m-1})EE_{t_{m-1}}\big(S_{ur}(t_{m-1}) - S_{ur}(t_m)\big).$$

1.2.5 CVA with wrong way risk

In the previous section, we have mentioned the dependence between exposure and the counterparty's default. A typical example of this dependence is known as wrong way risk, which describes the market behavior that exposure tends to increase when the counterparty credit quality becomes worse. And if the exposure tends to decrease when the counterparty credit quality becomes worse, then it is called right way risk.

To incorporate the dependence between exposure and default, one can use the concept of stochastic hazard rate to derive an analytical approximation of the expected exposure conditional on default. Suppose the counterparty's credit quality is characterized by a stochastic hazard rate process λ_t, without specifying its dynamics. The expected exposure conditional on default, $EE^*_{t_m,t_{m+1}}$, can be approximated by [49],

$$EE^*_{t_m,t_{m+1}} \approx \frac{\sum_{p=1}^{P} E_{t_m}(x_m(p)) \exp\big(-\sum_{i=1}^{m} \lambda_{t_i}(p)\Delta t\big)\lambda_{t_m}(p)}{\sum_{p=1}^{P} \exp\big(-\sum_{i=1}^{m} \lambda_{t_i}(p)\Delta t\big)\lambda_{t_m}(p)},$$

where P is the number of scenarios, $x_m(p)$ is the realisation of underlying market risk factors at time t_m, on scenario p, and $\lambda_{t_i}(p)$ denotes the realisation of the stochastic hazard rate at time t_i, on scenario p.

In the simulation, the market risk factors (or the credit exposure) and stochastic hazard rate are simulated jointly for P scenarios for a set of time points $t_0 = 0, t_1, ..., t_M$. All possible dependences between the market risk factors (or the credit exposure) and the hazard rate are taken into account in the simulation.

To model the dependence between the hazard rate and the underlying market risk factors, one approach is to assume the hazard rate to be a function of the market risk factors, i.e., $\lambda(X(t))$, where $X(t)$ denotes the risk factors. A simple example is an equity option written on the counterparty's equity price $S(t)$, for which the hazard rate of the counterparty is assumed to be a negative power function of $S(t)$, i.e.,

$$\lambda(S(t)) = AS(t)^B,$$

where A and B are constant parameters which can be estimated by a least squares linear regression method. This functional form assumes that the counterparty's equity price contains sufficient information to estimate its credit quality.

One can also model the dependence between the hazard rate and the portfolio value $V(t)$. As suggested by J. Hull and A. White (2012) [37], the hazard rate is assumed to be a function of the portfolio value $V(t)$. We further assume that $V(t)$ at state $(t, X(t))$ is a function of $X(t)$, i.e., $V(t) = g(X(t))$

or $X(t) = g^{-1}(V(t))$, where function g is invertible, and denote $\lambda(X(t)) = \lambda\big(g^{-1}(V(t))\big) = \widetilde{\lambda}(V(t))$. The functional form of the hazard rate is given as follows,

$$\widetilde{\lambda}(V(t)) = \exp\big(a(t) + bV(t)\big),$$

where $a(t)$ is a function of time, b is a constant parameter that measures the amount of wrong or right way risk in the model. In the case of wrong (right) way risk, b is positive (negative) and $\widetilde{\lambda}(V(t))$ is an increasing (decreasing) function of $V(t)$.

The calibration of the Hull-White wrong way risk model involves two major steps: (1) first, b has to be estimated properly; (2) second, $a(t)$ is determined by incorporating the credit spreads observed today into the model.

In summary, CVA with wrong way risk can be calculated by the following formula,

$$\text{CVA}_W \approx (1-\delta)\sum_{m=1}^{M} D(0, t_{m-1}) EE^*_{t_{m-1},t_m}\big(S_{ur}(t_{m-1}) - S_{ur}(t_m)\big),$$

where the expected exposure conditional on default, $EE^*_{t_{m-1},t_m}$, and the default probability $S_{ur}(t_{m-1}) - S_{ur}(t_m)$ are estimated via a specific model of hazard rate λ_t.

1.3 Setup of the thesis

The thesis is organized as follows.

In chapter 2, we explain the application of Monte Carlo simulation and an efficient Fourier inversion method, the COS method, to the exposure calculation of Bermudan options. Risk measures such as PFE and EE can then be obtained based on the empirical distribution of exposures. Different from the Longstaff-Schwartz method (LSM) which uses the least squares approximation in the computation of the continuation value at early exercise opportunities, a numerical integration method based on Fourier cosine expansions is used in our approach. For the one-dimensional case, this approach can calculate the exposures at each simulated state fast and accurately. The accuracy of exposure computation at each simulated state is important for an accurate estimation of the exposure profiles. The exposure profiles generated by our approach can serve as a benchmark to analyse the error of American Monte Carlo methods (LSM, etc.). In practice, PFE and EE should be calculated under the real world measure $\mathbb{P}$. We show the difference of exposure profiles under different measures (risk neutral measure $\mathbb{Q}$ and real world measure $\mathbb{P}$). We point out that the efficient computation of EE forms the basis for the computation of CVA.

In chapter 3, we study efficient computation methods for exposure profiles when the underlying is high-dimensional. In the case of multi-asset instruments, numerical integration methods (such as the approach introduced in chapter 2) are computationally expensive. The approach considered here is named Stochastic Grid Bundling Method (SGBM) [39]. The method is based on the 'regression later' technique [32] used for conditional expectation approximation and the bundling (or binning) technique used for state space partitioning [30, 31, 41]. To investigate the efficiency of SGBM, we focus on a numerical comparison (accuracy, computation speed and standard deviation of estimates) of SGBM, the standard regression method (SRM), and the standard regression bundling method (SRBM). Compared with the other two methods, it shows that SGBM has the advantage of smaller standard deviation for the direct estimates of option prices. Compared with SRM, the bundling technique used in SGBM and SRBM can significantly improve the accuracy of the exposure profiles.

In chapter 4, the risk neutral pricing of counterparty credit risk is discussed. An efficient computation method is provided for the CVA computation of Bermudan options when wrong way risk (positive dependence between default risk and exposure) exists. We use the approach described in chapter 2 to calculate the expected exposure (EE) of Bermudan options. To model the wrong way risk, we consider two approaches based on the hazard rate of the counterparty. In one approach, named portfolio value approach (PVA), the hazard rate is assumed to be a function of the portfolio value. In another approach, named empirical analysis approach (EAA), the hazard rate is assumed to be a function of the counterparty's stock price. Then we calculate the expected exposure conditional on default. We show that the effect of wrong way risk on the expected exposure and CVA can be significant. We also analyse the relationship between wrong way risk and the early exercise features via numerical examples.

In chapter 5, we give two extensions of the work of chapter 4. First, instead of Bermudan options written on the counterparty's stock, in this chapter, the underlying asset is not the counterparty's stock. We add (positive or negative) correlation between these two different stocks and investigate the wrong way risk effect under different values of correlation. Second, by using the computation methods introduced in chapter 3, we consider the CVA computation of multi-asset instruments. An efficiency comparison of different computation methods (SRBM, SGBM, SRM) for the computation of the option price and of CVA is also provided here. We show the effect of correlation between default risk and exposure on the results of the expected exposure profiles and CVA. We point out that the application of the bundling technique can improve the accuracy of exposure profiles and CVA of multi-asset instruments.

Chapter 2

A Benchmark Approach for the Counterparty Credit Exposure of Bermudan Options under Lévy Process: the Monte Carlo-COS Method

2.1 Introduction

The computation of counterparty credit exposure of exotic instruments without analytical solution is a challenging problem. According to Basel II and Basel III, counterparty credit risk is the risk that a counterparty in a derivatives transaction will default prior to the expiration of the instrument and will not therefore make the current and future payments required by the contract. For quantification of counterparty credit risk of exotic instruments with no analytical solution, such as calculation of potential future exposure (PFE), expected exposure (EE), and credit value adjustment (CVA), an efficient computation method for counterparty credit exposure is required.

In this chapter, we propose an advanced approach, which we call Monte Carlo-COS method (MCCOS), to give accurate results of the exposure profiles of a single asset Bermudan option under a Lévy process. Different from the American Monte Carlo method[1] [1, 22, 56], in the Monte Carlo-COS method,

[1]we call the Longstaff-Schwartz method, stochastic mesh method and other methods which are used for pricing Bermudan option and American option American Monte Carlo algorithms.

one can calculate the exposure profile without using any change of measure. Combined with the computational advantages of the COS method on accuracy and speed of option pricing, the exposure profile produced by the Monte Carlo-COS method can serve as a "benchmark" for analysing the reliability of American Monte Carlo methods.

The literature on the subject is quite rich. Canabarro and Duffie [17] and Duffie and Singleton [26] discuss techniques for measuring and pricing counterparty credit risk; Lomibao and Zhu [44] present a "direct jump to simulation date" method, and derive analytic expressions to calculate the exposure on a number of path-dependent instruments, except on Bermudan and American options; In Pykhtin and Zhu [51, 52], a modeling framework for counterparty credit exposure is proposed.

Based on this modeling framework, the American Monte Carlo method is proposed for exposure calculation in some literature. In Schöftner [56] a modified least squares Monte Carlo algorithm is applied; Cesari [22] combines the bundling technique [60] with the Longstaff-Schwartz method for exposure calculation; Ng [47] applies the stochastic mesh method to the credit exposure calculation.

The chapter is structured in the following way. Section 2.2 provides the definition of the exposure profiles of counterparty credit exposure, and describes the modeling approach for exposure calculation of exotic options. Section 2.3 shows the connection between dynamic programming and exposure calculation. Section 2.4 explains the application of the Monte Carlo-COS method to get a benchmark result for the Bermudan option. Section 2.5 gives numerical experiments and analyses the difference of exposure profiles and exercise intensity under different measures. Section 2.6 concludes the presented approach to calculate the exposure profiles.

2.2 Exposure valuation: the modeling framework

Let $(\Omega, \mathcal{F}, \mathbb{P})$ be a probability space, let T be a fixed positive number, and let $\mathcal{F}_t$, $0 \leq t \leq T$, be a filtration of sub-σ-algebras of $\mathcal{F}$. We define the value of a derivatives security under the risk-neutral measure $\mathbb{Q}$ [59] over time as a stochastic process $V(t), 0 \leq t \leq T$, which is driven by the stochastic process of risk factors $X(t), 0 \leq t \leq T$, such as stock prices, foreign exchange rates, and interest rates[33]. We call $(t, X(t))$ the state of the economy at time t. Denote the derivative's discounted net cashflow between t and T as $C_f(t,T)$ (i.e., all of the cashflows are discounted back to time t), then

$$V(t) = \mathbb{E}^{\mathbb{Q}}\big[C_f(t,T)|\mathcal{F}_t\big].$$

In chapter 1, the credit exposure E_t is defined as the positive part of $V(t)$. According to the definition of PFE and EE given in chapter 1, the main problem to calculate $PFE_{\alpha,t}$ and EE_t is to calculate the probability distribution of E_t (or $V(t)$) under the real-world measure $\mathbb{P}$. The exact probability distribution, which usually has no explicit solution, can be approximated by an empirical distribution of the sample results of E_t (or $V(t)$) on each simulated state $(t, X(t))$.

Assuming one has a model describing the stochastic process of risk factors $X(t)$, $0 \leq t \leq T$, which is already calibrated to the market data at time zero, then two basic steps are involved in the modelling framework [1, 22]:

1. Simulate the model under the real-world measure $\mathbb{P}$ (i.e., the market price of risk has to be incorporated into the model) to get the scenarios of risk factors $X(t)$, $t \in [0, T]$.

2. Calculate the option price for every simulated state $(t, X(t))$, under the risk-neutral measure $\mathbb{Q}$. The option can be seen as a newly issued one from a future state $(t, X(t))$, with time to maturity $T - t$.

2.3 Dynamic Programming and Exposure Calculation

In contrast to European options, which can only be exercised at maturity, a Bermudan option can be exercised at a fixed set of exercise opportunities, $\mathcal{T} = \{t_1, ..., t_M\}$,$0 = t_0 \leq t_1, t_M = T$. Assume the exercise dates are equally spaced, i.e., $t_i - t_{i-1} = \Delta t, i = 1, ...M$. If a put option is exercised at t_i, the option holder gets the exercise value $h(t_i, S_{t_i}) = (K - S_{t_i})^+$, where K is called the strike price [2].

To determine $V_0(S_0)$, the Bermudan option value at initial time 0, with initial stock price S_0, one needs to solve the following dynamic programming recursion:

$$\begin{aligned} V_M(S_M) &= h(t_M, S_M), && (2.1)\\ c(t_{m-1}, S_{m-1}) &= \exp(-r\Delta t)\mathbb{E}^{\mathbb{Q}}\left[V_m(S_m)|\mathcal{F}_{t_{m-1}}\right], m = M, ..., 1, && (2.2)\\ V_{m-1}(S_{m-1}) &= \max\{h(t_{m-1}, S_{m-1}), c(t_{m-1}, S_{m-1})\}, && (2.3)\\ V_0(S_0) &= c(t_0, S_0), && (2.4) \end{aligned}$$

where we use the simplified notation X_m for X_{t_m}. We assume a constant interest rate r, so $\exp(-r\Delta t)$ denotes the discount factor for time interval Δt, c is the continuation value of the option and V the value of the option immediately

[2] We have written the exercise value as $h(t_i, S_{t_i}) = (K - S_{t_i})^+$ rather than $h(t_i, S_{t_i}) = K - S_{t_i}$ so that exercising an out-of-the-money option produces a zero payoff rather than a negative payoff. This allows us to include the possibility that the option expires worthless within the event $\{\tau = T\}$ rather than writing, e.g., $\tau = \infty$ for this case, see [31].

before the exercise opportunity. As indicated in (2.1), the continuation value c at terminal time t_M equals 0.

Note that t_0 is not included in the exercise dates. If one issues a new Bermudan option from an intermediate state (t_{m-1}, S_{m-1}), with possible exercise dates $[t_m, ..., t_M]$ (Here t_{m-1} is not an exercise date.), then the price of this new option is equal to the continuation value $c(t_{m-1}, S_{m-1})$ in (2.2) [31]. Based on this observation, we can calculate the credit exposure for each exercise date, $\mathcal{T} = \{t_1, ..., t_M\}$, as a by-product of the option pricing procedure, which therefore yields estimated distributions of credit exposure, on each possible exercise date.

In an ordinary option pricing procedure of an American Monte Carlo method, such as LSM, the stock price S_t is usually simulated under the risk-neutral measure $\mathbb{Q}$. However, in risk management, industries are interested in values under the real-world measure $\mathbb{P}$, i.e., asset price processes evolve under the real-world measure $\mathbb{P}$. In [22, 56], the authors use the change of measure method to get the $\mathbb{P}$-distribution. In contrast to the American Monte Carlo method used in [22, 56], in the Monte Carlo-COS method, one can efficiently compute the option prices on all the grid points which are simulated under measure $\mathbb{P}$, without using any change of measure. The algorithm is explained in the following section.

2.4 A Benchmark Approach: The Monte Carlo-COS Method

The Monte Carlo-COS method is based on the work of [27, 28, 22]. We assume the underlying stochastic process is a Lévy process.

For a Bermudan option, regression-based approximation methods, such as the LSM method, are used to approximate the following conditional expectation on possible exercise dates:

$$c(t_{m-1}, s_{m-1}(p)) = \exp(-r\Delta t)\mathbb{E}^{\mathbb{Q}}\left[V_m(S_m)|S_{m-1} = s_{m-1}(p)\right], \tag{2.5}$$

with $p = 1, ..., P$, the simulated sample paths, $s_{m-1}(p)$ the realization of random variable S_{m-1}. If we define $X = \log\left(S_{m-1}/K\right)$, $x = \log\left(s_{m-1}(p)/K\right)$, $Y = \log\left(S_m/K\right)$, with K the strike price, and denote $\widetilde{V}_m(Y) = V_m(K\exp(Y)) = V_m(S_m)$, then it can be represented as,

$$c(t_{m-1}, x) = \exp(-r\Delta t)\mathbb{E}^{\mathbb{Q}}\left[\widetilde{V}_m(Y)|X = x\right] = \exp(-r\Delta t)\int_{\mathbb{R}} \widetilde{V}_m(y) f_{Y|X=x}(y)\mathrm{d}y, \tag{2.6}$$

where $f_{Y|X=x}(y)$ is the probability density function of y given x under risk-neutral measure $\mathbb{Q}$.

An alternative way for efficient calculation of (2.6) is by numerical integration, particularly we choose the COS method developed in [27] as the main component of our algorithm.

Different from the option pricing problem in [27], for the exposure profile problem, the option price on every grid point simulated under measure $\mathbb{P}$ has to be calculated. And the early exercise event has to be taken into account for each simulated path, since the option price should be floored to zero after the exercise event happens. This is done by finding the earliest exercise time, τ^p, for each path p and set the value after τ^p to zero.

There are three main components in the Monte Carlo-COS method for exposure profile calculation:

1. Scenario generation for the future economic state under measure $\mathbb{P}$;
2. Instrument valuation on all the simulated paths by the COS method;
3. Exposure profile calculation.

2.4.1 Fourier cosine expansions

In this section, we explain the COS method for instrument valuation on all the simulated grid points. The following proposition[27] gives another representation of (2.6):

Proposition 2.4.1. *Let the underlying stochastic process of stock price S_t be a Lévy process, then the continuation value at grid point $(t_{m-1}, s_{m-1}(p))$, $c(t_{m-1}, s_{m-1}(p))$, can be approximated by,*

$$\hat{c}(t_{m-1}, x) = \exp(-r\Delta t) \sum_{k=0}^{N-1}{}' Re\{\varphi_{levy}\big(\frac{k\pi}{b-a}; \Delta t\big) \exp(-ik\pi\frac{x-a}{b-a})\} V_k(t_m), \tag{2.7}$$

where $\varphi_{levy}(\omega; \Delta t) = \phi_{levy}(\omega; 0, \Delta t)$, and ϕ_{levy} is the characteristic function of a Lévy process. The $V_k(t_m)$ represent the Fourier-cosine series coefficients of $\widetilde{V}_m(y)$ on $[a, b]$,

$$V_k(t_m) = \frac{2}{b-a} \int_a^b \widetilde{V}_m(y) cos\big(k\pi\frac{y-a}{b-a}\big) \mathrm{d}y. \tag{2.8}$$

Here $[a, b]$ is the truncation interval of the integration of the risk-neutral evaluation formula in (2.6). $c(t_{m-1}, s_{m-1}(p))$ is equivalent to the value of a Bermudan option newly issued at grid point $(t_{m-1}, s_{m-1}(p))$, with maturity time t_M and possible exercise dates, $t_m, ..., t_M$. $\sum'$ indicates the first term in the summation is weighted by $1/2$.

Proof. The main proof can be found in [27]. ∎

2.4.2 Recovery of $V_k(t_m)$

To compute (2.7), one needs to know the Fourier cosine coefficients, $V_k(t_m)$, given in (2.8). The derivation of an induction formula for $V_k(t_m)$ for Bermudan options, backwards in time, was the basis of the work in [28]. It is briefly explained here.

First, the early exercise point, $x^*(t_m)$, at time t_m, which is the point where the continuation value equals the payoff, i.e., $c(x^*(t_m), t_m) = h(x^*(t_m))$, is determined by Newton's method.

Second, based on $x^*(t_m)$, $V_k(t_m)$ is split into two parts: one on the interval $[a, x^*(t_m)]$, and another on $(x^*(t_m), b]$, i.e.,

$$V_k(t_m)=\begin{cases} C_k(a, x^*(t_m), t_m) + G_k(x^*(t_m), b), & \text{for a call,} \\ G_k(a, x^*(t_m)) + C_k(x^*(t_m), b, t_m), & \text{for a put,} \end{cases}$$

for $m = M-1, ..., 1$, and at $t_M = T$,

$$V_k(t_M)=\begin{cases} G_k(x^*(0, b), & \text{for a call,} \\ G_k(x^*(a, 0), & \text{for a put.} \end{cases}$$

Here C_k and G_k are the Fourier coefficients for the continuation value and payoff function, respectively, which read,

$$G_k(x_1, x_2) = \frac{2}{b-a}\int_{x_1}^{x_2} h(x) cos\big(k\pi\frac{x-a}{b-a}\big)\mathrm{d}x,$$

and

$$C_k(x_1, x_2, t_j) = \frac{2}{b-a}\int_{x_1}^{x_2} c(x, t_j) cos\big(k\pi\frac{x-a}{b-a}\big)\mathrm{d}x.$$

For $k = 0, 1, ..., N-1$ and $m = 1, 2, ..., M$, $G_k(x_1, x_2)$ has an analytical solution, and the challenge is to compute the C_k efficiently. The following proposition from [28] claims that $C_k(x_1, x_2, t_m)$, $k = 0, 1, ..., N-1$, can be recovered from $V_l(t_{m+1})$, $l = 0, 1, ..., N-1$, with $O(N \log_2 N)$ complexity.

Proposition 2.4.2. *For $m = M$, $V_k(x_1, x_2, t_m)$ (and $C_k(x_1, x_2, t_m)$) has an analytical solution; for $m = M-1, ..., 1$, $G_k(x_1, x_2)$ has an analytical solution, and $C_k(x_1, x_2, t_m)$ can be approximated by $\widehat{C}_k(x_1, x_2, t_m)$, i.e.,*

$$\widehat{C}_k(x_1, x_2, t_m)=\begin{cases} \exp(-r\Delta t) Re\{\sum_{l=0}^{\prime N-1} \varphi_{levy}\big(\frac{l\pi}{b-a};\Delta t\big) V_l(t_{m+1}) \cdot \mathcal{M}_{k,l}(x_1, x_2)\} \\ \qquad\qquad \textit{for } m = M-1 \\ \exp(-r\Delta t) Re\{\sum_{l=0}^{\prime N-1} \varphi_{levy}\big(\frac{l\pi}{b-a};\Delta t\big) \widehat{V}_l(t_{m+1}) \cdot \mathcal{M}_{k,l}(x_1, x_2)\} \\ \qquad\qquad \textit{for } m = M-2, \ldots, 1 \end{cases}$$

with $\mathcal{M}_{k,l}(x_1, x_2)$ defined as

$$\mathcal{M}_{k,l}(x_1, x_2) = \frac{2}{b-a}\int_{x_1}^{x_2} \exp(il\pi\frac{x-a}{b-a})cos\big(k\pi\frac{x-a}{b-a}\big)\mathrm{d}x,$$

and $i = \sqrt{-1}$ being the imaginary unit. $\widehat{V}_l(t_{m+1})$ is the approximation of $V_l(t_{m+1})$ by replacing $C_k(x_1, x_2, t_{m+1})$ with $\widehat{C}_k(x_1, x_2, t_{m+1})$.

Proof. The derivation of the result can be found in [28]. □

2.4.3 Application for exposure calculation

Denote the integration interval for grid point $(t_{m-1}, s_{m-1}(p))$ by $[a_{m-1,p}, b_{m-1,p}]$, $m = 1, ..., M, p = 1, ..., P$, where

$$a_{m-1,p} = \xi_1 - L\sqrt{\xi_2 + \sqrt{\xi_4}} + \log\big(s_{m-1}(p)/K\big)$$
$$b_{m-1,p} = \xi_1 + L\sqrt{\xi_2 + \sqrt{\xi_4}} + \log\big(s_{m-1}(p)/K\big)$$

with $L \in [6, 12]$ depending on a user-defined tolerance level, TOL, and $\xi_1, ..., \xi_4$ being the cumulants of Lévy process[3], with time interval Δt. The error in the pricing formula connected to the size of the domain decreases exponentially with L, and in most cases, as shown in [27], with $L = 10$ the option price converges well for Lévy processes to accuracy of 10^{-9} or less.

The common truncation interval for all the grid points is chosen as $[a, b]$ in the following way,

$$a = \min\{a_{m-1,p} : m = 1, ..., M, p = 1, ..., P\},$$
$$b = \max\{b_{m-1,p} : m = 1, ..., M, p = 1, ..., P\}.$$

Consider the sample vector at time t_{m-1},

$$\mathbf{SV}_{m-1} = [s_{m-1}(1), ..., s_{m-1}(P)].$$

For a vector $\mathbf{xv}_{m-1} = [\log\big(s_{m-1}(1)/K\big), ..., \log\big(s_{m-1}(P)/K\big)]$, the COS formula (2.7) can be written as a vector form,

$$\begin{aligned}\hat{c}(t_{m-1}, \mathbf{xv}_{m-1}) &= \exp(-r\Delta t)\\ &\quad\times \sum_{k=0}^{N-1}{}' Re\{\varphi_{levy}\big(\frac{k\pi}{b-a}; \Delta t\big)\exp(-ik\pi\frac{\mathbf{xv}_{m-1}-a}{b-a})\}V_k(t_m),\end{aligned} \tag{2.9}$$

[3]For example, if the stochastic process is geometric Brownian motion, then $\xi_1 = (\mu - \frac{1}{2}\sigma^2)\Delta t$, $\xi_2 = \sigma^2\Delta t$, $\xi_4 = 0$, with μ the drift coefficient, and σ the diffusion coefficient.

which is useful for exposure calculation on all the grid points in a sample vector.

According to the proposition 2.4.2, for the case of Lévy processes, the Fourier cosine coefficients, $V_k(t_m)$, $k = 0, 1, ..., N-1$, can be recovered from $V_l(t_{m+1})$, $l = 0, 1, ..., N-1$, without knowing the option price for each time step. Once the Fourier cosine coefficients for each time step are calculated, one just inserts them into formula (2.9) to get the continuation value (or the Bermudan option price), i.e., $\hat{c}(t_{m-1}, \mathbf{xv}_{m-1})$.

2.4.4 The Monte Carlo-COS algorithm

We list the Monte Carlo-COS algorithm for exposure profile calculation of Bermudan options as follows,

1. Simulate sample paths for the stock price, $s_0(p), ..., s_M(p)$, at time steps $0 = t_0, ..., t_M = T$, with indices of paths $p = 1, ..., P$, under the real-world measure $\mathbb{P}$.

2. Calculate the common truncation interval for all simulated grid points, $[a, b]$.

3. For each time step, calculate the Fourier cosine coefficients, $V_k(t_m)$, $k = 0, 1, ..., N-1, m = 1, ..., M$.

4. At terminal date $t_M = T$, set

$$V_M(s_M(p)) = \max(h(t_M, s_M(p)), 0),$$

for $p = 1, ..., P$, and define the stopping time $\tau_M = T$.

5. Apply backward induction, i.e., $m \to m-1$ for $m = M, ..., 1$,

   (a) Calculate the continuation value, $\hat{c}(t_{m-1}, S_{m-1}(p))$, by inserting the Fourier cosine coefficients into formula (2.9).

   (b) Define a new stopping time according to the stopping rule for Bermudan options,

$$\tau^p_{m-1} = \min\{k \in \{m-1, ..., M\} | h(t_k, s_k(p)) \geq c(t_k, s_k(p))\}.$$

   (c) For each sample path $p = 1, ..., P$, set

$$V_{m-1}(s_{m-1}(p)) = \max(h(t_{m-1}, s_{m-1}(p)), c(t_{m-1}, s_{m-1}(p))),$$

   and $V_t(s_t(p)) = 0$ for $t > \tau^p_{m-1}$.

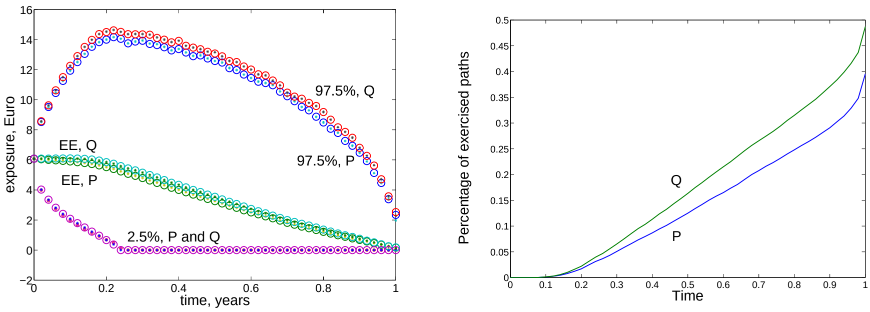

(a) (b)

Figure 2.1: (A), The exposure profiles of Bermudan options under different measures. (B), The exercise intensity of Bermudan options under different measures.

6. Calculate the exposure at initial time, $V_0(s_0) = c(0, s_0)$, because exercise is not allowed at time zero.
7. Set $E^p_{t_m} = \max(V_m(s_m(p)), 0)$ for the credit exposure.
8. The measure $\mathbb{P}$-exposure profiles of PFE_{α,t_m} and EE_{α,t_m} can be calculated directly by the empirical distribution of $E^p_{t_m}$. Since the scenario is simulated under measure $\mathbb{P}$, no change of measure needed.

2.5 Numerical Experiments: Exposure Profiles under Different Measures

In this section, we investigate the difference between the exposure profiles calculated under different measures, i.e., $\mathbb{Q}$ and $\mathbb{P}$. For comparison, we take the same parameters as in [56] for the Bermudan option, with initial price $S_0 = 100$, strike price $K = 100$, constant interest rate $r = 0.05$, real world drift $\mu = 0.1$, volatility $\sigma = 0.2$ and 50 exercise dates. The underlying stochastic process is the geometric Brownian motion process (GBM). We take 18000 paths and 50 time steps for the underlying value. Only the exposures on the possible exercise dates are considered.

We investigate the exposure profiles calculated under different measures by two settings:

Time	0.1	0.2	0.3	0.4	0.5
$\mathbb{P}$	5.8983	5.5188	4.7929	4.0037	3.2563
$\mathbb{Q}$	6.1020	5.8501	5.1485	4.3417	3.5437

Table 2.1: Expected Exposure (EE) under different measures.

Time	0.6	0.7	0.8	0.9	1
$\mathbb{P}$	2.5100	1.8140	1.2148	0.6762	0.1654
$\mathbb{Q}$	2.7390	1.9942	1.3643	0.7519	0.1799

Table 2.2: Expected Exposure (EE) under different measures.

1. $\mathbb{Q}$-exposure profile, i.e., the stock prices are simulated under measure $\mathbb{Q}$. The exposure profiles are obtained based on the $\mathbb{Q}$-probability distribution of credit exposure.

2. $\mathbb{P}$-exposure profile, i.e., the stock prices are simulated under measure $\mathbb{P}$. The exposure profiles are obtained based on the $\mathbb{P}$-probability distribution of credit exposure.

The difference between the $\mathbb{Q}$-exposure profile and the $\mathbb{P}$-exposure profiles is illustrated in figure 2.1a. Note that in this parameter setting, $\mu > r$, and we find the $\mathbb{P}$-exposure profiles are lower than $\mathbb{Q}$-exposure profiles. The initial prices V_0 for both settings coincide, because the risk-neutral pricing formula is independent of the different measures.

When $\mu > r$, at each time step t, the stock price S_t simulated under measure $\mathbb{P}$ tends to be higher than S_t simulated under measure $\mathbb{Q}$. For a Bermudan put option issued at time t, with maturity T and initial stock price S_t, a higher initial stock price S_t (i.e., simulated under measure $\mathbb{P}$) implies a lower option price, and a lower $\mathbb{P}$-exposure profile.

Tables 2.1 and 2.2 provide the expected exposure calculated under different measures, which can be further used in the computation of credit value adjustment (CVA).

Figure 2.1b shows the percentage of paths that has already been exercised at time t. In the example, the exercise intensity under measure $\mathbb{Q}$ is higher than that under measure $\mathbb{P}$. This significantly influences the future exposure values, since after exercise, the contract does not exist any more and the exposure is floored to zero.

Although paths are exercised more often under measure $\mathbb{Q}$ than under measure $\mathbb{P}$ (figure 2.1b), the $\mathbb{Q}$-exposure profile is still higher than the $\mathbb{P}$-exposure profile (figure 2.1a).

2.6 Conclusion

This chapter proposes an advanced method, named the Monte Carlo-COS method to calculate the exposure profile of single asset Bermudan options that have no analytical solutions, under Lévy processes. The result can serve as a benchmark for analysing the error from American Monte Carlo methods [1, 22, 56]. The difference of exposure profiles and exercise intensity under different measures(i.e., $\mathbb{P}$ and $\mathbb{Q}$) is also discussed.

Chapter 3

Algorithmic Counterparty Credit Exposure for Multi-Asset Bermudan Options

3.1 Introduction

The efficient quantification of counterparty credit risk of high-dimensional exotic options is an important and challenging problem both in academics and in the industry. For quantification of counterparty credit risk, two approaches are considered, which are associated with Basel II and Basel III, respectively.

The approach in Basel II consists of computing the counterparty credit exposure, which defines the loss in the event of a counterparty defaulting. Basel II proposes a number of risk measures. In this chapter we will concentrate on the potential future exposure (PFE) and the expected exposure (EE).

The approach in Basel III consists of computing the credit value adjustment (CVA), which is an adjustment to the price of financial instruments due to the possible default of a counterparty. CVA calculation requires the computation of counterparty credit exposure as well [8] [33].

Many authors have discussed the efficient quantification of counterparty credit risk. Canabarro and Duffie [17] and Duffie and Singleton [26] discuss techniques for measuring and pricing counterparty credit risk. The application of PFE and EE exposure profile in credit line limits and credit risk valuation (CVA) is also presented.

Lomibao and Zhu [44] present a "direct jump to simulation date" method, and propose a methodology to account for the possibilities of particular prior events (i.e., exercising an option, etc.) that may affect the exposure. By using the properties of the Brownian Bridge, they derived analytic expressions to calculate the exposure on a number of path-dependent instruments such as barrier options, average options, variance swaps, and swap-settled swaptions.

Pykhtin and Zhu [51] present a treatment of the counterparty credit risk of over-the-counter derivatives under Basel II. The calculation of the minimum capital requirement, which is related to the calculation of the counterparty credit exposure, is also discussed. In [51, 52], the modeling framework for counterparty credit exposure is explained, and in [52], the calculation of CVA is also presented based on the modeling framework.

In Schöftner [56] a modified least squares Monte Carlo algorithm is applied which fits into the context of credit exposure modeling. The algorithm incorporates a change of measure from the risk-neutral probability $\mathbb{Q}$ to the real-world probability measure $\mathbb{P}$, and, if appropriate, it partitions the state space of the payout function into continuous and discontinuous parts using multinomial regression techniques to allow for a more robust estimation. The author gives a benchmark result for the European option, however, benchmark results for Bermudan and American options are not discussed.

Cesari [22] combines the bundling technique, which is used to partition the state space, with the Longstaff-Schwartz method for exposure calculation. In [22], the scenarios are generated under the risk-neutral measure $\mathbb{Q}$, and the probability distribution of exposure under measure $\mathbb{P}$ is obtained by using a change of measure to the exposure distribution under measure $\mathbb{Q}$.

Ng [47] applies the stochastic mesh method into the credit exposure calculation for multi-asset cross currency products, especially for power reserve dual coupon swaps (PRDCs).

Antonov [1] presents an algorithmic approach for credit exposure calculation, such that the exposure calculation can be done during the backward pricing without changing the pseudo-code structure. The algorithmic approach is designed in the modeling framework and suitable for the American Monte Carlo algorithm. The purpose of the algorithmic approach is to avoid the cumbersome modifications of the pricing routines: for exposure calculation, the exercise conditions, or the possibilities of particular prior events have to be taken into account. The author discusses the application of the algorithmic approach for the barrier option, Bermudan swaption, and autocap.

This chapter contributes to the literature as follows.

1. To obtain accurate exposure profiles for multi-asset portfolios, an efficient simulation-based approach, the *Stochastic Grid Bundling Method* (SGBM) [39], is applied. In the case of high-dimensional underlying asset processes, by using a bundling technique, the accuracy of exposure profiles is improved significantly, and the computation speed is kept reasonably

high.

2. A detailed analysis of the bundling technique and regression approximation technique used in SGBM is provided via various numerical examples: assuming that closed-form formulas or analytical approximations exist for the conditional expectations of the basis functions, then

   - Compared with the Standard Regression Bundling Method (SRBM), when the same number of simulation paths, basis functions and bundles are used, the discontinuity of the conditional expectations appearing on the boundaries of bundles in SGBM is smaller. And this discontinuity in SGBM can become very small by increasing the number of simulation paths and bundles appropriately.
   - Compared with the Standard Regression Method (SRM) and SRBM, the numerical examples show that SGBM has the advantage of smaller standard deviation for the direct estimates of option prices. This result is consistent with the conclusion of Glasserman and Yu (2004) [32], in which they theoretically prove the advantage of 'regression later' (used in SGBM) compared with 'regression now' (used in SRBM and SRM) under some conditions (such as *martingale basis functions*, etc.). Generally, the estimates of option prices of SGBM are closer to the reference results than SRM and SRBM.

3. We also show that for discontinuous payoffs, such as digital options, by using the bundling technique appropriately, SGBM can get accurate and stable results of option prices and exposure profiles.

4. A numerical error analysis is provided by using benchmark results of one-dimensional European and Bermudan options via the Monte Carlo-COS method (MCCOS) [58]. It shows that with an appropriate choice of basis functions and application of the bundling technique, SGBM can get very accurate results of the exposure profiles. In addition, the difference between the $\mathbb{P}$-exposure and $\mathbb{Q}$-exposure profiles is also discussed.

The chapter is structured in the following way. Section 3.2 specifies the models of underlying asset prices and discusses the exposure of different instruments. Section 3.3 explains the computation methods, including SRM, SGBM, and SRBM. The bundling method is introduced in detail. The example of single asset options (European, Bermudan and digital options) is given. The discontinuity of the conditional expectation on the bundles boundaries is discussed. In section 3.4 we benchmark the result for the single asset European and Bermudan option by using MCCOS method, and provide an error analysis for SGBM. In section 3.5 we give a numerical comparison (accuracy and speed of computation) of different computation methods, including SGBM, SRM, and SRBM, via several multi-asset instruments. Section 3.6 concludes the presented approach by solving the credit exposure problem.

3.2 Model specification and different instruments

To get the sample results of E_t (or $V(t)$) on each state, one possibility is by using a simulation approach. We will use the modeling framework introduced in chapter 2. Assuming one has a model describing the stochastic process of risk factors $X(t)$, $0 \leq t \leq T$, then two basic steps are involved in the modelling framework:

1. Simulate the model under the real-world measure $\mathbb{P}$ to get the scenarios of risk factors $X(t)$, $t \in [0, T]$.
2. Evaluate the instrument price for each simulated state $(t, X(t))$.

To work under the modeling framework, we need to specify the model for the underlying asset prices. The exposure of different instruments will also be discussed in this section.

3.2.1 Multi-dimensional Models

Consider the exposure evaluation of exotic instruments with multi-dimensional underlying assets. For a derivative security with multiple underlying assets $\mathbf{S}_t = \left(S_t^1, ..., S_t^d\right)$, we assume that each asset price is driven by a geometric Brownian motion (GBM),

$$\frac{\mathrm{d}S_t^i}{S_t^i} = (r - q_i)\mathrm{d}t + \sigma_i \mathrm{d}W^i(t), \quad i = 1, ..., d, \tag{3.1}$$

where each asset pays a dividend at a continuous rate of q_i, r is the risk free interest rate, and σ_i are the volatility coefficients. The multi-dimensional process $\left(W^1(t), ..., W^d(t)\right)$ is d-dimensional Brownian motion under measure $\mathbb{Q}$. The instantaneous correlation coefficients between the increments W^i and W^j are $\rho_{i,j}$, $i, j = 1, ..., d$. The increment of this process for time interval Δt is joint normally distributed,

$$\left(W^1(\Delta t), ..., W^d(\Delta t)\right) = L\left(Z^1, ..., Z^d\right),$$

where $Z^1, ..., Z^d$ are independent standard normal random variables. $LL^\top = \Sigma$ is the Cholesky decomposition of the symmetric positive definite $d \times d$ matrix Σ, with $\Sigma_{i,j} = \rho_{i,j}\Delta t$, $i, j = 1, ..., d$.

The multi-dimensional model (3.1) admits analytical conditional moments of several functions of underlying assets S_t^i, such as $\left(\prod_{i=1}^d S_t^i\right)^{\frac{1}{d}}$ and $\frac{1}{d}\left(\sum_{i=1}^d S_t^i\right)$, which are used in the payoff functions of geometric and arithmetic basket options (see the following section). For some functions, such as $\max(S_t^1, ..., S_t^d)$, the Clark algorithm [23, 39], can be applied to calculate the first four exact moments of the maximum of a pair of jointly normal variables ($d = 2$). However, for $d \geq 3$, the Clark algorithm can only be used to approximate the moments of $\max(S_t^1, ..., S_t^d)$. These formulas of conditional moments are listed in table 3.1 and will be used in the application of the multi-dimensional model.

Remark 3.2.1. *For one-dimensional models, more general stochastic processes, such as the jump-diffusion model, can be found with analytical conditional moments. For high-dimensional models, since many random variables are involved (complicated cases including stochastic interest rate, stochastic volatility, etc.), the analytical conditional moments of functions of underlying assets may become very complicated or may not exist, for which one has to find an accurate approximation, then.*

3.2.2 Exposure of Different Instruments

To calculate the exposure on time interval $[0, T]$, we first set up the vector of *observation dates* as $\mathcal{T} = \{t_1, ..., t_M\}$, with $0 = t_0 \leq t_1$ and $t_M = T$, which are assumed to be equally spaced, $t_m - t_{m-1} = \Delta t, m = 1, ...M$. For an accurate computation of CVA, the observation dates should be dense enough (such as monthly or weekly).

Given the multi-dimensional model of the underlying assets, the exposure of a European option at time t_{m-1} can be calculated based on its option value $V_{t_{m-1}}(\mathbf{S}_{t_{m-1}})$,

$$\begin{aligned} V_{t_M}(\mathbf{S}_{t_M}) &= h(t_M, \mathbf{S}_{t_M}), \\ V_{t_{m-1}}(\mathbf{S}_{t_{m-1}}) &= \exp(-r\Delta t)\mathbb{E}^{\mathbb{Q}}\big[V_{t_m}(\mathbf{S}_{t_m})|\mathbf{S}_{t_{m-1}}\big], m = M, ..., 1, \end{aligned} \tag{3.2}$$

We assume a constant interest rate r, so $\exp(-r\Delta t)$ denotes the discount factor for time interval Δt. $h(t_M, \mathbf{S}_{t_M})$ is the non-negative payoff function at maturity time T. For basket options, the following three types of payoff functions are considered (geometric average, arithmetic average and max options),

$$\begin{aligned} h_1(t_M, \mathbf{S}_{t_M}) &= \big(K - (\prod_{i=1}^{d} S_{t_M}^i)^{\frac{1}{d}}\big)^+, \\ h_2(t_M, \mathbf{S}_{t_M}) &= \big(K - \frac{1}{d}(\sum_{i=1}^{d} S_{t_M}^i)\big)^+, \\ h_3(t_M, \mathbf{S}_{t_M}) &= \big(\max(S_{t_M}^1, ..., S_{t_M}^d) - K\big)^+, \end{aligned}$$

where K is the strike price.

Function $h(\cdot)$ can also be discontinuous. A typical example is a digital option, for which the payoff function at maturity reads (in the case of geometric basket put options),

$$h(t_M, \mathbf{S}_{t_M}) = \begin{cases} Q, & \left(\prod_{i=1}^{d} S_{t_M}^i\right)^{\frac{1}{d}} \leq K, \\ 0, & \left(\prod_{i=1}^{d} S_{t_M}^i\right)^{\frac{1}{d}} > K, \end{cases}$$

where Q is a constant amount received if the geometric average value of underlying assets finishes below the strike price. Another typical example is a gap option.

When the underlying asset is one-dimensional and also follows a GBM process, European vanilla options, digital options and gap options have analytical solutions for their option values (exposure) at the observation dates. However, if the underlying assets are multi-dimensional and the payoff function is basket type (such as arithmetic average or max options), even for European vanilla options with the underlying asset prices following a GBM process, the exposure has to be computed approximately [1].

A more complicated example is a Bermudan option. Recalling from chapter 2, the exposure of Bermudan options can be calculated by following a dynamic programming recursion:

$$V_{t_M}(\mathbf{S}_{t_M}) = h(t_M, \mathbf{S}_{t_M}), \tag{3.3}$$

$$c(t_{m-1}, \mathbf{S}_{t_{m-1}}) = \exp(-r\Delta t)\mathbb{E}^{\mathbb{Q}}\left[V_{t_m}(\mathbf{S}_{t_m})|\mathbf{S}_{t_{m-1}}\right], m = M, ..., 1, \tag{3.4}$$

$$V_{t_{m-1}}(\mathbf{S}_{t_{m-1}}) = \begin{cases} \max\{h(t_{m-1}, \mathbf{S}_{t_{m-1}}), c(t_{m-1}, \mathbf{S}_{t_{m-1}})\}, & \text{possible exercise date,} \\ c(t_{m-1}, \mathbf{S}_{t_{m-1}}), & \text{extra date,} \end{cases} \tag{3.5}$$

$$V_{t_0}(\mathbf{S}_{t_0}) = c(t_0, \mathbf{S}_{t_0}). \tag{3.6}$$

Remark 3.2.2. *The extra dates are the time grid points between two consecutive possible exercise dates. Since the observation dates should be dense enough (such as monthly or weekly) in exposure profiles and CVA calculation, we need more time grid points than possible Bermudan option exercise dates. Taking into account the extra dates significantly influences the results of Bermudan options' exposure profiles, which is illustrated in the numerical examples part of this chapter.*

Let $\mathbf{s}_{t_m}(p)$ be the realized value of random variable $\mathbf{S}_{t_m}$, i.e., the stock price at observation date t_m, on sample path p, $m = 1, ..., M$, $p = 1, ..., P$. For each path p, the earliest exercise time τ^p can be written as,

$$\tau^p = \min\{k \in \{1, ..., M\}|h(t_k, \mathbf{s}_{t_k}(p)) \geq c(t_k, \mathbf{s}_{t_k}(p))\}, \tag{3.7}$$

[1] In this model assumption, however, the geometric basket options can be priced via one dimensional BS formula [54].

where we simply set $h(t_k, \mathbf{s}_{t_k}(p)) = 0$ if time t_k is an extra date.

The exposure of the Bermudan option on path p is then obtained by setting the option value after τ^p to zero, which can be written as,

$$E^p_{t_m} = \begin{cases} \max(V_{t_m}(\mathbf{s}_{t_m}(p)), 0) & t_m \leq \tau^p, \\ 0 & t_m > \tau^p. \end{cases}$$

In the framework of American Monte Carlo methods, such as LSM, the stock price $\mathbf{S}_t$ is usually simulated under the risk-neutral measure $\mathbb{Q}$, which implies that the credit exposure distribution is generated under measure $\mathbb{Q}$, i.e., a $\mathbb{Q}$-exposure profile. However, in risk management, industries are more interested in exposure distribution under the real-world measure $\mathbb{P}$, i.e., a $\mathbb{P}$-exposure profile, because asset price processes evolve in the real-world measure $\mathbb{P}$ [22, 33, 37, 56]. In [22, 56], the authors use different strategies based on the change of measure method to get the $\mathbb{P}$-exposure profile, as explained in appendix 3.7.1. We discuss the difference of the $\mathbb{Q}$-exposure profile and $\mathbb{P}$-exposure profile in section 3.3.4.

3.3 Computation of Exposure Profiles for Multi-Asset Instruments

For multi-asset instruments (European or Bermudan), an efficient computation method is needed for the continuation value,

$$c(t_{m-1}, \mathbf{s}_{tm-1}(p)) = \exp(-r\Delta t)\mathbb{E}^{\mathbb{Q}}\big[V_{t_m}(\mathbf{S}_{t_m})|\mathbf{S}_{t_{m-1}} = \mathbf{s}_{t_{m-1}}(p)\big], \tag{3.8}$$

Based on the well known least squares approximation of conditional expectations [45], the *standard regression method* (SRM) is proposed in [31]. In SRM, the conditional expectation $\mathbb{E}^{\mathbb{Q}}[V_{t_m}(\mathbf{S}_{t_m}) \mid \mathbf{S}_{t_{m-1}}]$ is approximated as a linear combinations of *basis functions*, $\widetilde{f}_i : \mathbb{R}^d \to \mathbb{R}$, $i = 1, ..., K$,

$$\mathbb{E}^{\mathbb{Q}}[V_{t_m}(\mathbf{S}_{t_m}) \mid \mathbf{S}_{t_{m-1}}] \approx \beta^\top_{t_{m-1}} \widetilde{f}(\mathbf{S}_{t_{m-1}}),$$

where $\beta_{t_{m-1}} = (\beta_{t_{m-1}}(1), ..., \beta_{t_{m-1}}(K))^\top$ is a vector of constants, and $\widetilde{f} = (\widetilde{f}_1, ..., \widetilde{f}_K)^\top$. To minimize the *expected squared error* in the approximation w.r.t the coefficient $\beta_{t_{m-1}}$, we differentiate the expression

$$\mathbb{E}^{\mathbb{Q}}\big(\mathbb{E}^{\mathbb{Q}}[V_{t_m}(\mathbf{S}_{t_m}) \mid \mathbf{S}_{t_{m-1}}] - \beta^\top_{t_{m-1}} \widetilde{f}(\mathbf{S}_{t_{m-1}})\big)^2,$$

w.r.t. $\beta_{t_{m-1}}$ and set the result to zero. This gives us the solution [31],

$$\beta_{t_{m-1}} = \big(\mathbb{E}^{\mathbb{Q}}[\widetilde{f}(\mathbf{S}_{t_{m-1}})\widetilde{f}(\mathbf{S}_{t_{m-1}})^\top]\big)^{-1}\mathbb{E}^{\mathbb{Q}}[\widetilde{f}(\mathbf{S}_{t_{m-1}})V_{t_m}(\mathbf{S}_{t_m})].$$

The coefficient $\beta_{t_{m-1}}$ can be further estimated by Monte Carlo simulation. Starting with initial grid point $\mathbf{s}_{t_0}$, suppose we have generated P independent simulation paths $\mathbf{s}_{t_m}(p), m = 1, ..., M, p = 1, ..., P$. The $K \times K$ matrix $\mathbb{E}^{\mathbb{Q}}[\widetilde{f}(\mathbf{S}_{t_{m-1}})\widetilde{f}(\mathbf{S}_{t_{m-1}})^\top]$ can be approximated as

$$\frac{1}{P}\sum_{p=1}^{P}\widetilde{f}(\mathbf{s}_{t_{m-1}}(p))\widetilde{f}(\mathbf{s}_{t_{m-1}}(p))^\top,$$

and the K-vector $\mathbb{E}^{\mathbb{Q}}[\widetilde{f}(\mathbf{S}_{t_{m-1}})V_{t_m}(\mathbf{S}_{t_m})]$ can be approximated as

$$\frac{1}{P}\sum_{p=1}^{P}\widetilde{f}(\mathbf{s}_{t_{m-1}}(p))V_{t_m}(\mathbf{s}_{t_m}(p)),$$

where we assume that $V_{t_m}(\mathbf{s}_{t_m}(p))$, $p = 1, ..., P$, is known (or it has been estimated). The least squares estimation of $\beta_{t_{m-1}}$ reads,

$$\widehat{\beta}_{t_{m-1}} = \Big(\sum_{p=1}^{P}\widetilde{f}(\mathbf{s}_{t_{m-1}}(p))\widetilde{f}(\mathbf{s}_{t_{m-1}}(p))^\top\Big)^{-1}\sum_{p=1}^{P}\widetilde{f}(\mathbf{s}_{t_{m-1}}(p))V_{t_m}(\mathbf{s}_{t_m}(p)), \quad (3.9)$$

and the least squares approximation of $\mathbb{E}^{\mathbb{Q}}[V_{t_m}(\mathbf{S}_{t_m}) \mid \mathbf{S}_{t_{m-1}}]$ reads,

$$\mathbb{E}^{\mathbb{Q}}[V_{t_m}(\mathbf{S}_{t_m}) \mid \mathbf{S}_{t_{m-1}}] \approx \widehat{\beta}_{t_{m-1}}^\top \widetilde{f}(\mathbf{S}_{t_{m-1}}).$$

Generally, the following SRM algorithm can be used for the exposure calculation of multi-asset instruments (European and Bermudan type),

1. Simulate sample paths for the underlying assets, $\mathbf{s}_{t_0}(p), ..., \mathbf{s}_{t_M}(p)$, at time steps $0 = t_0, ..., t_M = T$, with indices of paths $p = 1, ..., P$, under the risk-neutral measure $\mathbb{Q}$.
2. At terminal nodes, set $V_{t_M}(\mathbf{s}_{t_M}(p)) = h(t_M, \mathbf{s}_{t_M}(p))$.
3. Apply backward induction, for $m = M - 1, ..., 1$:
   - Given values $V_{t_{m+1}}(\mathbf{s}_{t_{m+1}}(p))$, $p = 1, ..., P$, use least squares regression to estimate the continuation value, $c(t_m, \mathbf{s}_{t_m}(p))$, $p = 1, ..., P$.
   - – If t_m is a possible exercise date (see remark 3.2.2 for an explanation of the distinction between possible exercise date and extra date.), set

     $$V_{t_m}(\mathbf{s}_{t_m}(p)) = \max\big(h(t_m, \mathbf{s}_{t_m}(p)), c(t_m, \mathbf{s}_{t_m}(p))\big).$$

     For exposure calculation, if $h(t_m, \mathbf{s}_{t_m}(p)) > c(t_m, \mathbf{s}_{t_m}(p))$, set

     $$V_{t_{m+1}}(\mathbf{s}_{t_{m+1}}(p)) = 0, ..., V_{t_M}(\mathbf{s}_{t_M}(p)) = 0.$$

  - If t_m is an extra date, set $V_{t_m}(\mathbf{s}_{t_m}(p)) = c(t_m, \mathbf{s}_{t_m}(p))$.

4. Set $V_{t_0}(\mathbf{s}_{t_0}) = \big(V_{t_1}(\mathbf{s}_{t_1}(1)) + ... + V_{t_M}(\mathbf{s}_{t_1}(P))\big)/P$; set $E^p_{t_m} = \max(V_{t_m}(\mathbf{s}_{t_m}(p), 0)$, $m = 0, 1, ..., M, p = 1, ..., P$.

Remark 3.3.1. *In implementation, since the true value of $V_{t_{m+1}}(\mathbf{s}_{t_{m+1}}(p))$ is unknown, it has to be replaced by estimated values [31].*

Remark 3.3.2. *For ease of comparison, all of the exposure algorithms in this section are presented under the risk neutral measure. To get the exposure profiles under the real world measure, two possible methods can be used: (i) Based on the $\mathbb{Q}$-probability distribution of $E^p_{t_m}$ (i.e., approximated by the empirical distribution of samples obtained from the algorithm.), the $\mathbb{P}$-probability distribution of $E^p_{t_m}$ can be estimated by using change of measure [22]. (ii), the risk factors have to be simulated under the measure $\mathbb{P}$ instead of $\mathbb{Q}$, and the continuation value has to be calculated under the measure $\mathbb{P}$ instead of $\mathbb{Q}$, by using change of measure [56]. A short review is given in the appendix 3.7.1 for these methods.*

To obtain an efficient computation of the exposure profiles, one has to have an accurate result for the option value at time t_m, $m = 0, \ldots, M$, not only at time t_0. Particularly, in SRM, when the dimension of problem increases, it could become problematic to obtain accurate exposure profiles because of the following observations:

1. The computation may become inefficient since lots of basis functions are required in an accurate regression. The problem becomes more involved when the payoffs is non-smooth or discontinuous.

2. The SRM suggests a regression to the whole data set. This may generate a bigger approximation error, compared with more sophisticated regression methods, such as localized regression.

Before making an improvement of SRM, we first give a short review of several related attempts in the literature. In Glasserman and Yu (2004), the regression method of SRM is termed as 'regression now', because the basis functions are chosen at t_{m-1} instead of t_m. Another regression method, for which the basis functions are chosen at t_m, is termed as 'regression later'. Through theoretical analysis, Glasserman and Yu (2004) [32] prove that the 'regression later' technique has two attractive features: under appropriate conditions, (i) it results in less-dispersed estimates, and (ii) it provides a dual estimate (an upper bound) with modest additional effort. Note that these features are based on using *martingale basis functions*, i.e., in their comparison study, they impose martingale property to the basis functions,

$$\mathbb{E}^{\mathbb{Q}}[f(\mathbf{S}_{t_m}) \mid \mathbf{S}_{t_{m-1}}] = f(\mathbf{S}_{t_{m-1}}), m = 1, \ldots, M,$$

thus it is not a comparison for a general set of basis functions. Based on the work of Glasserman and Yu (2004), in Firth (2005) [29], the author gives a general formula of martingale basis functions under the one-dimensional GBM model. This is applied in several numerical experiments to compare the results of regression now and later. The results indicates that 'regression later' gives more accurate option price estimates than 'regression now'. Based on these literature conclusions, it is natural to consider the advantages and disadvantages of 'regression later' compared with 'regression now' when the choice of basis functions is not as restrictive as the martingale basis functions requirement.

Another direction to reduce the regression error is by using localized regression, i.e., regressing on part of the data set instead of the whole data set. A typical example is to use a bundling technique to partition the state space [60]. In Fries (2007) [30], it is referred to as 'binning'. Intuitively, when the data set is partitioned into different small groups, one could expect that the regression in a group will generally become better.

In the following sections, we focus on a numerical comparison of different computation methods, particularly, for the purpose of multi-asset exposure profiles computation. A method of combining the 'regression later' technique with bundling, which is called *Stochastic Grid Bundling Method* (SGBM), can be found in Jain and Oosterlee (2013) [39]. To give a comparison, we also propose another method, named *Standard Regression Bundling Method* (SRBM), in which a 'regression now' technique is combined with bundling. A similar method can be found in [22]. A theoretical analysis of the comparison is put to future work.

3.3.1 Option Value Approximation via Regression Later

In contrast to SRM ('regression now'), the approximation of $\mathbb{E}^{\mathbb{Q}}[V_{t_m}(\mathbf{S}_{t_m}) \mid \mathbf{S}_{t_{m-1}}]$ in SGBM ('regression later') starts with approximating the option value $V_{t_m}(\mathbf{S}_{t_m})$ as linear combination of *basis functions* $f_i : \mathbb{R}^d \to \mathbb{R}$, $i = 1, ..., K$,

$$V_{t_m}(\mathbf{S}_{t_m}) \approx \alpha_{t_m}^{\top} f(\mathbf{S}_{t_m}),$$

where $\alpha_{t_m} = (\alpha_{t_m}(1), ..., \alpha_{t_m}(K))^{\top}$ is a vector of constants, and $f = (f_1, ..., f_K)^{\top}$. By using the same methodology as SRM, the coefficient α_{t_m} can be estimated by generating P independent simulation paths $\mathbf{s}_{t_m}(p)$, $m = 1, ..., M, p = 1, ..., P$, starting from an initial grid point $\mathbf{s}_{t_0}$,

$$\widehat{\alpha}_{t_m} = \big(\sum_{p=1}^{P} f(\mathbf{s}_{t_m}(p)) f(\mathbf{s}_{t_m}(p))^{\top}\big)^{-1} \sum_{p=1}^{P} f(\mathbf{s}_{t_m}(p)) V_{t_m}(\mathbf{s}_{t_m}(p)), \tag{3.10}$$

where we assume that $V_{t_m}(\mathbf{s}_{t_m}(p))$ is known or has been estimated. The least squares approximation of $V_{t_m}(\mathbf{S}_{t_m})$ reads,

$$V_{t_m}(\mathbf{S}_{t_m}) \approx \widehat{\alpha}_{t_m}^{\top} f(\mathbf{S}_{t_m}),$$

$f_k(\mathbf{S}_{t_m})$, $\mathbf{S}_{t_m} = (S^1_{t_m}, ..., S^d_{t_m})$, $k \geq 1$	$\mathbb{E}^{\mathbb{Q}}[f_k(\mathbf{S}_{t_m}) \mid \mathbf{S}_{t_{m-1}} = \mathbf{s}_{t_{m-1}}(p)]$
$\left(S^i_{t_m}\right)^{k-1}$	$\left(s^i_{t_{m-1}}(p)\exp((r_i + \frac{k-2}{2}\sigma_i^2)\Delta t)\right)^{k-1}$
$\left((\prod_{i=1}^d S^i_{t_m})^{\frac{1}{d}}\right)^{k-1}$	$\left((\prod_{i=1}^d s^i_{t_{m-1}}(p))^{\frac{1}{d}}\exp((\widehat{\mu} + \frac{k-1}{2}\widehat{\sigma}^2)\Delta t)\right)^{k-1}$
$\left(\frac{1}{d}\sum_{i=1}^d S^i_{t_m}\right)^{k-1}$	$\frac{1}{d^{k-1}} \sum_{k_1+...+k_d=k-1} \binom{k-1}{k_1, ..., k_d}$ $\times \mathbb{E}^{\mathbb{Q}}[\prod_{1\leq i\leq d}(S^i_{t_m})^{k_i}) \mid \mathbf{S}_{t_{m-1}} = \mathbf{s}_{t_{m-1}}(p)]$
$\left(\log(\max(S^1_{t_m}, ..., S^d_{t_m}))\right)^{k-1}$	Clark's algorithm

Table 3.1: Basis functions and the corresponding conditional expectations [39]. Each asset price S^i_t is driven by a geometric Brownian motion, with the model assumptions in section 3.2.1. Here: $\widehat{\mu} = \frac{1}{d}\sum_{i=1}^d(r - q_i - \frac{\sigma_i^2}{2})$, $\widehat{\sigma} = \sqrt{\frac{1}{d^2}\sum_{j=1}^d\sum_{k=1}^d \rho_{j,k}\sigma_j\sigma_k}$. The expression $\mathbb{E}^{\mathbb{Q}}[\prod_{1\leq i\leq d}(S^i_{t_m})^{k_i}) \mid \mathbf{S}_{t_{m-1}} = \mathbf{s}_{t_{m-1}}(p)]$ can be seen as the moments of the geometric average of the assets, as listed in the third row.

and the conditional expectation will be approximated as,

$$\mathbb{E}^{\mathbb{Q}}[V_{t_m}(\mathbf{S}_{t_m}) \mid \mathbf{S}_{t_{m-1}}] \approx \widehat{\alpha}_{t_m}^{\top}\mathbb{E}^{\mathbb{Q}}[f(\mathbf{S}_{t_m}) \mid \mathbf{S}_{t_{m-1}}]. \tag{3.11}$$

The last expression enables us to reduce the calculation problem into the computation of conditional expectations of basis functions. Note that a similar expression can be found in Glasserman and Yu (2004), in which the authors show that a weighted Monte Carlo technique for American option pricing problem developed by Broadie, Glasserman, and Ha (2000) (BGH) [13] is equivalent to the regression later method. More precisely, proposition 2 in [32] shows that the conditional expectation estimator of BGH admits the representation (3.11).

While in Glasserman and Yu (2004) and Firth (2005), the authors impose the martingale property to the basis functions $f(\mathbf{S}_{t_m})$, in our comparison study, we restrict the choice of basis functions such that the expression $\mathbb{E}^{\mathbb{Q}}[f(\mathbf{S}_{t_m}) \mid \mathbf{S}_{t_{m-1}}]$ has an *analytical formula or approximation formula*. This condition makes the choice of basis functions more flexible than martingale basis functions, especially in high-dimensional problems. In table 3.1, we list the basis functions and the corresponding formulas of conditional expectations which are used frequently in the later numerical comparison study.

3.3.2 Bundling Methods

In order to get an accurate computation of

$$\mathbb{E}^{\mathbb{Q}}[V_{t_m}(\mathbf{S}_{t_m}) \mid \mathbf{S}_{t_{m-1}} = \mathbf{s}_{t_{m-1}}(p)],$$

for which the integration representation can be written as

$$\int_{\mathbb{R}^d} V_{t_m}(x)\mathbb{Q}[\mathbf{S}_{t_m} \in \mathbf{d}x \mid \mathbf{S}_{t_{m-1}} = \mathbf{s}_{t_{m-1}}(p)], \tag{3.12}$$

one has to find a regression approximation of $V_{t_m}(\mathbf{S}_{t_m})$ as accurate as possible for the region where $\mathbf{S}_{t_m}$ has 'most' probability mass, originating from the grid point $\mathbf{s}_{t_{m-1}}(p)$. Given a set of basis functions, this is equivalent to getting an accurate estimate of the regression coefficient $\widehat{\alpha}_{t_m}$ in SGBM (or $\widehat{\beta}_{t_{m-1}}$ in SRM).

However, the estimation formulas of $\widehat{\alpha}_{t_m}$ (and $\widehat{\beta}_{t_{m-1}}$) given in the last section are based on a Monte Carlo simulation starting from *initial grid point* $\mathbf{s}_{t_0}$, not from $\mathbf{s}_{t_{m-1}}(p)$. These coefficient estimations may generate significant error in the computation of the conditional expectation $\mathbb{E}^{\mathbb{Q}}[V_{t_m}(\mathbf{S}_{t_m}) \mid \mathbf{S}_{t_{m-1}} = \mathbf{s}_{t_{m-1}}(p)]$.

One observation is that the probability distribution of grid points originally from grid point $\mathbf{s}_{t_{m-1}}(p)$ can be approximated by the probability distribution of grid points originating from the 'neighbourhood' of $\mathbf{s}_{t_{m-1}}(p)$ (see figure 3.1). Intuitively, since the grid points in the neighbourhood of $\mathbf{s}_{t_{m-1}}(p)$ are close to each other, grid points $\mathbf{S}_{t_m}$, which are originally from different grid points in the neighborhood of $\mathbf{s}_{t_{m-1}}(p)$, can be approximated as being from the same origin.

Based on this observation, in the calculation of $\mathbb{E}^{\mathbb{Q}}\left[V_{t_m}(\mathbf{S}_{t_m})|\mathbf{S}_{t_{m-1}} = \mathbf{s}_{t_{m-1}}(p)\right]$, we use the option value $V_{t_m}(\mathbf{S}_{t_m})$ on the grid points originating from the 'neighbourhood' of $\mathbf{s}_{t_{m-1}}(p)$ to find a regression approximation of function form of $V_{t_m}(\mathbf{S}_{t_m})$ (or the coefficient $\widehat{\alpha}_{t_m}$), which we call 'localized regression'. By separately considering the points that originate from the 'neighbourhood' of $\mathbf{s}_{t_{m-1}}(p)$, intuitively the regression is forced to be precise around values for $V_{t_m}(\mathbf{S}_{t_m})$ where the conditional density,

$$\mathbb{Q}\left[\mathbf{S}_{t_m} \in \mathbf{d}x \mid \mathbf{S}_{t_{m-1}} = \mathbf{s}_{t_{m-1}}(p)\right],$$

has most of its probability mass.

In order to define the 'neighbourhood' of $\mathbf{s}_{t_{m-1}}(p)$, we apply the bundling method. Bundling is a method to partition the state space into non-overlapping regions, so that any point in the space can be identified to lie in exactly one of the regions, see [22, 39, 41, 60]. If we denote the 'neighbourhood' of $\mathbf{s}_{t_{m-1}}(p)$ as bundle $\mathcal{B}^h_{m-1}$, where $h = 1, ..., H$ represent the indices of the bundles, then $\mathbf{s}_{t_{m-1}}(p) \in \mathcal{B}^h_{m-1}$.

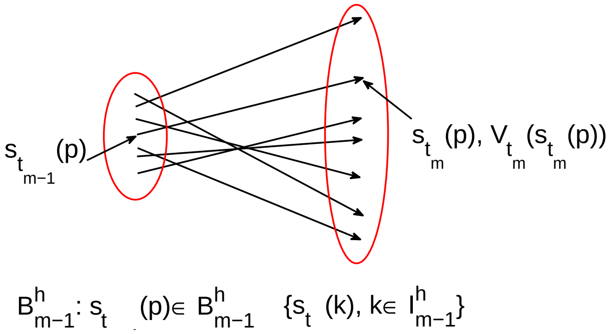

Figure 3.1: Paths $S_{t_m}(p)$ are originally from bundle $\mathcal{B}^h_{m-1}$; I^h_{m-1} is the set of path indices in bundle $\mathcal{B}^h_{m-1}$.

To explain the method, we take a two-dimensional example, i.e., $\mathbf{S}_t = (S^1_t, S^2_t)$. Suppose we want to bundle P grid points $\mathbf{s}_{t_m}(p) = (s^1_{t_m}(p), s^2_{t_m}(p))$, $p = 1, 2, .., P$ at time step t_m for some $m = 1, ..., M$. The following steps need to be performed recursively.

1. Estimate the mean value for each stock at time t_m, i.e.,

$$\hat{\mu}^i_m = \frac{1}{P}\sum_{p=1}^{P} s^i_{t_m}(p), i = 1, 2.$$

2. Define the following subsets of grid points:

$$G^i_m = \left\{\mathbf{s}_{t_m}(p) : s^i_{t_m}(p) > \hat{\mu}^i_m\right\}, \qquad \overline{G}^i_m = \{\mathbf{s}_{t_m}(p) : \mathbf{s}_{t_m}(p) \notin G_i\}$$

3. Four (i.e., 2^2) unique bundles are obtained through combinations of different groups, i.e.,

$$\begin{aligned} \mathcal{B}^1_m &= G^1_m \cap G^2_m, & \mathcal{B}^2_m &= \overline{G}^1_m \cap G^2_m, \\ \mathcal{B}^3_m &= G^1_m \cap \overline{G}^2_m, & \mathcal{B}^4_m &= \overline{G}^1_m \cap \overline{G}^2_m. \end{aligned}$$

4. If more bundles are required, the same procedure, from (1) to (3), can be performed, either for each bundles, $\mathcal{B}^1_m, ..., \mathcal{B}^4_m$ or some of them.

The number of partitions, or bundles, after q iterations, where each of the bundles is involved, would be equal to 4^q (i.e., in the case of 2 assets).

Remark 3.3.3. *The approach described above could be problematic when some of the subsets do not have enough grid points or even become empty because of the probability distribution of the grid points; it will also become computationally expensive for high-dimensional problems, since the number of bundles obtained after each iteration would be very large. Rather than partitioning the actual state space, an alternative method is to bundle the grid points on a* dimensionally reduced state space *[3, 39]. A mapping function, such as (in the case of geometric average, arithmetic average and max option, for example.)*

$$
\begin{aligned}
g_1(t, \mathbf{S}_t) &= \big(\prod_{i=1}^{d} S_t^i\big)^{\frac{1}{d}},\\
g_2(t, \mathbf{S}_t) &= \frac{1}{d}\big(\sum_{i=1}^{d} S_t^i\big),\\
g_3(t, \mathbf{S}_t) &= \max(S_t^1, ..., S_t^d),
\end{aligned}
$$

can be used to map the d-asset state space into a one-dimensional state space. The same bundling scheme of the two asset example (or generally for d-dimensional case) above can be applied now into the one-dimensional case (i.e., function $g(\cdot)$), and the number of bundles obtained after q iterations will be 2^q. We give an example of this bundling method on the dimensionally reduced state space via the numerical example of max options with five stocks.

Assuming that the state space at t_{m-1} has been partitioned into H distinct bundles, $\mathcal{B}^h_{m-1}$, $h = 1, ..., H$. For the grid points $\mathbf{s}_{t_{m-1}}(p) \in \mathcal{B}^h_{m-1}$, the continuation value can be written as

$$
c^h(t_{m-1}, \mathbf{s}_{t_{m-1}}(p)) \approx \exp(-r\Delta t)\mathbb{E}^{\mathbb{Q}}\big[f(\mathbf{S}_{t_m})^\top \widehat{\alpha}^h_{t_m} | \mathbf{S}_{t_{m-1}} = \mathbf{s}_{t_{m-1}}(p)\big]. \tag{3.13}
$$

Here $\widehat{\alpha}^h_{t_m}$ represents the coefficients estimated by using formula (3.10), based on observations of pairs

$$
\big(\mathbf{s}_{t_m}(p), V_{t_m}(\mathbf{s}_{t_m}(p))\big), p = 1, ..., P,
$$

for which $\mathbf{s}_{t_m}(p)$ is the consecutive grid point of $\mathbf{s}_{t_{m-1}}(p) \in \mathcal{B}^h_{m-1}$. We can also write it as, for a general grid point $\mathbf{s}_{t_{m-1}}(p)$,

$$
c(t_{m-1}, \mathbf{s}_{t_{m-1}}(p)) \approx \exp(-r\Delta t)\mathbb{E}^{\mathbb{Q}}\big[\sum_{h=1}^{H} \mathbf{1}_{\mathbf{s}_{t_{m-1}}(p)\in\mathcal{B}^h_{m-1}}\big(f(\mathbf{S}_{t_m})^\top \widehat{\alpha}^h_{t_m}\big)|\mathbf{S}_{t_{m-1}} = \mathbf{s}_{t_{m-1}}(p)\big].
$$

3.3.3 Algorithm

In summary, the SGBM algorithm [39] for exposure of multi-asset instruments (European and Bermudan type) reads,

1. Simulate sample paths for the stock price, $\mathbf{s}_{t_0}, \mathbf{s}_{t_1}(p), ..., \mathbf{s}_{t_M}(p)$, at time steps $0 = t_0, ..., t_M = T$, with indices of paths $p = 1, ..., P$, under the risk-neutral measure $\mathbb{Q}$.

2. At terminal date $t_M = T$, set

$$V_{t_M}(\mathbf{s}_{t_M}(p)) = h(t_M, \mathbf{s}_{t_M}(p)),$$

for $p = 1, ..., P$.

3. Apply backward induction, i.e., $m \to m-1$ for $m = M, ..., 1$.

   (a) i. Bundle the grid points at t_{m-1}, into H distinct bundles (except at t_0, where there is only one grid point.), using the bundling algorithm in section 3.3.2.

   ii. For each bundle $\mathcal{B}^h_{m-1}$, calculate the option value approximation,

$$f(\mathbf{S}_{t_m})^\top \widehat{\alpha}^h_{t_m}.$$

   iii. For each grid point $\mathbf{s}_{t_{m-1}}(p) \in \mathcal{B}^h_{m-1}$, calculate the continuation value,

$$c^h(t_{m-1}, \mathbf{s}_{t_{m-1}}(p)) \approx \exp(-r\Delta t)\mathbb{E}^{\mathbb{Q}}\left[f(\mathbf{S}_{t_m})^\top \widehat{\alpha}^h_{t_m} | \mathbf{S}_{t_{m-1}} = \mathbf{s}_{t_{m-1}}(p)\right].$$

   (b) For each sample path $p = 1, ..., P$,

   - If t_{m-1} is a possible exercise date, set

$$V_{t_{m-1}}(\mathbf{s}_{t_{m-1}}(p)) = \max(h(t_{m-1}, \mathbf{s}_{t_{m-1}}(p)), c(t_{m-1}, \mathbf{s}_{t_{m-1}}(p)));$$

   if $h(t_{m-1}, \mathbf{s}_{t_{m-1}}(p)) > c(t_{m-1}, \mathbf{s}_{t_{m-1}}(p))$, set

$$V_{t_m}(\mathbf{s}_{t_m}(p)) = 0, V_{t_{m+1}}(\mathbf{s}_{t_{m+1}}(p)) = 0, ..., V_{t_M}(\mathbf{s}_{t_M}(p)) = 0.$$

   - If t_{m-1} is an extra date, set

$$V_{t_{m-1}}(\mathbf{s}_{t_{m-1}}(p)) = c(t_{m-1}, \mathbf{s}_{t_{m-1}}(p)).$$

4. The initial option price reads $V_{t_0}(\mathbf{s}_{t_0}) = c(0, \mathbf{s}_0)$ (exercise is not allowed at t_0.).

5. The exposure for each grid point reads $E^p_{t_m} = \max(V_{t_m}(\mathbf{s}_{t_m}(p)), 0)$.

Following the methodology above, the *standard regression bundling method* (SRBM) ('regression now'), which combines the bundling method and SRM, can also be applied for the computation of exposure profiles. In SRBM, similar as SGBM, for the grid points $\mathbf{s}_{t_{m-1}}(p) \in \mathcal{B}^h_{m-1}$, the continuation value can be written as

$$c^h(t_{m-1}, \mathbf{s}_{t_{m-1}}(p)) \approx \exp(-r\Delta t)\widetilde{f}(\mathbf{S}_{t_{m-1}})^\top \widehat{\beta}^h_{t_{m-1}}. \tag{3.14}$$

Here $\widehat{\beta}^h_{t_{m-1}}$ is the coefficients estimated by using formula (3.9), based on observations of pairs

$$\left(\mathbf{s}_{t_{m-1}}(p), V_{t_m}(\mathbf{s}_{t_m}(p))\right), p = 1, ..., P,$$

for which $\mathbf{s}_{t_m}(p)$ is the consecutive grid point of $\mathbf{s}_{t_{m-1}}(p) \in \mathcal{B}^h_{m-1}$.

In the numerical example part, we will call $V_{t_0}(\mathbf{s}_{t_0})$ the *direct estimator* of the initial option price; another estimator of the initial option price, which is obtained based on simulating a new set of paths and finding the optimal exercise policy, is called *path estimator* $\underline{V_{t_0}}(\mathbf{s}_{t_0})$ [12, 39]. These two estimators are used in the efficiency comparison of SRM, SGBM, and SRBM.

3.3.4 Examples of Single Asset Options

An example of single asset Bermudan options was already given in chapter 2, in which we have already looked at the difference of the $\mathbb{Q}$-exposure and $\mathbb{P}$-exposure profiles.

The difference between the $\mathbb{Q}$-exposure and $\mathbb{P}$-exposure profiles of the European put option is illustrated in figure 3.2. In this example we assume that $\mu > r$. With this condition, at each time step t, the stock price S_t simulated under measure $\mathbb{P}$ tends to be higher than S_t simulated under measure $\mathbb{Q}$. For a European put option issued at time t, with maturity T and initial stock price S_t, a higher initial stock price S_t (i.e., simulated under measure $\mathbb{P}$) leads to a lower option price, thus a lower $\mathbb{P}$-exposure profile. Particularly, in this example, we observe that $\mathbb{P}$-EE_t decreases w.r.t t, and $\mathbb{Q}$-EE_t increases w.r.t t.

In the situation of discontinuous payoffs, such as digital options and gap options, because many basis functions are needed for an accurate regression, the regression-based methods (including SGBM, SRBM, SRM, LSM) may be problematic. However, for the simple cases, increasing the number of bundles is helpful to get an accurate and stable result of PFE and EE. In figure 3.3a and figure 3.3b, we show the PFE generated by SGBM with different strike prices K in the case of one-dimensional European type digital put options.

Recalling that the payoff function at maturity reads,

$$h(t_M, \mathbf{S}_{t_M}) = \begin{cases} Q, & S_{t_M} \leq K, \\ 0, & S_{t_M} > K, \end{cases}$$

where Q is a constant amount received if S_{t_M} is below the strike price K. Note that in this case an analytical solution exists for the option price. Because the

Method	$K = 25$	$K = 30$
SGBM (direct est.)	0.2023 (0.0039)	1.9091 (0.0085)
Analytical solution	0.2029	1.9087

Table 3.2: Comparison of digital put option price with different strike prices. Parameters: $Q = 40$, $s_0 = 40$, $r = 0.06$, $q = 0$, $T = 1$, $\sigma = 0.2$, observation dates =12, number of bundles=32. The numbers in the parentheses are the standard deviation of estimates.

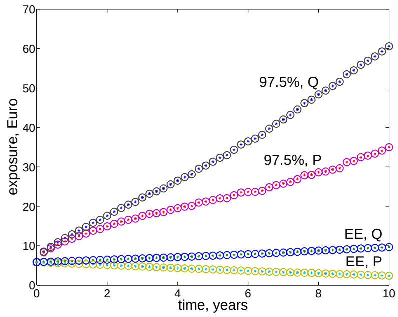

Figure 3.2: European put option, single asset, by SGBM (o) with 16 bundles and BS formula(*). Parameters: $s_0 = 100$, $K = 100$, $r = 0.05$, real world drift $\mu = 0.1$, $\sigma = 0.2$, $T = 10$.

digital option's payoff at maturity depends on the comparison of S_{t_M} and K, the PFE and EE can change substantially when choosing two different strike prices (for example, $K = 25$ in figure 3.3a and $K = 30$ in figure 3.3b). With $K = 25$, since the probability of $S_{t_M} > K$ is high, the payoffs at t_M on most of the simulation paths are equal to zero and the 97.5% PFE at t_M is zero. With $K = 30$, since the probability of $S_{t_M} > K$ becomes lower, the payoffs at maturity on some of the simulation paths are equal to Q and the 97.5% PFE at maturity t_M becomes Q ($Q = 40$ in the example). Compared with the analytical results, with 32 bundles, the results from SGBM are quite accurate and stable. The results of option prices can be seen from table 3.2.

3.3.5 Discontinuity On the Bundle Boundaries

Consider a grid point $\mathrm{s}_{t_{m-1}}(p)$ which crosses the boundary of two consecutive bundles $\mathcal{B}^h_{m-1}$ and $\mathcal{B}^{h+1}_{m-1}$, $h = 1, ..., H$. In the implementation of the bundling

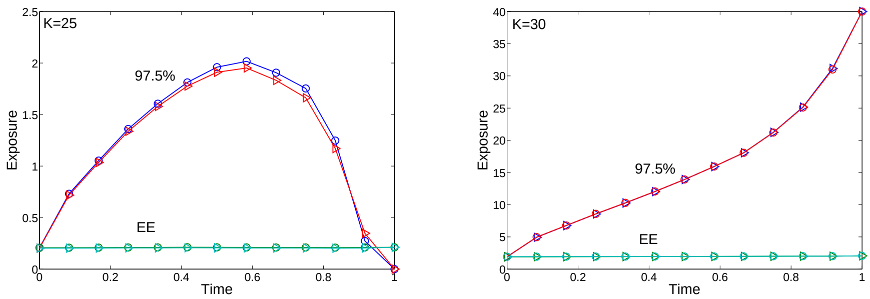

(a) (b)

Figure 3.3: European digital put options, by SGBM (o) and analytical solution ($\triangle$). In SGBM, 32 bundles are used. In all of the examples, 100000 simulation paths are generated to get the profiles. (A) Strike price $K = 25$. (B) Strike price $K = 30$. The other parameters can be found in the caption of table 3.2.

technique, the bundles do not overlap. In order to investigate the property of grid points at the boundaries, here we assume that $\mathcal{B}^h_{m-1} \cap \mathcal{B}^{h+1}_{m-1} = \{\mathbf{s}_{t_{m-1}}(p)\}$.

According to equation (3.13), in bundle $\mathcal{B}^h_{m-1}$, the continuation value

$$c(t_{m-1}, \mathbf{s}_{t_{m-1}}(p))$$

can be approximated as

$$\exp(-r\Delta t)\mathbb{E}^{\mathbb{Q}}[f(\mathbf{S}_{t_m})^\top \widehat{\alpha}^h_{t_m} \mid \mathbf{S}_{t_{m-1}} = \mathbf{s}_{t_{m-1}}(p)],$$

while in bundle $\mathcal{B}^{h+1}_{m-1}$ it can be approximated as

$$\exp(-r\Delta t)\mathbb{E}^{\mathbb{Q}}[f(\mathbf{S}_{t_m})^\top \widehat{\alpha}^{h+1}_{t_m} \mid \mathbf{S}_{t_{m-1}} = \mathbf{s}_{t_{m-1}}(p)].$$

Apparently the difference of coefficients $\widehat{\alpha}^h_{t_m}$ and $\widehat{\alpha}^{h+1}_{t_m}$ will lead to a discontinuity of $c(t_{m-1}, \mathbf{S}_{t_{m-1}})$ at grid point $\mathbf{s}_{t_{m-1}}(p)$, which could make difference in the exposure distribution and risk profiles.

The discontinuity of continuation value at the boundary is illustrated via numerical experiments in tables 3.4 and 3.5. The example is taken from single asset European type digital put options, for which we consider the option price (it is equivalent to the continuation value in the case of European type options) at time step $t = 0.75$ and the parameters are taken from table 3.3. In the example, the basis functions are specified as $f_k(S_{t_m}) = (S_{t_m})^{k-1}, k = 1, 2, 3, 4$.

In table 3.4, the state space is partitioned by two bundles (one boundary). The number in the table is the *mean absolute value of the difference* between two option price estimates on the same boundary, which is based on 500 independent simulation trials, i.e., if we denote V_1 and V_2 to be two different option

$s_0 = 40$	$K = 25$	$r = 0.06$	$q = 0$
$\sigma = 0.6$	$T = 1$	observation dates $= 12$	$Q = 40$

Table 3.3

price estimates for the same grid point on the boundary, then the *mean absolute value of the difference* reads,

$$\frac{1}{500}\sum_{i=1}^{500} \mid V_1(i) - V_2(i) \mid,$$

where i denotes different simulation trials. With the same number of simulation paths, the discontinuity of SGBM is less than of SRBM. If we increase the number of simulation paths, in the case of two bundles, the discontinuity does not decrease.

In table 3.5, the number of bundles increases to four (three boundaries). Compared with the results of two bundles from table 3.4, both for SGBM and SRBM the discontinuity decreases significantly. If we increase the number of simulation paths, the discontinuity decreases. With the same number of simulation paths, the discontinuity of SGBM is generally smaller than of SRBM. Though it is risky to extrapolate from limited numerical results, this example suggests that using enough simulation paths and bundles, especially for SGBM, the discontinuity at the boundaries can become very small.

In figures 3.4a and 3.4b, by using SGBM, we give a histogram of the difference between two different option price estimates for the same grid point on the boundary, based on 500 independent simulation trials at time step $t = 0.75$. In figure 3.4a two bundles (one boundary) are used, while in figure 3.4b four bundles (three boundaries) are used. From these two figures, we see that increasing the number of bundles can significantly decrease the differences.

3.4 Benchmark

To analyse the reliability of the SGBM method, we employ the Monte Carlo-COS method (MCCOS) to benchmark the exposure profile of the Bermudan option under the GBM model. The algorithm is explained in chapter 2.

There are three main components in MCCOS for exposure profile calculation:

Method	6000 paths	60000 paths	120000 paths
SGBM	0.9435	1.0615	1.0900
SRBM	2.4941	2.6396	2.6673

Table 3.4: Two bundles (one boundary), at time step $t = 0.75$. The numbers are the *mean absolute value of the difference* between two different option price estimates for the same grid point on the boundary, which is based on 500 independent simulation trials. Different numbers of simulation paths are used to compare the performance of both SGBM and SRBM. For each comparison, the same number of basis functions is used in SGBM and SRBM. Since the grid point at the boundary will change if we use different number of simulation paths, the option value at the boundary is around 4.88.

Method	6000 paths	60000 paths	120000 paths
SGBM	$(0.0747, 0.0506, 0.0821)$	$(0.0344, 0.0181, 0.1021)$	$(0.0316, 0.0135, 0.1080)$
SRBM	$(0.9701, 0.7534, 0.1680)$	$(0.4882, 0.2262, 0.1373)$	$(0.4617, 0.1736, 0.1358)$

Table 3.5: Four bundles (boundary I, II and III), at time step $t = 0.75$. The vector of numbers in parentheses are the *mean absolute value of the difference* between two different option price estimates for the same grid point on boundary I, II and III, which is based on 500 independent simulation trials. Different numbers of simulation paths are used to compare the performance of both SGBM and SRBM. For each comparison, the same number of basis functions is used in SGBM and SRBM. The option values at boundaries I, II, III are around 19.56, 4.80, and 0.36, respectively.

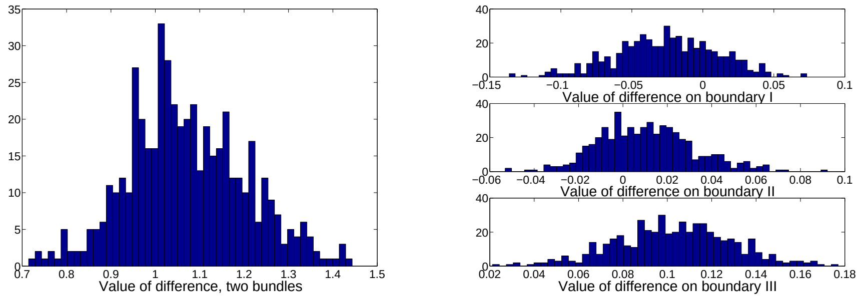

(a) Two bundles in SGBM

(b) Four bundles in SGBM

Figure 3.4: The distribution (histogram) of the difference between two different option price estimates for the same grid point on the boundary by SGBM at time step $t = 0.75$, based on 500 independent simulation trials. For each simulation trial, 60000 simulation paths are used to get the PFE and option price. (A), the option value at the boundary is around 4.88. (B), the option values at boundaries I, II, III are around 19.56, 4.80, and 0.36, respectively.

1. Scenario generation for the future economic state (risk factors);
2. Instrument valuation of all the simulated grid points by the COS method;
3. Exposure profile calculation.

3.4.1 Numerical Error Analysis

In this section we analyse the error of the approximation by the SGBM method, by using benchmark results. We use the examples of single asset options from section 3.3.4, including the European put and Bermudan put option. For a European put option, the Black-Scholes formula is available for a benchmark result; for a Bermudan put option, which has no analytical solution, we use the Monte Carlo-COS method to get the benchmark result. In the example of the Bermudan option, we set the number of exercise dates $M = 50$, and only the exposure on exercise dates is considered. To focus the discussion, all of the analysis is based on the results of $\mathbb{Q}$-exposure profiles as explained in section 3.3.4.

To verify the performance of the SGBM method, we use the error criteria established in [56]. For a grid point at time t_m and simulation path p, $(t_m, s_{t_m}(p))$, $m = 1, ..., M$, $p = 1, ..., P$, let $V_{t_m}(s_{t_m}(p))$ be the benchmark result for the option value. And let $\widehat{V}_{t_m}(s_{t_m}(p))$ be the approximated result by the SGBM method. Note that in case of Bermudan options, the option value after exercise

Number of bundles	AMAE	AMSE
2^3	0.0063	2.1950×10^{-4}
2^4	0.0027	1.9424×10^{-5}
2^5	0.0030	1.5337×10^{-5}
2^6	0.0053	4.4199×10^{-5}

Table 3.6: Error measure results for the $\mathbb{Q}$-exposure profile of the European put option.

time are set to be zero. The mean absolute error (MAE) and the mean squared error (MSE) are defined as follows,

$$\begin{aligned}
\mathrm{MAE}_{t_m} &= \frac{1}{P}\sum_{p=1}^{P} |V_{t_m}(s_{t_m}(p)) - \widehat{V}_{t_m}(s_{t_m}(p))|, \\
\mathrm{MSE}_{t_m} &= \frac{1}{P}\sum_{p=1}^{P} |V_{t_m}(s_{t_m}(p)) - \widehat{V}_{t_m}(s_{t_m}(p))|^2.
\end{aligned}$$

And the corresponding total average errors over time are defined as,

$$\begin{aligned}
\mathrm{AMAE} &= \frac{1}{M}\sum_{m=1}^{M} \mathrm{MAE}_{t_m}, \\
\mathrm{AMSE} &= \frac{1}{M}\sum_{m=1}^{M} \mathrm{MSE}_{t_m}.
\end{aligned}$$

3.4.2 European Options

We calculate the above formulated exposure errors for a European put option with the same parameter set as in section 3.3.4. In the example, we specify the basis functions as $f_k(S_{t_m}) = (S_{t_m})^{k-1}, k = 1, 2, 3, 4$ and analyse the dependence of accuracy on different numbers of bundles.

The results summarized in table 3.6 show that, the approximation error with 2^4 and 2^5 bundles is smaller than the ones with 2^3 and 2^6 bundles. A smaller number of bundles can generate larger approximation error, and the extreme case is without bundles, i.e., the vanilla regression method; on the other hand, excessive bundles will also produce significant error, since there may be not enough simulation paths in some bundles for an accurate regression. Compared with the best result shown in the same example from [56], with AMAE $= 0.2099$ and AMSE $= 0.1025$, the error in SGBM method is much smaller.

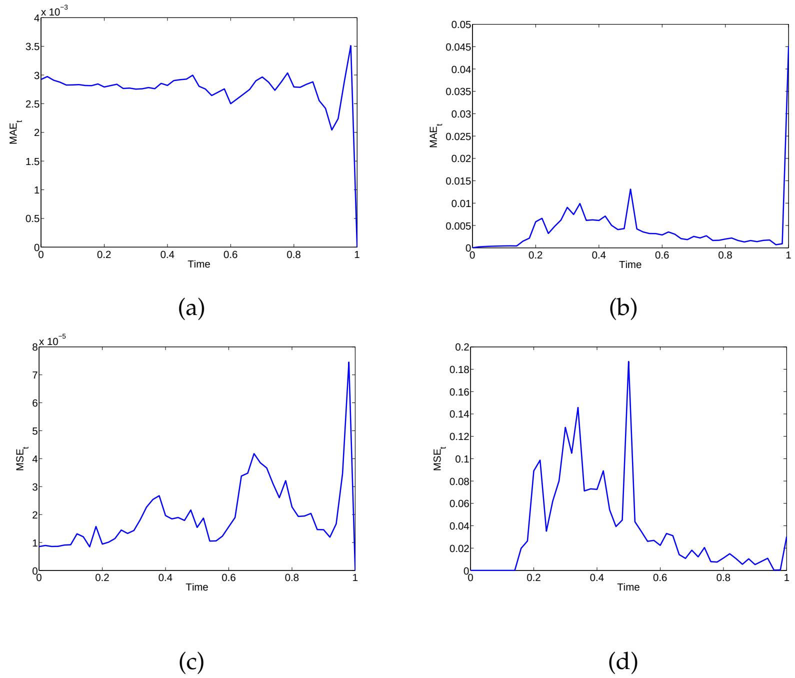

Figure 3.5: (A), The MAE_{t_m} of European put option. (B), The MAE_{t_m} of Bermudan put option. (C), The MSE_{t_m} of European put option. (D), The MSE_{t_m} of Bermudan put option.

Number of bundles	AMAE	AMSE
2^3	0.0203	0.2256
2^4	0.0054	0.0502
2^5	0.0041	0.0360
2^6	0.0053	0.0473

Table 3.7: Error measure results for the $\mathbb{Q}$-exposure profile of the Bermudan put option.

3.4.3 Bermudan Options

For Bermudan put options, a similar conclusion can be obtained. We specify the basis functions as $f_k(S_{t_m}) = (S_{t_m})^{k-1}$, $k = 1, 2, 3, 4$. In table 3.7, the experiment with 2^5 bundles gives the best results. We can see that increasing the number of bundles does not necessarily yield better performance results, while decreasing the number of bundles can yield worse performance results. Figure 3.5 depicts the MAE_{t_m} and MSE_{t_m} over time.

3.5 Results and Efficiency Comparison

An efficiency comparison of different computation methods, SGBM, SRBM and SRM, is given in this section via several numerical examples of multi-asset options. Each example follows the model assumptions given in section 3.2.1. To focus the discussion on efficient computation of exposure, we will not list the results for CVA, although it is quite straightforward. A practical formula of CVA in the case of no wrong way risk can be found in [33], for which the main component is the multiplication of expected exposure and counterparty's default probability.

The efficiency comparison includes comparison of computation speed and accuracy for exposure profiles (PFE and EE) and option prices. The initial option prices are provided for the reason that an accurate result for the option prices (especially the path estimator of the option price) represents a good estimate of the early exercise policy, which can significantly influence the exposure profile in the case of Bermudan options. To compare with the reference literature in which the option prices are usually obtained under the risk neutral measure, we concentrate on the numerical comparison of PFE, EE and option prices generated under the risk-neutral measure. To obtain the exposure profiles and the direct estimator of the option price, we use 60000 simulation paths in SGBM, SRBM and SRM; and for the path estimators, 240000 simulation paths are generated. The standard deviations of the estimates (the num-

$s_0^i = 40$	$K = 40, d = 2$	$r = 0.06$
$\sigma = 0.2$	$T = 1, M = 10$	observation dates $= 20$
$q = 0$	$\rho_{i,j} = 0.25, i \neq j, i, j = 1, ..., d$	

Table 3.8

bers in the parentheses) are based on 100 independent simulation trials. All of the computations are implemented in Matlab on Intel (R) Core (TM) i5-2400 CPU 3.10 GHz with 4 GB memory.

3.5.1 Geometric Basket Options

As a special case of basket options, the geometric basket options can be reduced to a one-dimensional problem [5], for which we have shown in section 3.4 that SGBM can give accurate results for PFE and EE. The exercise value for d-asset geometric basket Bermudan options is given by,

$$h(\mathbf{S}_{t_m}) = \big(K - \big(\prod_{i=1}^{d} S_{t_m}^i\big)^{\frac{1}{d}}\big)^+.$$

Given the model assumptions for the underlying assets, we specify the parameters of the model in table 3.8. For the regression approximation at time step t_m, basis functions

$$f_k(\mathbf{S}_{t_m}) = \big((\prod_{i=1}^{d} S_{t_m}^i)^{\frac{1}{d}}\big)^{k-1}, k = 1, ..., 5,$$

are used in SGBM, while basis functions

$$f_k(\widetilde{\mathbf{S}}_{t_{m-1}}) = \big((\prod_{i=1}^{d} S_{t_{m-1}}^i)^{\frac{1}{d}}\big)^{k-1}, k = 1, ..., 5,$$

are used in SRBM and SRM. The formulas of the conditional expectations of $f_k(\mathbf{S}_{t_m})$ can be found in table 3.1.

In table 3.9, the CPU time scale shows us that SRM is the fastest method. In this relatively low-dimensional case, since the moments of the basis functions are simple, we find that the computation speed of SGBM is a bit faster than

Method	CPU time (secs)	Direct est.	Path est.
SGBM	3.8299	1.7558 (0.000184)	1.7554 (0.0033)
SRBM	4.6696	1.7596 (0.0040)	1.7497 (0.0029)
SRM	1.4710	1.8100 (0.0044)	1.7507 (0.0036)

Table 3.9: Geometric basket Bermudan option with two stocks. The CPU time represents the computation time of PFE and EE. The direct estimator and path estimator represent the different estimates of option prices. The reference option price is 1.7557 [5].

SRBM [2]. The results of option prices from different methods are quite close, however, compared with the reference result, the estimates of SGBM seem to be better than the other two results. Particularly, for the direct estimator, SGBM has the lowest standard deviation of estimates, which is the contribution of the moment computation in each bundle. This is consistent with the conclusion from Glasserman and Yu [32]. The standard deviation of option price estimates from SRBM and SRM is quite similar.

The effect of the bundling technique on the exposure computation can be seen in figure 3.6a. For both PFE and EE, the results of SGBM are close to the results of SRBM. The results of SRM are higher than both SGBM and SRBM. Particularly, in the case of only one bundle, SRBM is equivalent to SRM. The computation time of SGBM and SRBM with different numbers of bundles is illustrated in figure 3.6b. In figure 3.6c, we also show the CPU time scale of SGBM, SRBM, and SRM with respect to different numbers of simulation paths.

Remark 3.5.1. *The saw-toothed shape of PFE and EE comes from the early exercise feature, since the exposure becomes zero after exercise. It is important to take into account more dense time grid points than only possible exercise dates for accuracy reasons. Otherwise the exposure profiles will be quite different, which can significantly influence the computation of CVA.*

3.5.2 Arithmetic Basket Options

In this section, we give an efficiency comparison of SGBM, SRBM, and SRM for the exposure computation of d-asset arithmetic basket Bermudan options,

[2]Generally, the computation speed of SRBM should be faster than SGBM because no moment calculation is needed in SRBM. However, in this simple two-dimensional case, since lots of basis functions are used, the regression computation step in the implementation of SRBM can be rank deficient, which makes the computation slower than SGBM.

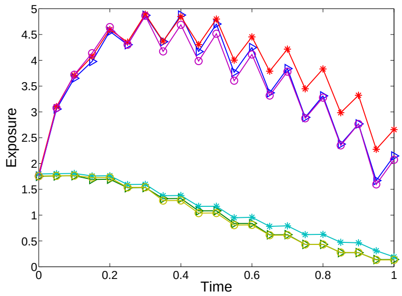

(a)

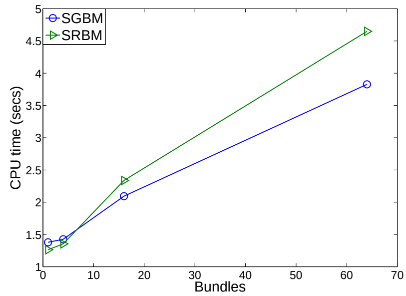

(b)

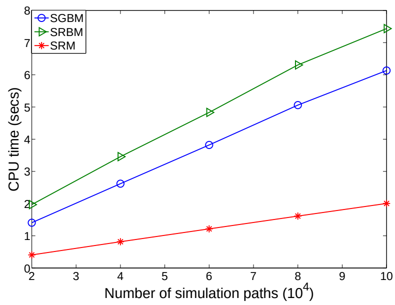

(c)

Figure 3.6: Geometric basket Bermudan option with two stocks. (A) Comparison of SGBM with 64 bundles (o), SRM (*), and SRBM ($\triangle$) with 64 bundles. High profile: 97.5% PFE. Low profile: EE. (B) CPU time scale of PFE and EE computation in number of bundles. (C) CPU time scale of PFE and EE computation in number of simulation paths.

$s_0^1 = 90, s_0^2 = 110$	$K = 100, d = 2$	$r = 0.04$
$\sigma_1 = 0.2, \sigma_2 = 0.3$	$T = 1, M = 10$	observation dates $= 20$
$q = 0$	$\rho_{i,j} = 0.25, i \neq j, i, j = 1, ..., d$	

Table 3.10

for which the exercise value reads,

$$h(\mathbf{S}_{t_m}) = \big(K - \frac{1}{d}\big(\sum_{i=1}^{d} S_{t_m}^i\big)\big)^+$$

Given the model assumptions of the underlying assets and counterparty's stock price, the parameters in table 3.10 are used for the numerical examples. For the regression approximation at time step t_m, basis functions

$$f_k(\mathbf{S}_{t_m}) = \big(\frac{1}{d}\sum_{i=1}^{d} S_{t_m}^i\big)^{k-1}, k = 1, ..., 4,$$

are used in SGBM, while basis functions

$$f_k(\widetilde{\mathbf{S}}_{t_{m-1}}) = \big(\frac{1}{d}\sum_{i=1}^{d} S_{t_{m-1}}^i\big)^{k-1}, k = 1, ..., 4,$$

are used in SRBM and SRM. The formulas of the conditional expectations of $f_k(\mathbf{S}_{t_m})$ can be found in table 3.1.

According to the results reported in table 3.11, the CPU time scale shows us that SRM is the fastest method, and SRBM the middle. For the direct estimator of the option price, SGBM has the lowest standard deviation of estimates, whereas the standard deviation of the option price estimates from SRBM and SRM is similar. For the standard deviation of path estimator, all of the three methods seem to be similar. Compared with the option prices estimated by SRM and SRBM, the results generated by SGBM are closer to the reference result.

Similar as for the geometric basket options, the application of the bundling technique improves PFE and EE significantly, which can be seen from figure 3.7a. For both PFE and EE, the results of SGBM are close to the results of SRBM. The results of SRM, which is the special case of SRBM with *one bundle*,

Method	CPU time (secs)	Direct est.	Path est.
SGBM	3.7233	6.6108 (0.000809)	6.6096 (0.0103)
SRBM	3.1158	6.6280 (0.0184)	6.5990 (0.0090)
SRM	1.0863	6.8508 (0.0128)	6.5796 (0.0078)

Table 3.11: Arithmetic basket Bermudan option with two stocks. The CPU time represents the computation time of PFE and EE exposure profiles. The direct estimator and path estimator represent the different estimates of option prices. The reference option price is 6.6109 [54].

are higher than both SGBM and SRBM. The computation time of SGBM and SRBM with different numbers of bundles is shown in figure 3.7b. Because of the moment calculation, SGBM needs more time for computation. For SRBM, since no moment computation is needed, the CPU time is kept almost the same for both geometric and arithmetic basket options. In figure 3.7c, we also show the CPU time scale of SGBM, SRBM, and SRM with respect to different numbers of simulation paths.

3.5.3 Max Options

Given the model assumptions of the underlying assets, one common feature shared by the numerical examples discussed (single-asset options, geometric basket options and arithmetic basket options) is that in the application of SGBM, all of the option payoffs allow for closed-form solutions of the conditional expectations of the basis functions f_k. Particularly, in the case of relatively low-dimensional problems, as we have discussed for the two stock examples, the closed-form formula of the moments is quite simple which makes the CPU time for geometric and arithmetic basket options quite similar, even with different computation methods (i.e., SGBM and SRBM).

Although the property of closed-form formulas of the conditional expectations of basis functions f_k is relatively rare in quantitative finance calculation, especially for high-dimensional problems when many random variables are involved, if we can find an approximation formula, it is very helpful for an efficient computation. In this section, the example of multi-asset max options with five stocks is given, for which an approximation of the conditional expectation is obtained by Clark's algorithm [23, 39].

The exercise value of d-asset Bermudan max options is given by,

$$h(\mathbf{S}_{t_m}) = \big(\max(S_{t_m}^1, ..., S_{t_m}^d) - K\big)^+.$$

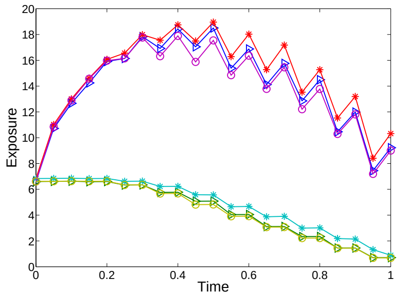

(a)

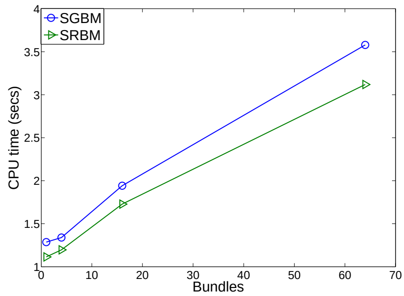

(b)

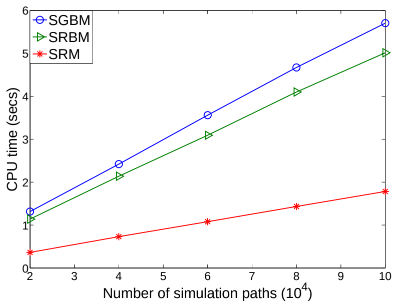

(c)

Figure 3.7: Arithmetic basket Bermudan option with two stocks. (A) Comparison of SGBM with 64 bundles (o), SRM (*), and SRBM ($\triangle$) with 64 bundles. High profile: 97.5% PFE. Low profile: EE. (B) CPU time scale of exposure profile computation in number of bundles. (C) CPU time scale of exposure profile computation in number of simulation paths.

$s_0^i = 100$	$K = 100, d = 5$	$r = 0.05$
$\sigma = 0.2$	$T = 3, M = 9$	observation dates $= 36$
$q = 0.1$	$\rho_{i,j} = 0, i \neq j, i, j = 1, ..., d$	

Table 3.12

Under the model assumption of multi-dimensional geometric Brownian motion, the parameters are given in table 3.12.

As already discussed in section 3.3.2, the bundling method used for two stocks becomes computationally expensive in the case of five stocks. In this section, we apply the bundling method on a *dimensionally reduced state space*, for which the mapping function reads

$$g(t, \mathbf{S}_t) = \max(S_t^1, ..., S_t^d).$$

For the regression approximation at time step t_m, basis functions

$$f_k(\mathbf{S}_{t_m}) = \big(\log(\max(S_{t_m}^1, ..., S_{t_m}^d))\big)^{k-1}, k = 1, ..., 5,$$

$$f_6(\mathbf{S}_{t_m}) = \big(\prod_{i=1}^{d} S_{t_m}^i\big)^{\frac{1}{d}},$$

$$f_{6+i}(\mathbf{S}_{t_m}) = S_{t_m}^i, i = 1, ..., d,$$

are used in SGBM as in [39], while basis functions

$$\widetilde{f}_k(\mathbf{S}_{t_{m-1}}) = \big(\log(\max(S_{t_{m-1}}^1, ..., S_{t_{m-1}}^d))\big)^{k-1}, k = 1, ..., 5,$$

$$\widetilde{f}_6(\mathbf{S}_{t_{m-1}}) = \big(\prod_{i=1}^{d} S_{t_{m-1}}^i\big)^{\frac{1}{d}},$$

$$\widetilde{f}_{6+i}(\mathbf{S}_{t_{m-1}}) = S_{t_{m-1}}^i, i = 1, ..., d,$$

are used in SRBM and SRM. By using the Clark algorithm [23, 39], an exact formula of $\mathbb{E}^{\mathbb{Q}}[f_k(\mathbf{S}_{t_m}) \mid \mathbf{S}_{t_{m-1}} = \mathbf{s}_{t_{m-1}}(p)]$, $k = 1, ..., 5$, exists for two assets (the first four moments). For more than two assets, Clark's algorithm can provide an accurate approximation.

In table 3.13, the CPU time scale shows us that SRM is the fastest method, and SRBM the middle. For the direct estimator of option price, SGBM has the lowest standard deviation of estimates. For the standard deviation of the path estimator, all of the three methods are similar. If we use the reference as the benchmark, SGBM seems to have the best estimates of option prices among theses three methods.

Method	CPU time (secs)	Direct est.	Path est.
SGBM	18.5511	26.1673 (0.0127)	26.0871 (0.0320)
SRBM	8.4731	26.3164 (0.0607)	26.0474 (0.0335)
SRM	2.9839	26.4223 (0.0413)	26.0049 (0.0361)

Table 3.13: Max options with 5 stocks. 16 bundles are used in SGBM and SRBM. The CPU time represents the computation time of the PFE and EE profiles. The direct estimator and path estimator represent the different estimates of option prices. The literature reference of the option price is $[26.115, 26.164]$, with 95% CI [11].

Similar as for the geometric and arithmetic basket options, the application of bundling method changes PFE and EE significantly, which can be observed from figure 3.8a. For both PFE and EE, the results of SGBM are close to the results of SRBM. The results of SRM are higher than both SGBM and SRBM. The computation time of SGBM and SRBM with different numbers of bundles is shown in figure 3.8b. Because of the moment calculation, SGBM needs more time for computation. Compared with the geometric and arithmetic basket options, since more basis functions are used for max options (11 basis functions for five assets), and the conditional expectation of basis functions have more complicated formulas, the corresponding CPU time of SGBM is higher. However, for SRBM, since no moment computation is needed, the CPU time is kept relatively low. In figure 3.8c, we show the CPU time scale of SGBM, SRBM, and SRM with respect to different numbers of simulation paths. Although SRM is the fastest one, the exposure profile and option price estimates are not as accurate as SRBM and SGBM. While the computation speed of SRBM is faster than SGBM, the exposure profiles and option price estimates are quite similar. The standard deviation of option price estimates by SGBM is the lowest among the three methods, although merely an approximation of conditional expectation of basis functions is used in computation.

3.6 Conclusion

This chapter provides an efficient simulation-based method, SGBM from [39], to estimate the counterparty credit exposure profiles of multi-asset options. In the one-dimensional case, by using a benchmark of European and Bermudan

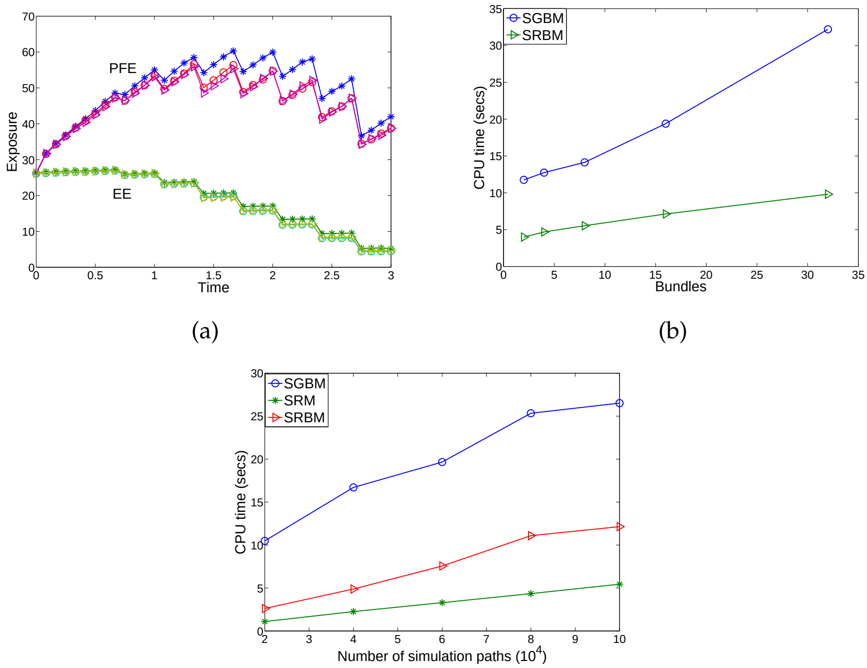

(c)

Figure 3.8: Max Bermudan option with 5 stocks. (A) Comparison of SGBM with 16 bundles (o), SRM (*), and SRBM ($\triangle$) with 16 bundles. High profile: 97.5% PFE. Low profile: EE. (B) CPU time scale of exposure profiles computation in number of bundles. (C) CPU time scale of exposure profile computation in number of simulation paths, with 16 bundles in SGBM and SRBM.

options via MCCOS, it shows that with an appropriate choice of basis functions and application of bundling, SGBM achieves high accuracy. Particularly, for discontinuous payoffs, such as digital options, by using the bundling technique, SGBM can get an accurate and stable result for the option price and exposure profiles. The numerical experiments show that the discontinuity of conditional expectations on the boundary of bundles can be reduced significantly by increasing the number of simulation paths and bundles appropriately. In addition, compared with SRBM, when the same number of simulation paths, basis functions and bundles are used, the discontinuity on the boundary of bundles in SGBM is less pronounced. In the case of multi-asset instruments (two stocks and five stocks in the examples), the numerical comparison of SGBM, SRBM and SRM shows that SGBM has the advantage of lower standard deviation for the direct estimates of the option prices. This is consistent with the conclusion of Glasserman and Yu (2004), in which they have a theoretical proof of the advantage of 'regression later' (used in SGBM) compared with 'regression now' (used in SRBM and SRM) under some conditions. Generally, the estimates for the option prices of SGBM are closer to the reference results than SRM and SRBM. Even though the computation speed of SGBM will be generally slower than the other two methods, it is still reasonably fast. The bundling method is shown to be quite useful in improving the accuracy of exposure profiles. The exposure profiles generated by SGBM and SRBM are similar when the same number of bundles are used. And the exposure profiles generated by SRM are not as accurate as SGBM and SRBM. We conclude that SGBM is an efficient method for exposure calculation, and the efficient calculation of the expected exposure (EE) [33] for multi-asset options can be further applied to the computation of the credit value adjustment (CVA) [22, 33].

3.7 Appendix

3.7.1 $\mathbb{P}$-Probability Distribution of Credit Exposure: Change of Measure

We simulate the scenario of risk factors under measure $\mathbb{Q}$, and we use an American Monte Carlo method to go through the dynamic programming procedure for Bermudan options. The algorithm results in samples of the exposure probability distribution under $\mathbb{Q}$. To get the exposure probability distribution under measure $\mathbb{P}$, we need to use the change of measure technique [22].

Define the Randon-Nikodym derivative of $\mathbb{P}$ relative to $\mathbb{Q}$ on $\mathcal{F}_t$ as,

$$z(t) = \frac{\mathrm{d}\mathbb{P}}{\mathrm{d}\mathbb{Q}} \,|_{\mathcal{F}_t} \,. \tag{3.15}$$

Particularly, if the stochastic process of stock price S_t is geometric Brownian motion, with μ the drift part under measure $\mathbb{P}$, σ the diffusion part, r the constant risk-free interest rate, then $z(t)$ has the following explicit formula,

$$z(t) = \frac{\mathrm{d}\mathbb{P}}{\mathrm{d}\mathbb{Q}} |_{\mathcal{F}_t} = \exp(\theta W_t^{\mathbb{Q}} - \frac{1}{2}\theta^2 t),$$

with $\theta = (\mu - r)/\sigma$, the market price of risk and $W_t^{\mathbb{Q}} = \int_0^t \mathrm{d}W_s^{\mathbb{Q}}$.

By a change of measure, EE_t can be calculated as,

$$\begin{aligned} EE_t &= \mathbb{E}^{\mathbb{P}}\big[E_t\big] \\ &= \mathbb{E}^{\mathbb{Q}}\big[E_t z(t)\big]. \end{aligned}$$

From the samples of E_t obtained from the algorithm, EE_t can be calculated empirically, i.e.,

$$\widehat{EE}_t = \frac{1}{P}\sum_{p=1}^{P} E_t^p z^p(t),$$

with p denotes the p-th sample path, $p = 1, ..., P$.

The quantity $PFE_{\alpha,t}$ is closely related to the empirical distribution of E_t under measure $\mathbb{P}$. Denote the exact distribution of E_t under $\mathbb{P}$ at time t as $F_t^{\mathbb{P}}(x)$, which can be written as,

$$\begin{aligned} F_t^{\mathbb{P}}(x) &= \mathbb{E}^{\mathbb{P}}\big[1_{E_t \leq x}\big] \\ &= \mathbb{E}^{\mathbb{Q}}\big[1_{E_t \leq x} z(t)\big]. \end{aligned}$$

From the estimated samples of the algorithm, $F_t^{\mathbb{P}}(x)$ can be approximated by an empirical distribution function, i.e.,

$$\hat{F}_t^{\mathbb{P}}(x) = \frac{1}{P}\sum_{p=1}^{P} 1_{E_p^t \leq x} z^p(t), x \in \mathbb{R}.$$

Given a confidential level α, we can calculate the $PFE_{\alpha,t}$ by inverting the empirical function $\hat{F}_t^{\mathbb{P}}$, which can be obtained by an interpolation procedure, i.e.,

$$PFE_{\alpha,t} = \big(\hat{F}_t^{\mathbb{P}}\big)^{-1}\big(\alpha\big).$$

If the risk factors are simulated under the real world measure $\mathbb{P}$, the conditional expectation (and the exposures) has to be computed under measure $\mathbb{P}$ by using a change of measure [56],

$$c(t_{m-1}, \mathbf{S}_{t_{m-1}}) = \exp(-r\Delta t)\mathbb{E}^{\mathbb{P}}\big[\frac{z(t_m)}{z(t_{m-1})} V_{t_m}(\mathbf{S}_{t_m}) | \mathbf{S}_{t_{m-1}}\big], m = M, M-1, ..., 1.$$

In practice, an approximation such as $\frac{z(t_m)}{z(t_{m-1})} \approx 1$ can be used in implementation, when the drift μ is close to r. The exposure distribution resulting in this case is under measure $\mathbb{P}$.

Chapter 4

Credit Value Adjustment with Wrong Way Risk for Bermudan Options

4.1 Introduction

High-profile defaults of important financial institutions during the financial crisis of 2007 to 2009 highlight the importance of counterparty credit risk in over-the-counter (OTC) derivative contracts. According to the Basel II and III accords, counterparty credit risk is the risk that a counterparty in a financial OTC derivative contract will default prior to the expiration of the contract and will fail to make all the payments required by the contract. The market value of counterparty credit risk is called credit value adjustment (CVA): the difference between the risk free portfolio value and the true portfolio value that takes into account the counterparty's default risk.

Many authors have discussed the challenges of intensive computation in CVA calculations. In [33], the author discusses the bilateral nature of credit exposure imbedded in many derivative portfolios, which makes the pricing of counterparty risk more difficult than in the unilateral situation. For many OTC exotic options, because of the exotic features and complicated underlying asset processes, no explicit pricing formulas exist, which makes the calculation of expected exposure (one component that is required for CVA calculation) even more complicated and time-consuming. In addition, one also has to be careful regarding the proper modeling of positive (negative) correlation between exposure and counterparty's default risk, which is called wrong (right) way risk, because the effect of this correlation on CVA could be significant [10, 33, 37].

The purpose of this chapter is to propose an efficient calculation method for CVA of exotic options when wrong way risk exists, and investigate the relationship between the wrong way risk effect on CVA and the exotic features. Particularly, considering a simple but nontrivial example of exotic options, we focus on the efficient calculation for CVA of Bermudan equity options with counterparty credit risk. For ease of exposition, we assume the option is written on the counterpary's own stock. By using the proposed method, we are able to analyse the effect of the early exercise feature and wrong way risk on CVA, and the relationship between the wrong way risk effect and the early exercise feature in general.

The calculation problem of CVA originates from the pricing problem of 'vulnerable options' (i.e., an option with credit risk) in Johnson and Stulz (1987) [42]. Johnson and Stulz (1987) studied the pricing of European options and American options with default risk, where the underlying asset follows a pure jump process or a lognormal diffusion process. Hull and White (1995) [36] and Jarrow and Turnbull (1995) [40] generalized the ideas of Johnson and Stulz (1987), and the impact of default risk on the price of an American option was also discussed in Hull and White (1995). Since then many authors have been working on this topic. In addition, because of the financial crisis and risk management requirements from the Basel committee, Monte Carlo methods have been developed in practice for the CVA computation of large portfolios. Canabarro and Duffie (2003) [17] provided a general Monte Carlo algorithm to obtain an estimation of the market value of counterparty credit risk in bilateral OTC portfolios. Pykhtin (2011) [48] gives an overview of approaches for managing counterparty credit risk and reviews different aspects of modeling of counterparty credit risk. Differently from the aforementioned work, here we study the 'vulnerable' Bermudan options. We are interested in the effect of the wrong way risk and the early exercise feature on CVA, and the relationship between the wrong way risk effect and the early exercise feature.

A closely related paper is Hull and White (2012) [37], in which the authors propose a model to incorporate wrong way risk into CVA calculations. In the model, the hazard rate of the counterparty is postulated to be an increasing function of the bank's portfolio value, while it becomes a decreasing function in the case of right way risk. This model is named "portfolio value approach" (PVA) in Ruiz (2013) [55]. Hull and White (2012) focuses on the study of the effect of wrong way risk on CVA and the Greeks letters of CVA. They also find that the effect depends on the collateral arrangements. Here we consider a different but related hazard rate model in which the counterparty's hazard rate is negatively related to its stock price. This model is named "empirical analysis approach" (EAA) in Ruiz (2013) to stress the empirical evidence background. We show the mathematical equivalence of PVA and EAA, and provide a comparison of the calibration. Our study shows that the effect of wrong way risk on CVA of a Bermudan option depends on its early exercise features. These issues are not discussed in Hull and White (2012).

To take into account the correlation between the credit exposure and default risk, Rosen and Saunders (2012) [53] proposed a joint market-credit model by building a co-dependence structure between the exposures and the credit events. Brigo and Pallavicini (2008) [10] proposed a stochastic intensity jump diffusion model for the default event, and a short-rate Gaussian shifted two-factor process for the interest rate. The two processes are coupled by correlating their Brownian shocks. Both papers assume specific models for the counterparty's default event and add correlation between the default event and the market variables of the portfolio. Differently from their work, we use the hazard rate approach to incorporate the correlation, where the hazard rate is assumed to be a function of the counterparty's stock price. The specific functional form of the hazard rate is estimated by using empirical data which shows a negative relationship between counterparty's hazard rate and its stock price, see also Duffie and Singleton (2003, p. 206) [26] and Ruiz (2013) [55].

Duffie and Singleton (2003, p. 206) [26] model the risk-neutral hazard rate as a (negative power) function of the equity price of the counterparty, and give an equity derivative pricing algorithm with default and recovery in the binomial-tree model. In Linetsky (2006) [43], Carr and Linetsky (2006) [18] and Carr and Madan (2010) [19], the authors use a negative power function of the equity price to model the hazard rate, and give a solution for European options with credit risk under different models for volatility (i.e., constant, constant elasticity of variance, and local volatility). Here we use this negative relationship to model the wrong way risk embedded in Bermudan put options.

The main issues contained in the current chapter are the following:

1. By using the concept of stochastic hazard rate, we derive an approximation of the expected exposure conditional on default, which is applicable for the calculation of expected exposure and CVA with wrong way risk;

2. Regarding the wrong way risk modeling, we compare the empirical analysis approach (EAA) and the portfolio value approach (PVA), and show the advantages of EAA in our problem setting;

3. Based on Monte Carlo simulation and a Fourier inverse option pricing method, an efficient calculation method for Bermudan options' CVA is proposed. The method is also applicable when the underlying stock price follows a Lévy process;

4. The numerical results show that the wrong way risk has significant effect on the expected exposure (EE) and CVA of Bermudan options, however, this effect depends on the Bermudan option's early exercise feature. More precisely, a high exercise intensity (i.e., high volatility, high

strike price, or high number of possible early exercise dates) may lead to $\text{CVA}_W < \text{CVA}_I$ (see formulas (4.1) and (4.5) and the explanations in the corresponding sections.), which is different from the conclusion if one uses the α multiplier approach with $\alpha > 1$ (see formula (4.8) and the explanation.).

This chapter is structured in the following way. Section 4.2 introduces the problem of interest. Section 4.3 describes the computation of Bermudan options' CVA when the wrong way risk is not considered. In section 4.4 we mainly discuss the hazard rate approach to model the wrong way risk imbedded in the Bermudan equity put options, and provide an analytical approximation of the expected exposure conditional on default. In section 4.5 we propose an efficient calculation method for the credit exposure of Bermudan options. After that we provide the computation method for Bermudan options' CVA when wrong way risk exists. In section 4.6, through several numerical examples, we study the effect of wrong way risk on Bermudan options' CVA, and the relationship between the wrong way risk effect and the early exercise feature. Section 4.7 gives a conclusion of the current research.

4.2 Problem Formulation

Consider a bank (the contract holder) holding a derivative security with a given counterparty which has default risk. Following the same notation as in chapter 3, let $(\Omega, \mathcal{F}, \mathbb{P})$ be a probability space, let T be a fixed positive number, and let $\mathcal{F}_t$, $0 \le t \le T$, be a filtration of sub-σ-algebras of $\mathcal{F}$, representing the information available up to time t. We define the risk free value (i.e., no counterparty risk) of the derivative security under the risk-neutral measure $\mathbb{Q}$ [59] over time as a stochastic process $V(t), 0 \le t \le T$, which is driven by the stochastic process of risk factors $X(t), 0 \le t \le T$, such as stock prices, foreign exchange rates, and interest rates[33]. We call $(t, X(t))$ the state of the economy at time t. Denote the derivative's discounted net cash flow between t and T as $C_f(t,T)$ (i.e., all of the cashflows are discounted back to time t), then $V(t) = \mathbb{E}^{\mathbb{Q}}\left[C_f(t,T)|\mathcal{F}_t\right]$.

For the counterparty's default risk, denote the counterparty's default time by τ. Let $S_{ur}(t)$ denote the risk neutral survival (no default) function of the counterparty,

$$S_{ur}(t) = \mathbb{Q}[\tau > t]$$

We are interested in the value of the bank's derivative security traded with the counterparty subject to default risk, which is denoted as $\widetilde{V}(t)$. $\widetilde{V}(t)$ is always smaller than $V(t)$ and the difference $V(t) - \widetilde{V}(t)$ is named credit value adjustment (CVA). Particularly, in this chapter, we analyse in detail the CVA of Bermudan equity options when the underlying asset is one-dimensional.

4.3 Simulation Approach for CVA Valuation

In some simple cases (such as European options, when the exposure process and counterparty's default are independent.), one can obtain analytical solution for CVA; however, in practice, CVA is almost invariably calculated using Monte Carlo simulation [37].

Consider a Bermudan equity option which can be exercised at a fixed set of equally spaced time points (possible early exercise dates), $\mathcal{T} = \{t_1, ..., t_M\}$, $0 = t_0 \leq t_1, t_M = T$, $t_m - t_{m-1} = \Delta t, m = 1, ...M$. We choose the set of time points $\mathcal{T}$ for discretization [1]. Based on the risk neutral pricing formula of CVA introduced in chapter 1, if the exposure is independent of the default risk, then CVA of Bermudan options can be approximated as follows,

$$\text{CVA}_I \approx (1-\delta)\sum_{m=1}^{M} D(0, t_{m-1}) EE_{t_{m-1}} \big(S_{ur}(t_{m-1}) - S_{ur}(t_m)\big) \tag{4.1}$$

Here $D(0, t_{m-1})$ is the deterministic discount factor from t_{m-1} to 0, and $EE_{t_{m-1}}$ is the expected exposure, as defined in chapter 1. Note that $EE_{t_{m-1}}$ is calculated under the risk neutral measure $\mathbb{Q}$. We use CVA_I to denote that exposures and counterparty's defaults are independent, and use the simplified notation CVA for CVA(0, T).

Formula (4.1) implies that two terms, the expected exposure $EE_{t_{m-1}}$ and the default probability $S_{ur}(t_{m-1}) - S_{ur}(t_m)$, have to be calculated efficiently. We explain it in the following section.

4.3.1 Valuation of Expected Exposure

By using the modeling framework introduced in chapter 2, we can get the sample results of Bermudan option's credit exposure under the measure $\mathbb{Q}$. Then EE_{t_m} can be obtained directly by averaging the exposures E_{t_m} over all scenarios, $x_m(p), p = 1, ..., P$,

[1] A smaller time interval can be used for discretization; for ease of exposition, we use the set of time points which represents the possible early exercise dates of Bermudan option.

$$
\begin{aligned}
EE_{t_m} &= \mathbb{E}^{\mathbb{Q}}[E_{t_m}] \\
&\approx \frac{1}{P}\sum_{p=1}^{P} E_{t_m}(x_m(p)).
\end{aligned}
$$

Here (and below) we use the simplified notation X_m for $X(t_m)$ and $x_m(p)$ denotes the realization of underlying variables $X(t)$ at time t_m, on scenario p. One can also write it in another form[2],

$$
\begin{aligned}
EE_{t_m} &= \mathbb{E}^{\mathbb{Q}}[E_{t_m}] \\
&\approx \sum_{p=1}^{P} E_{t_m}(x_m(p))\mathbb{Q}(X_m = x_m(p)).
\end{aligned}
\tag{4.2}
$$

Here $E_{t_m}(x_m(p))$ denotes the exposure at the simulated state $(t_m, x_m(p))$, and $\mathbb{Q}(X_m = x_m(p))$ is the probability mass of $X_m = x_m(p)$.

4.3.2 Counterparty's Default Probability

If we use the concept of hazard rate λ_t to represent the survival function of a counterparty, then the survival function $S_{ur}(t)$ can be written as,

$$
S_{ur}(t) = \mathbb{E}^{\mathbb{Q}}[\exp(-\int_0^t \lambda_u du)]. \tag{4.3}
$$

The default probability during the time interval (t_{m-1}, t_m) reads,

$$
S_{ur}(t_{m-1}) - S_{ur}(t_m) = \mathbb{E}^{\mathbb{Q}}[\exp(-\int_0^{t_{m-1}} \lambda_u \mathrm{d}u)] - \mathbb{E}^{\mathbb{Q}}[\exp(-\int_0^{t_m} \lambda_u \mathrm{d}u)]. \tag{4.4}
$$

4.4 Hazard Rate Approach for Wrong Way Risk Modeling

Based on the simulation approach discussed above, we further consider a more complicated situation where the counterparty's default probability is positively dependent on credit exposure, which is termed as 'wrong way risk' (WWR).

[2]For a continuous probability distribution, no overlap sample results exist, so at time step t_m, the total number of sample results is equal to the number of scenarios P.

4.4.1 Wrong Way Risk in Put Options

Assume that a bank buys a put option from a counterparty which has default risk, and the option's underlying asset S is highly correlated to the counterparty's credit quality (an example is that S is the counterparty's own stock). The put option will only be valuable if the stock S goes down, in which case the counterparty is expected to be underperforming (i.e., credit quality decreases). This means that as the bank's counterparty exposure (the option value) increases, the counterparty is more likely to default. This positive dependence between the exposure and default risk is called wrong way risk.

To capture the wrong way risk, one has to model the dependence between the exposure and the counterparty's default. Recalling from chapter 1, the following formula can be used for the computation of CVA with wrong way risk CVA_W,

$$\mathrm{CVA}_W \approx (1-\delta)\sum_{m=1}^{M} D(0,t_{m-1})EE^*_{t_{m-1},t_m}\big(S_{ur}(t_{m-1})-S_{ur}(t_m)\big), \tag{4.5}$$

where

$$\begin{aligned} EE^*_{t_{m-1},t_m} &= \mathbb{E}^{\mathbb{Q}}[E_{t_{m-1}} \mid t_{m-1} < \tau \le t_m] \\ &\approx \sum_{p=1}^{P} E_{t_{m-1}}(x_{m-1}(p))\mathbb{Q}(X_{m-1} = x_{m-1}(p) \mid t_{m-1} < \tau \le t_m). \end{aligned} \tag{4.6}$$

The dependence between the credit exposure and the default risk is embedded in the conditional expectation, $EE^*_{t_{m-1},t_m}$. A simple way of dealing with wrong way risk is the 'α multiplier approach', which is used by the Basel Committee for the calculation of regulatory capital. In this approach, $EE^*_{t_{m-1},t_m}$ is obtained by multiplying a constant factor α to $EE_{t_{m-1}}$,

$$EE^*_{t_{m-1},t_m} = \alpha EE_{t_{m-1}}. \tag{4.7}$$

The effect of this is to increase CVA by the α multiplier,

$$\mathrm{CVA}_W = \alpha \mathrm{CVA}_I. \tag{4.8}$$

Basel II sets α equal to 1.4 or allows banks to use their own models, with a floor for $\alpha = 1.2$. Estimation of α reported by banks range from 1.07 to 1.10.

We will use a different approach. Instead of multiplying by a constant α, we propose a more sophisticated model which uses the concept of hazard rate to model the wrong way risk. The following proposition gives an approximation of $EE^*_{t_m,t_{m+1}}$:

Proposition 4.4.1. *(Hazard rate approach) The expected exposure conditional on default, or the expected exposure with wrong way risk (WWR EE), $EE^*_{t_m,t_{m+1}}$, can be approximated as,*

$$EE^*_{t_m,t_{m+1}} \approx \frac{\sum_{p=1}^{P} E_{t_m}(x_m(p)) \exp\big(-\sum_{i=1}^{m} \lambda(x_i(p))\Delta t\big)\lambda(x_m(p))}{\sum_{p=1}^{P} \exp\big(-\sum_{i=1}^{m} \lambda(x_i(p))\Delta t\big)\lambda(x_m(p))}, \tag{4.9}$$

where P is the number of scenarios, $x_m(p)$ is the realization of underlying variables at time t_m, on scenario p, and the hazard rate at time t_m is a function of $x_m(p)$, i.e., $\lambda(x_m(p))$.

Proof. The conditional expectation $EE^*_{t_m,t_{m+1}}$ can be written as

$$\begin{aligned} EE^*_{t_m,t_{m+1}} &= \mathbb{E}^{\mathbb{Q}}[E_{t_m} \mid t_m < \tau \le t_{m+1}] \\ &= \mathbb{E}^{\mathbb{Q}}[E_{t_m} \frac{\mathbb{Q}(t_m < \tau \le t_{m+1} \mid X_s, s \le t_m)}{\mathbb{Q}\big(t_m < \tau \le t_{m+1}\big)}]. \end{aligned}$$

The expectation above can also be estimated (in an unbiased way) by averaging over all of the scenarios,

$$EE^*_{t_m,t_{m+1}} \approx \frac{1}{P}\sum_{p=1}^{P} E_{t_m}(x_m(p)) \frac{\mathbb{Q}(t_m < \tau \le t_{m+1} \mid X_s = x_s(p), s \le t_m)}{\mathbb{Q}\big(t_m < \tau \le t_{m+1}\big)}. \tag{4.10}$$

If we assume the stochastic hazard rate is a function of X_m, $\lambda(X_m)$, then we can derive the following approximation,

$$\begin{aligned} \mathbb{Q}(t_m < \tau \le t_{m+1} \mid X_s = x_s(p), s \le t_m) &= \mathbb{E}^{\mathbb{Q}}[\exp(-\int_0^{t_m} \lambda(X_u)\mathrm{d}u) \\ &\quad - \exp(-\int_0^{t_{m+1}} \lambda(X_u)\mathrm{d}u) \mid X_s = x_s(p), s \le t_m] \\ &= \exp(-\int_0^{t_m} \lambda(x_u(p))\mathrm{d}u) \\ &\quad \times \mathbb{E}^{\mathbb{Q}}[1 - \exp(-\int_{t_m}^{t_{m+1}} \lambda(X_u)\mathrm{d}u) \mid X_s = x_s(p), s \le t_m] \\ &\approx \exp\big(-\sum_{i=1}^{m} \lambda(x_i(p))\Delta t\big)\lambda(x_m(p))(t_{m+1} - t_m), \end{aligned}$$

and

$$\begin{aligned}\mathbb{Q}(t_m < \tau \le t_{m+1}) &= \mathbb{E}^{\mathbb{Q}}[\mathbb{Q}(t_m < \tau \le t_{m+1} \mid X_s, s \le t_m)] \\ &\approx \frac{1}{P}\sum_{p=1}^{P} \exp\big(-\sum_{i=1}^{m} \lambda(x_i(p))\Delta t\big)\lambda(x_m(p))(t_{m+1}-t_m),\end{aligned}$$

then we have the following equation,

$$\frac{\mathbb{Q}(t_m < \tau \le t_{m+1} \mid X_s = x_s(p), s \le t_m)}{\mathbb{Q}\big(t_m < \tau \le t_{m+1}\big)} \approx \frac{\exp\big(-\sum_{i=1}^{m} \lambda(x_i(p))\Delta t\big)\lambda(x_m(p))P}{\sum_{p=1}^{P}\exp\big(-\sum_{i=1}^{m} \lambda(x_i(p))\Delta t\big)\lambda(x_m(p))}. \tag{4.11}$$

Substitute (4.11) into formula (4.10), we can get,

$$EE^*_{t_m,t_{m+1}} \approx \frac{\sum_{p=1}^{P} E_{t_m}(x_m(p))\exp\big(-\sum_{i=1}^{m} \lambda(x_i(p))\Delta t\big)\lambda(x_m(p))}{\sum_{p=1}^{P}\exp\big(-\sum_{i=1}^{m} \lambda(x_i(p))\Delta t\big)\lambda(x_m(p))}.$$

□

The numerical tests show us that, compared with the approximation in the proposition above, the following simplified approximation makes little difference for the results of CVA,

$$EE^*_{t_m,t_{m+1}} \approx \frac{\sum_{p=1}^{P} E_{t_m}(x_m(p))\lambda(x_m(p))}{\sum_{p=1}^{P}\lambda(x_m(p))}, \tag{4.12}$$

which can be easily used in practice. For ease of exposition, in the later section with numerical examples, we will use this simplified approximation to explain the numerical results. Formula (4.12) represents an average value of E_{t_m} over all of the paths, but with different weights

$$\frac{\lambda(x_m(p))}{\sum_{p=1}^{P}\lambda(x_m(p))},$$

for different paths p. The path with a higher hazard rate will get a larger weight, which leads to the difference between $EE^*_{t_m,t_{m+1}}$ and EE_{t_m}.

Remark 4.4.1. *In the trivial case of no wrong way risk (and right way risk), where the hazard rate λ is not related to $x_m(p)$, we have*

$$EE^*_{t_m,t_{m+1}} \approx \frac{1}{P}\sum_{p=1}^{P} E_{t_m}(x_m(p))$$

which is equal to EE_{t_m}.

4.4.2 Empirical Analysis Approach

The computation of $EE^*_{t_m,t_{m+1}}$ in (4.9) requires the knowledge of function $\lambda(X(t))$. In this section, we consider possible methods to find an explicit function form of the hazard rate, $\lambda(X(t))$. The hazard rate represents the relationship between the hazard rate of the counterparty and the underlying variable (or variables) $X(t)$. To find an analytical approximation formula of $\lambda(X(t))$, the following two approaches can be used,

- Empirical analysis approach (EAA) [55]. In the case of Bermudan equity put options, $X(t)$ is the counterparty's stock price. The functional form of $\lambda(X(t))$ is estimated by empirical data of hazard rate and the stock price of the counterparty.

- Portfolio value approach (PVA) [37]. Note that the portfolio value $V(t)$ at state $(t, X(t))$ is a function of $X(t)$, i.e., $V(t) = g(X(t))$ or $X(t) = g^{-1}(V(t))$. Instead of finding the relationship between hazard rate and $X(t)$, one can also try to find the relationship between hazard rate and $V(t)$, i.e.,

$$\lambda(g^{-1}(V(t))) = \widetilde{\lambda}(V(t)).$$

Here we use a simplified notation $\widetilde{\lambda}(V(t))$ to denote that $\lambda(g^{-1}(V(t)))$ is a function of $V(t)$.

Remark 4.4.2. *An alternative approach mentioned in [37] is to find the relationship between the hazard rate and the portfolio's exposure $E_t = \widetilde{g}(X(t))$. However, as we will see in the Bermudan option example, $\widetilde{g}$ is not invertible, because in the case of $E_t = 0$, more than one $X(t)$ exists. This may explain why this method does not work as well as PVA [37].*

We first consider PVA. PVA is a straightforward method in the sense that it directly gives the dependence between a counterparty's default probability and the portfolio value which is closely related to the credit exposure. In [37], the authors postulate a functional form of $\widetilde{\lambda}(V(t))$,

$$\widetilde{\lambda}(V(t)) = \exp\big(a(t) + bV(t)\big), \tag{4.13}$$

where $a(t)$ is a function of time. b is a constant parameter that measures the amount of wrong or right way risk in the model. In the case of wrong way risk, b is positive and $\widetilde{\lambda}(V(t))$ is an increasing function of $V(t)$.

The calibration method of model (4.13) is given in [37]: first of all, b has to be estimated properly; secondly, $a(t)$ is determined by incorporating the credit spreads observed today into the model. Particularly, parameter b can be estimated by two different approaches,

- collecting historical data of $V(t)$ and credit spreads of the counterparty. The credit spread can be converted into a hazard rate and b then can be estimated. However, for different portfolios (such as Bermudan option $V_1(t)$, barrier option $V_2(t)$, lookback option $V_3(t)$, etc.), different data is needed, which makes the estimation inconvenient; and if data with high quality is not available, the estimation will be unstable.

- or giving a subjective judgement about the amount of right way or wrong way risk the counterparty has [37]. Although this method is straightforward and easy to implement, it may be difficult to justify the subjective judgment which is just a manager's view.

To have a convenient and stable calibration and get rid of subjective judgment as much as possible, while, importantly, taking into account the market data and observed market behaviour, particularly in the set up of the Bermudan option example, EAA could be a suitable alternative.

The fundamental reason of using EAA is that, the evidence of a clear (negatively related) dependence structure between the equity price $S(t)$ and the default probability is quite rich both in academics and in industry. When the stock price of the counterparty falls, its return volatility σ often increases [20]. A traditional explanation that dates back to Black (1976) is the leverage effect [6]. So long as the face value of debt is not adjusted, a falling stock price increases the company's leverage and hence its risk, which shows up in the stock return volatility [3]. As the return volatility increases, the credit spread of the company will also increase; This is because credit spreads of a company are positively related to the equity return volatilities of the same company [4]. The conclusion is that, if we convert the credit spread into a hazard rate, then the stock price is negatively related to the hazard rate. Evidence from industry also confirms this dependence, see [55]. In figure 4.1, we give an example of Allianz SE-REG from [55]. The application of this relationship can be found in Duffie and Singleton (2003, p. 206) [26], Linetsky (2006) [43], Carr and Linetsky (2006) [18], and Carr and Madan (2010) [19].

This dependence between $S(t)$ and the default probability can be described in the hazard rate function $\lambda(S(t))$. To describe the counterparty's default probability, we use the one year average hazard rate, which represents the market's view on the short term default probability. The one year average hazard rate can be estimated by a well-known formula,

[3] Various other explanations have also been proposed in the literature; for example, Haugen, Talmor, and Torous (1991) [34], Campbell and Hentschel (1992) [14], Campbell and Kyle (1993) [15], Bekaert and Wu (2000) [4], and Carr and Wu (2011) [21].

[4] In [20], the authors use this issue for modeling; the evidence of this issue from literature can be found in, for example, Collin-Dufresne, Goldstein, and Martin (2001) [24], Campbell and Taksler (2003) [16], Baskshi, Madan, and Zhang (2006) [2], and Zhu, Zhang, and Zhou (2005) [61].

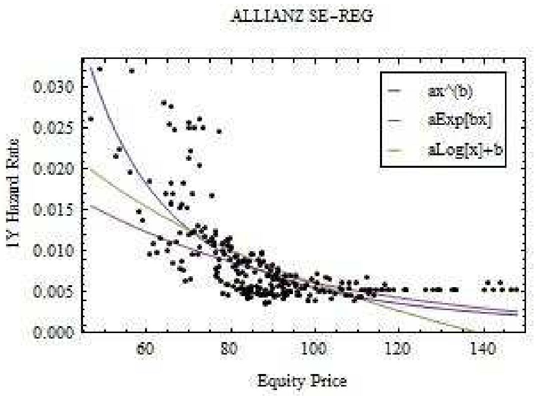

Figure 4.1: Empirical data from [55]: dependence between one year hazard rate and equity price of Allianz SE-REG

$$\lambda_t \approx \frac{c(t)}{1-\delta},$$

with $c(t)$ the one year par credit spread, which is embedded in the one year CDS prices.

Here we use a negative power functional form of $\lambda(S(t))$, i.e.,

$$\lambda(S(t)) = AS(t)^B,$$

where A and B are constant parameters that can be estimated by a least squares linear regression method. In the case of Allianz SE-REG, the calibration results given in [55] give us,

$$\widehat{\lambda}(S(t)) = 230S(t)^{-2.3}. \tag{4.14}$$

Using formula (4.14), the hazard rate for each simulated state can be calculated. After knowing E_{t_m} for each simulated state, the calculation of the expected exposure with wrong way risk $EE^*_{t_m,t_{m+1}}$ is completed by substituting the hazard rate of each simulated state into formula (4.9).

4.4.3 Counterparty's Default Probability in EAA

In the example of Allianz SE-REG, let λ_{mp} denote the hazard rate $\lambda(s_m(p))$ calculated by formula (4.14), where $s_m(p)$ is the simulated stock price on the pth path, at time t_m, $p = 1, ..., P, m = 1, ..., M$. Then the survival function (4.3)

$$S_{ur}(t_m) = \mathbb{E}^{\mathbb{Q}}[\exp(-\int_0^{t_m} \lambda_u \mathrm{d}u)],$$

can be approximated by

$$S_{ur}(t_m) \approx \frac{1}{P}\sum_{p=1}^{P}[\exp\big(-\sum_{i=1}^{m}\lambda_{ip}\Delta t\big)]. \tag{4.15}$$

Given the simulation results of the hazard rate, the default probability,

$$S_{ur}(t_{m-1}) - S_{ur}(t_m),$$

during the time interval $\big(t_{m-1}, t_m\big)$ can be estimated by formula (4.15).

4.4.4 Comparison of EAA and PVA

It is interesting to have a comparison of EAA and PVA. It is reasonable to expect that, for the same portfolio and the same counterparty, the results of CVA from EAA and PVA should be the same. In appendix 4.8.1, we find an 'objective estimation' of b in the PVA approach, by using the equivalence of CVA results from EAA and PVA. This objective estimation can be used to compare with a manager's 'subjective judgement' of b (if it is not estimated by empirical data). In the example of Allianz SE-REG, through our approach, we find the value of $b \approx 0.0598$.

4.5 Computation Method

In this section, we first calculate the credit exposure of a Bermudan option under a GBM process by a combination of Monte Carlo simulation and the Fourier COS method [27], which is named Monte Carlo-COS method (MC-COS) in chapter 2. Based on the results of credit exposure, the WWR EE is then calculated by EAA. In the end, the calculation of CVA of the Bermudan option is completed by combining the results of WWR EE with the default probability estimated by EAA.

There are three main components in the Monte Carlo-COS method for WWR EE and CVA calculation:

1. Scenario generation for the future economic state under measure $\mathbb{Q}$ (For CVA computation, the expected exposure is proposed to be calculated under the risk neutral measure $\mathbb{Q}$, see formula (4.6) and [9].);

2. Computation of portfolio value (and credit exposure) for each simulated state by the COS method;

3. Computation of WWR EE and CVA.

The technical details of MCCOS can be found in chapter 2.

In summary, the following formula

$$\text{CVA}_W \approx (1-\delta)\sum_{m=1}^{M} D(0,t_{m-1})EE^*_{t_{m-1},t_m}\big(S_{ur}(t_{m-1})-S_{ur}(t_m)\big), \qquad (4.16)$$

will be used for the CVA computation of Bermudan options with wrong way risk.

First of all, we use the hazard rate approach of proposition 4.4.1 to calculate $EE^*_{t_{m-1},t_m}$, which reads

$$EE^*_{t_{m-1},t_m} \approx \frac{\sum_{p=1}^{P} E_{t_{m-1}}(s_{m-1}(p))\exp\big(-\sum_{i=1}^{m-1}\lambda(s_i(p))\Delta t\big)\lambda(s_{m-1}(p))}{\sum_{p=1}^{P}\exp\big(-\sum_{i=1}^{m-1}\lambda(s_i(p))\Delta t\big)\lambda(s_{m-1}(p))},$$

or the simplified one,

$$EE^*_{t_{m-1},t_m} \approx \sum_{p=1}^{P} E_{t_{m-1}}\big(s_{m-1}(p)\big)\frac{\lambda\big(s_{m-1}(p)\big)}{\sum_{p=1}^{P}\lambda\big(s_{m-1}(p)\big)},$$

where the hazard rate function $\lambda\big(S(t)\big)$ is estimated by EAA. The exposure of each state, $E_{t_{m-1}}\big(s_{m-1}(p)\big)$, is calculated by the Monte Carlo-COS method.

Secondly, the counterparty's default probability in time interval $(t_{m-1},t_m]$,

$$S_{ur}(t_{m-1})-S_{ur}(t_m),$$

can be estimated as,

$$\frac{1}{P}\sum_{p=1}^{P}[\exp\big(-\sum_{i=1}^{m-1}\lambda_{ip}\Delta t\big)]-\frac{1}{P}\sum_{p=1}^{P}[\exp\big(-\sum_{i=1}^{m}\lambda_{ip}\Delta t\big)],$$

with λ_{ip} the hazard rate $\lambda(s_i(p))$.

4.6 Numerical Examples

In this section, we use several numerical examples to show the impact of the early exercise feature and wrong way risk on CVA of Bermudan options.

Recalling the α multiplier approach in section 4.4.1 suggested by the Basel Committee, which is used as a basic way of taking into account the wrong way risk for the calculation of expected exposure and CVA,

$$EE^*_{t_{m-1},t_m} = \alpha EE_{t_{m-1}}. \tag{4.17}$$

The effect of this is to increase CVA by the α multiplier, $\text{CVA}_W = \alpha\text{CVA}_I$. Note that a constant $\alpha > 1$, which is usually used as a default value in a bank, implies that $EE^*_{t_{m-1},t_m} > EE_{t_{m-1}}$ and $\text{CVA}_W > \text{CVA}_I$.

We want to show that, however, if we use a more sophisticated and realistic method to model the wrong way risk, such as the hazard rate approach that we have proposed, the situation $EE^*_{t_{m-1},t_m} > EE_{t_{m-1}}$ and $\text{CVA}_W > \text{CVA}_I$ may be reversed. More precisely, the effect of wrong way risk on EE and CVA for Bermudan options depends on their early exercise features.

To expose the problem, in the example we assume the stochastic process of the underlying asset follows geometric Brownian motion under measure $\mathbb{Q}$,

$$\frac{\mathrm{d}S(t)}{S(t)} = r\mathrm{d}t + \sigma\mathrm{d}W^{\mathbb{Q}}(t). \tag{4.18}$$

The generalization of the stochastic process to any Lévy process is straightforward since the Monte Carlo-COS method can be applied when the underlying asset follows a Lévy process and can be simulated accurately. In the following sections, we first explain the relationship between the wrong way risk effect and the early exercise feature. Based on this explanation, we consider three different variables which are closely related to the early exercise features of the Bermudan option: (i) return volatility σ in formula (4.18), (ii) Bermudan option's strike price K, and (iii) the number of possible early exercise dates M, and investigate the impact of the change of these variables on the results of EE and CVA when wrong way risk is modeled by EAA.

To focus on the main discussion, we will not list the impact of collateral, although it is quite straightforward.

4.6.1 Wrong Way Risk and Early Exercise Feature

In this section, we show that the wrong way risk effect on CVA of a Bermudan option depends on its early exercise features.

We first consider the effect of the early exercise feature and wrong way risk on Bermudan option's EE. Figure 4.2 shows the risk profiles of EE of a Bermudan option by different approaches, i.e., the α multiplier approach and the hazard rate approach (EAA and PVA). For comparison, the expected exposure without wrong way risk of a European option ($M = 1$) is also provided.

The effect of the early exercise feature ($M > 1$) indicates that, compared with the European option's increasing EE,the Bermudan option's EE is a decreasing function of time t (see the risk profiles of Bermudan option's EE without

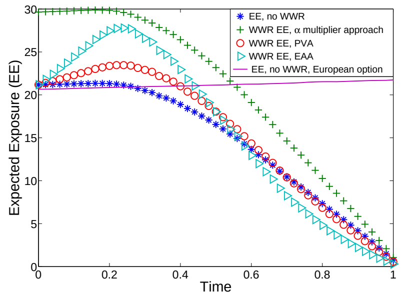

Figure 4.2: Different approaches for the expected exposure profile of a Bermudan option with $S_0 = K = 100, T = 1, \sigma = 0.6, M = 50, r = 0.05$: EE without WWR ('*'), WWR EE by hazard rate approaches (PVA ('o') and EAA ('$\triangleright$')), WWR EE by α multiplier approach ('+'), with $\alpha = 1.4$. Compared with the Bermudan option, the expected exposure profile of a European option ($M = 1$) without wrong way risk is an increasing line ('-').

wrong way risk in figure 4.2). This can be explained by the increasing exercise intensity (percentage of exercised paths) at each time step of Bermudan options, see figure 4.3. When more paths are exercised and the exposures on these paths become 0, the average value of the exposures on all of the paths,

$$EE_{t_m} \approx \frac{1}{P}\sum_{p=1}^{P} E_{t_m}(x_m(p)),$$

becomes smaller and approaches to 0.

The wrong way risk can also affect the shape of the Bermudan option's EE risk profile. In the examples of figure 4.2, compared with the EE without wrong way risk, the WWR EE which is calculated by EAA is higher at the beginning and then becomes lower. This can be explained by the hazard rate approach (EAA) for the calculation of WWR EE,

$$EE^*_{t_m,t_{m+1}} \approx \sum_{p=1}^{P} E_{t_m}\big(s_m(p)\big)\frac{\lambda\big(s_m(p)\big)}{\sum_{p=1}^{P}\lambda\big(s_m(p)\big)}. \tag{4.19}$$

At the beginning of the time period, for a fix time step, according to the negatively related dependence structure of the stock price and hazard rate, a simulated state with a low stock price implies a high hazard rate. However, the option value and exposure at this state will be high because it is a put option. It implies that a high (low) exposure $E_{t_m}\big(s_m(p)\big)$ will get a high (low) weight

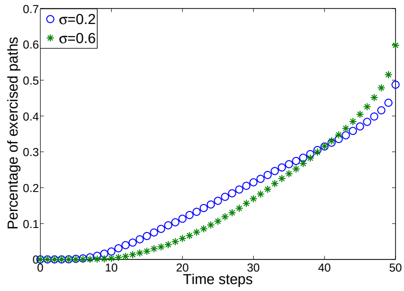

Figure 4.3: Exercise intensity of Bermudan option with different values of volatility σ of stock price, $S_0 = K = 100, T = 1, M = 50, r = 0.05$.

$\frac{\lambda\left(s_m(p)\right)}{\sum_{p=1}^{P}\lambda\left(s_m(p)\right)}$, which leads to $EE^*_{t_m,t_{m+1}} > EE_{t_m}$.

At the end of the time period, however, because of the early exercise feature, most of the paths have been exercised and the exposures on these paths become 0. Note that on these exercised paths, the stock prices tend to be lower than the ones on the non-exercised paths, which means that these exercised paths (with 0 exposure) get higher weights. In this situation, the value of $EE^*_{t_m,t_{m+1}}$ is pulled down and finally $EE^*_{t_m,t_{m+1}} < EE_{t_m}$.

In summary, because of the Bermudan option's early exercise feature, regarding the wrong way risk, if we use the hazard rate approach (EAA or PVA), then $EE^*_{t_m,t_{m+1}}$ (or $EE^*_{t_{m-1},t_m}$) is not necessarily greater than EE_{t_m} (or $EE_{t_{m-1}}$), which implies that the result of CVA with wrong way risk for a Bermudan option,

$$\text{CVA}_W \approx (1-\delta)\sum_{m=1}^{M} D(0,t_{m-1})EE^*_{t_{m-1},t_m}\big(S_{ur}(t_{m-1}) - S_{ur}(t_m)\big),$$

is not necessarily greater than the one without wrong way risk,

$$\text{CVA}_I \approx (1-\delta)\sum_{m=1}^{M} D(0,t_{m-1})EE_{t_{m-1}}\big(S_{ur}(t_{m-1}) - S_{ur}(t_m)\big).$$

On the other hand, if we use the α multiplier approach, with $\alpha > 1$, then $EE^*_{t_{m-1},t_m} > EE_{t_{m-1}}$ (see figure 4.2) and $\text{CVA}_W > \text{CVA}_I$ always holds.

Remark 4.6.1. *The analysis above works in the same way for PVA.*

The following numerical examples show that the decrease of $EE^*_{t_m,t_{m+1}}$ is faster with a higher exercise intensity, which may lead to $\text{CVA}_W < \text{CVA}_I$.

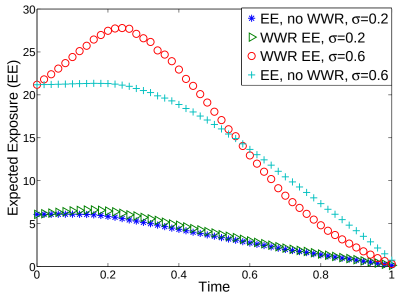

Figure 4.4: Decrease of EE with different values of volatility σ: the expected exposure profile of the Bermudan option with different values of $\sigma = 0.2$ or 0.6, $S_0 = K = 100$, $T = 1, M = 50, r = 0.05$. Wrong way risk is modeled by EAA.

4.6.2 Volatility σ

In this section, we explain the impact of the change of volatility σ (in formula (4.18)) on the Bermudan option's EE and CVA.

First, we consider the relation between volatility σ and the early exercise feature of a Bermudan option. Figure 4.3 illustrates the exercise intensity of the Bermudan option with different values of σ. When approaching to maturity time, the exercise intensity with volatility $\sigma = 0.6$ becomes higher than the one with volatility $\sigma = 0.2$. This implies that with $\sigma = 0.6$, we will get a higher percentage of exercised paths and 0 exposures than in the case of $\sigma = 0.2$.

Figure 4.4 provides a comparison of the decrease of $EE^*_{t_m,t_{m+1}}$ with $\sigma = 0.2$ and 0.6. With $\sigma = 0.6$, because of a higher percentage of 0 exposures, the decrease of $EE^*_{t_m,t_{m+1}}$ is faster than in the case of $\sigma = 0.2$, which increases the part for which $EE^*_{t_m,t_{m+1}} < EE_{t_m}$. The part of $EE^*_{t_m,t_{m+1}} < EE_{t_m}$ pulls down the value of CVA$_W$, which may lead to CVA$_W <$ CVA$_I$.

Figure 4.5 illustrates the values of CVA$_W$ and CVA$_I$ with respect to the values of σ. Both CVA$_W$ and CVA$_I$ are increasing functions of σ. This is because of the increase of EE with respect to the increase of σ [5], as shown in figure 4.4. In this experiment, with volatility $\sigma = 0.2$, we have CVA$_W >$ CVA$_I$. However, when σ is increasing, we observe that CVA$_I$ increases faster than CVA$_W$ and in the end we will get CVA$_W <$ CVA$_I$ (for example, when $\sigma = 0.8$).

[5] In EAA, the change of σ will also affect the default probability, however, the increasing effect on EE will dominate the increasing of CVA.

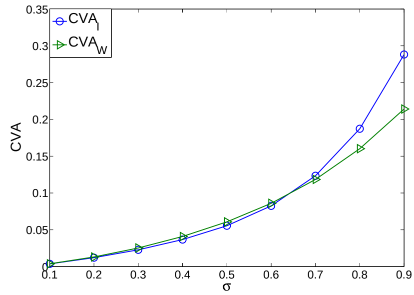

Figure 4.5: The wrong way risk effect (i.e., the difference between CVA_W and CVA_I) on Bermudan option's CVA depends on volatility σ, where $S_0 = K = 100, T = 1, M = 50, r = 0.05$. CVA is an increasing function of σ. We subdivide the time interval in 100 time steps. The wrong way risk is modeled by EAA.

4.6.3 Strike Price K

The variation of strike price K can also affect the exercise intensity of Bermudan options, and finally affects the results of EE and CVA as well.

As illustrated in figure 4.6, compared with the at-the-money option ($K = 100$), with the same initial stock price and all the other parameters identical, an in-the-money put option ($K = 110$) has higher exercise intensity while an out-of-the-money put option ($K = 90$) has lower exercise intensity. As shown in figure 4.7, with the same initial stock price $S_0 = 100$, the Bermudan option's $EE^*_{t_m,t_{m+1}}$ with $K = 110$ decreases faster than the one with $K = 90$, which enlarges the part of $EE^*_{t_m,t_{m+1}} < EE_{t_m}$.

In figure 4.8 we show the change of CVA w.r.t strike price K. Both CVA_W and CVA_I are increasing when K is increasing; this is because of the increase of EE with increasing K, see figure 4.7. Further more, with different strike price, the relationship between CVA_W and CVA_I can change. In this example, if $K = 90$, $\text{CVA}_W > \text{CVA}_I$ holds. When $K = 110$, since the part of $EE^*_{t_m,t_{m+1}} < EE_{t_m}$ pulls down the value of CVA_W, we will get $\text{CVA}_W < \text{CVA}_I$.

4.6.4 Early Exercise Rights M

Intuitively, a higher value of M provides the contract holder a more flexible choice to exercise the contract and 'hedge' the counterparty's default risk. In the extreme case, when $M = 1$, the EE of a European option is always increasing. When $M > 1$, because of the effect of the early exercise feature, EE is decreasing.

In figure 4.9, we show the risk profiles of EE with $M = 10$. For discretiza-

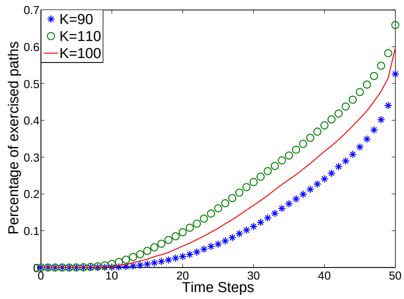

Figure 4.6: Exercise intensity of the Bermudan option with different values of strike price K, with $S_0 = 100$, $\sigma = 0.6$, $T = 1, M = 50, r = 0.05$.

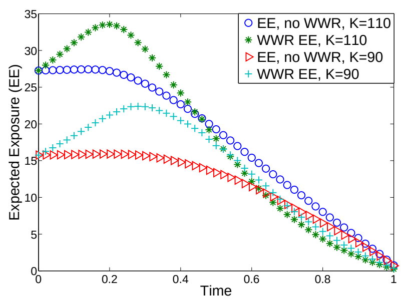

Figure 4.7: Comparison of EE without WWR and with WWR by EAA: the expected exposure profile of a Bermudan option with different strike prices (i.e., out-the-money and in-the-money) $K = 90$ or 110, $S_0 = 100$, $\sigma = 0.6$, $T = 1, M = 50, r = 0.05$.

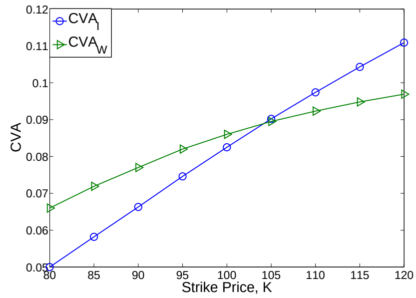

Figure 4.8: The wrong way risk effect on Bermudan option's CVA depends on the strike price K, where $S_0 = 100$, $\sigma = 0.6$, $T = 1, M = 50, r = 0.05$. CVA is an increasing function of K. We discretize the time interval by 100 time steps. The wrong way risk is modeled by EAA.

M	1	2	5	10	20	25	50
CVA$_I$	0.1724	0.1269	0.1070	0.1008	0.0980	0.0978	0.0967
CVA$_W$	0.3190	0.1623	0.1159	0.1036	0.0983	0.0977	0.0958

Table 4.1: CVA w.r.t different values of M

tion, we use 50 time points. It is worth mentioning that a discretization with a small time step is important for an accurate calculation of CVA. This is because of the 'zigzag' shape of EE for Bermudan options (see figure 4.9). Particularly, between two consecutive possible exercise dates, the option can be seen as a European option which has an increasing EE; however, at the time point immediately after one exercise date, because of the 0 exposures on the exercised paths, a 'jump' to a lower EE occurs.

With a fixed discretization of 100 time points[6], we calculate the CVA$_W$ and CVA$_I$ with different values of M. The change of CVA$_W$ and CVA$_I$ w.r.t to the values of M is shown in figure 4.10 and table 4.1. Different from the case of σ or K, both CVA$_W$ and CVA$_I$ are decreasing functions of M; this is because of the decrease of EE w.r.t the increase of M, see figure 4.9 for a comparison of risk profiles of EE with $M = 1$ and $M = 10$. The comparison of CVA$_W$ and CVA$_I$ is similar as in the case where σ or K changes. Our experiments show that when $M = 1$, we have CVA$_W$ $>$ CVA$_I$; it will become CVA$_W$ $<$ CVA$_I$ when $M > 25$.

[6]The possible exercise dates have been taken into account already.

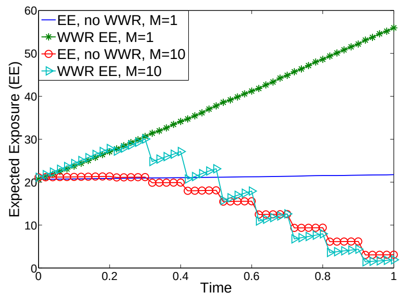

Figure 4.9: Comparison of EE without WWR and WWR EE by EAA: the expected exposure profiles of Bermudan options with different numbers of early exercise opportunities, $M = 1$ (European option) or $M = 10$, $K = S_0 = 100$, $\sigma = 0.6$, $T = 1$, $r = 0.05$. We use 50 time points for discretization of $[0, 1]$.

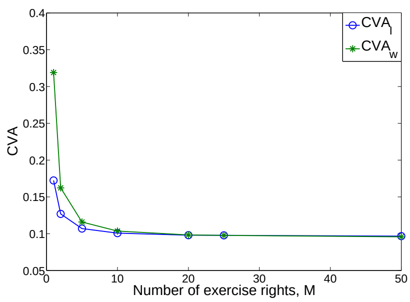

Figure 4.10: The wrong way risk effect on Bermudan option's CVA depends on the number of possible early exercise dates M, where $S_0 = 95$, $K = 100$, $\sigma = 0.6$, $T = 1$, $r = 0.05$. CVA is a decreasing function of M. We discretize the time interval by 100 time steps. The wrong way risk is modeled by EAA.

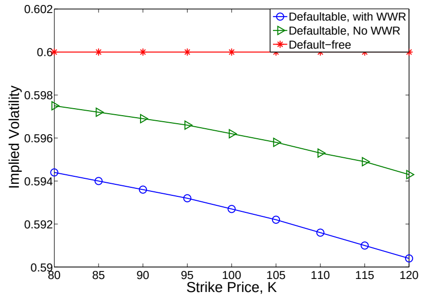

Figure 4.11: Implied volatility skew of a defaultable European put option.

4.6.5 Change of Implied Volatility

When CVA is taken into account for pricing a European put option, the implied volatility will change. Figure 4.11 plots the option implied volatilities against different strike prices of an option under the GBM model, with $S_0 = 100$, $\sigma = 0.6$, $T = 1$, $r = 0.05$. We discretize the time interval by 100 time steps. The implied volatilities are obtained by first computing the risky value of the put option under counterparty credit risk, $\widetilde{V}(s) = V(s) - \text{CVA}(s, T)$, for a given strike price, with $s = 0$, and then implying the Black-Scholes implied volatility. Compared with the trivial case of a no-default option, which has a constant implied volatility under the GBM model, the defaultable option has an implied volatility skew. Particularly, when wrong way risk is taken into account, the skew becomes lower and the impact is significant. The results imply a connection between the implied volatility skew and counterparty's default risk.

4.7 Conclusion

To analyze the effect of wrong way risk on CVA, this chapter provides the example of Bermudan options. Since no explicit pricing formula exists for Bermudan options, we propose an efficient numerical method which is based on Monte Carlo simulation and a Fourier inverse option pricing method. The method is applicable for Lévy processes. To incorporate the wrong way risk, we apply the technique from John Hull and Alan White and model the hazard rate of the counterparty as a function of the counterparty's equity price. The analysis from the numerical experiments implies that, in the example of Bermudan options, the wrong way risk effect depends on its early exercise features. With a high exercise intensity for Bermudan options, which is caused by, for example, high volatility of the stock price process, high strike price, or high number of possible early exercise dates, the value of CVA with wrong way risk (i.e., CVA_W) can be smaller than the value of CVA when wrong way risk is not considered (i.e., CVA_I). Note that if one uses the α multiplier approach, with $\alpha > 1$, then $\text{CVA}_W > \text{CVA}_I$ always holds. We also have compared two different methods for wrong way risk modeling.

The current work can be extended to the situation where the underlying asset of the option is different from the counterparty's stock. Apart from the counterparty's default risk, the default risk from the underlying asset can also be considered. Another possible extension is to consider the high-dimensional case, i.e., the option is written on multiple assets, see chapter 5.

4.8 Appendix

4.8.1 Comparison of Empirical Analysis Approach (EAA) and Portfolio Value Approach (PVA)

In EAA, the explicit formula of $\lambda(X(t))$, where $X(t)$ are the underlying risk factors, is estimated by using empirical data of a counterparty's hazard rate λ_t and $X(t)$. For a Bermudan equity put option written on the counterparty's stock, $X(t)$ is the counterparty's stock price S_t. We further assume a functional form of $\lambda(X(t))$ as follows,

$$\lambda(S_t) = AS_t^B, \tag{4.20}$$

where A and B are constant parameters. Based on the empirical data of the counterparty's one-year hazard rate (estimated from one-year CDS prices) and its historical stock prices, parameters A and B can be estimated by the least squares linear regression method.

In PVA, the hazard rate is represented as a function of the portfolio value $V(t)$. Note that the portfolio value $V(t)$ at state $(t, X(t))$ is a function of $X(t)$, i.e., $V(t) = g(X(t))$ or $X(t) = g^{-1}(V(t))$, where g is invertible. The hazard rate $\lambda(X(t))$ can be written as follow,

$$\lambda(X(t)) = \lambda(g^{-1}(V(t))) = \widetilde{\lambda}(V(t)).$$

Here we use a simplified notation $\widetilde{\lambda}(V(t))$ to denote that $\lambda(g^{-1}(V(t)))$ is a function of $V(t)$. In [37], the authors assume a functional form of $\widetilde{\lambda}(V(t))$ in the following way,

$$\widetilde{\lambda}(V(t)) = \exp\big(a(t) + bV(t)\big), \tag{4.21}$$

where $a(t)$ is a function of time; b is a constant parameter that measures the amount of wrong or right way risk in the model, particularly, in the case of wrong way risk, b is positive and $\widetilde{\lambda}(V(t))$ is an increasing function of $V(t)$.

The calibration of $\widetilde{\lambda}(V(t))$ requires the estimates of parameters $a(t)$ and b. In the main text we have discussed the estimation of b. In the simulation framework, we denote the simulation trials of hazard rate as follows,

$$\widetilde{\lambda}_{m,p} = \exp\big(a(t_m) + bV_{m,p}\big),$$

where $\widetilde{\lambda}_{m,p}$ and $V_{m,p}$ are simulation results of $\widetilde{\lambda}(V(t))$ and $V(t)$ at time step t_m, $m = 1, ..., M$, on simulation path p, $p = 1, ..., P$.

We further require [37] that

$$\frac{1}{P}\sum_{p=1}^{P} \exp\big(-\sum_{m=1}^{k} \widetilde{\lambda}_{m,p}\Delta t\big) = \exp\big(-\frac{c_k t_k}{1-\delta}\big), \text{for } 1 \leq k \leq M, \tag{4.22}$$

where c_k is the credit spread for a maturity of t_k. Equation (4.22) means that the average survival probability up to t_k, across all simulations, equals the survival probability inferred from the term structure of the credit spreads [37]. The formula of CVA without wrong way risk can be written as,

$$\begin{aligned}
\text{CVA}_I &\approx (1-\delta)\sum_{m=1}^{M} D(0,t_{m-1})EE_{t_{m-1}}\big(S_{ur}(t_{m-1}) - S_{ur}(t_m)\big) \\
&= (1-\delta)\sum_{m=1}^{M} D(0,t_{m-1})EE_{t_{m-1}}\big(\exp\big(-\frac{c_{m-1}t_{m-1}}{1-\delta}\big) - \exp\big(-\frac{c_m t_m}{1-\delta}\big)\big) \\
&= (1-\delta)\sum_{m=1}^{M} D(0,t_{m-1})EE_{t_{m-1}}\big(\exp\big(-\frac{\overline{c}t_{m-1}}{1-\delta}\big) - \exp\big(-\frac{\overline{c}t_m}{1-\delta}\big)\big),
\end{aligned} \tag{4.23}$$

where the last equality comes from an assumption of the same credit spread $\overline{c}$ for all maturities.

Credit spread $\overline{c}$

It is reasonable to expect that for the same portfolio and the same counterparty, the result of CVA from EAA and PVA should be the same. If we take the Bermudan put option as an example and denote the results from EAA as CVA_I^e and CVA_W^e, the results from PVA as CVA_I^p and CVA_W^p, then an equivalent relationship between EAA and PVA should hold as follows,

$$\text{CVA}_I^e = \text{CVA}_I^p, \tag{4.24}$$

and

$$\mathrm{CVA}_W^e = \mathrm{CVA}_W^p. \tag{4.25}$$

Equation (4.23) implies that CVA_I is a function of $\overline{c}$, i.e., $\mathrm{CVA}_I^e = \mathrm{CVA}_I^p = F(\overline{c})$, where F is a short notation for formula (4.23). Based on the values of CVA_I^e from EAA, we can estimate $\overline{c}$ by solving the equation $\mathrm{CVA}_I^p = F(\overline{c})$.

Estimation of b

In order to provide an 'objective estimate' of b in (4.21), we assume that the results of CVA by EAA (CVA_I^e and CVA_W^e) are from an objective market point of view. We are interested in the value of b if both (4.24) and (4.25) hold (or the results are as close as possible).

Note that given a value of $\overline{c}$, CVA_W^p is actually a function of b, i.e., $\mathrm{CVA}_W^p = G(b;\overline{c})$. More precisely, if b and $\overline{c}$ are known, the values of $a(t_k)$ for $1 \leq k \leq M$ can be determined sequentially. First, k is set to be 1. Based on the results of $V_{1,p}$, $p = 1, ..., P$, $a(t_1)$ can be determined by solving equation (4.22) with $k = 1$. After $a(t_1)$ is known, $\widetilde{\lambda}_{1,p}$ can be calculated. Second, k is set to be 2. Based on the values of $V_{2,p}$ and $\widetilde{\lambda}_{1,p}$, $a(t_2)$ can be determined. It also determines the $\widetilde{\lambda}_{2,p}$, and so on. When the values of $\widetilde{\lambda}_{m,p}$ are determined, the value of CVA_W^p can be calculated. An example of this calibration procedure can be found in the appendix of [37].

In summary, given a value of $\overline{c}$, an 'objective estimate' of b can be obtained by solving equation $\mathrm{CVA}_W^p = G(b;\overline{c})$, where the values of CVA_W^p are equal to the values of CVA_W^e obtained from EAA. Here we use G to denote the computation of CVA based on the calibration procedure described above.

Numerical test

We take the empirical data of Allianz SE-REG as an example (see figure 4.1) for the calculation of CVA_I^e and CVA_W^e. We choose the portfolio to be a Bermudan put option, with $M = 50$ exercise rights, $S_0 = 100$, $\sigma = 0.6$, $T = 1$, and we discretize the time interval by 50 steps (i.e., the same as the possible exercise dates). We use the calibration procedure discussed above for PVA. By using equation (4.24), we first invert the credit spread $\overline{c}$. Based on the results of $\overline{c}$ and equation (4.25), we can estimate the value of b as explained above. In table 4.2, we provide the estimates of $\overline{c}$ and b for options with different strike prices K. If we take an average of all of the b-values, then $\overline{b} = 0.0598$.

K	80	85	90	95	100
$\overline{c}$	0.00607	0.00602	0.005955	0.0059	0.00585
b	0.095	0.08	0.065	0.036	0.014

Table 4.2: Estimates of $\overline{c}$ and b for Bermudan options with different strike prices K.

K	105	110	115	120
$\overline{c}$	0.005795	0.00574	0.005685	0.005635
b	0.065	0.063	0.061	0.059

Table 4.3: Estimates of $\overline{c}$ and b for Bermudan options with different strike prices K.

Chapter 5

Credit Value Adjustment with Wrong Way Risk for Multi-asset Options

5.1 Introduction

This chapter is an extension of the work in the chapters 3 and 4. Recalling that, in chapter 3, we have discussed efficient computation methods for the exposure profiles of multi-asset instruments. And in chapter 4, we switched from the exposure profiles computation to CVA in the one-dimensional case, which is based on the risk neutral pricing technique of counterparty credit risk. In this chapter, we combine the methods used in chapters 3 and 4 to provide an efficient computation of CVA for multi-asset instruments, which is the final task in this thesis.

A general risk-neutral Monte Carlo simulation approach for CVA computation (or the market value of credit risk) can be found in Canabarro and Duffie (2003) [17]. As pointed out in [17], the traditional exposure framework discussed in chapter 3 takes a static buy-and-hold view of counterparty risk, without incorporating the possibility of dynamic hedging of credit risk. However, because of the expansion of the credit derivatives markets, 'liquid' counterparty risk becomes hedgeable which causes a fundamental change in the perception and management of these risks. To hedge the counterparty risk, an accurate pricing is very important, and is the first line of defense in credit risk management. For example, underestimation of the market value of a counterparty's default risk may bias prices which will *accumulate* larger risks with that counterparty. Then potentially large hidden losses may come to light at unfavorable events. Thus, in order to provide proper incentives to traders, the pricing of counterparty credit risk should be *accurate*.

However, because of the complexity of CVA, the computation can be very expensive, especially for multi-asset portfolios. Related literature, such as Pierre Henry-Labordère (2012) [35], proposed a marked branching diffusion approach which can deal with multi-asset portfolios. American options are also discussed. In addition, the author points out that accurate modeling of dependence between the underlying risk factors and the counterparty's hazard rate (or stochastic intensity) is a key issue in CVA computation, however, it is not addressed in [35].

This chapter aims to propose an efficient computation method for CVA of multi-asset (European and Bermudan type) options, while the correlation between the exposure and default risk is also included. The credit exposure of the multi-asset instruments is calculated by SGBM (see Jain and Oosterlee (2013) [39], Shen et al. (2014) [57]) introduced in chapter 3, and the dependence between the credit exposure and default risk is modeled by the hazard rate approach introduced in chapter 4. We give an efficiency comparison (accuracy, computation speed, and standard deviation of estimates) of different computation methods (SGBM, SRBM, and SRM) for CVA.

This chapter is structured in the following way. Section 5.2 gives the model specification of underlying assets and the model of the counterparty's default risk. Section 5.3 gives the algorithm and an example for single asset options. The effect of correlation between exposure and default risk on exposure profiles and CVA is also shown. Section 5.4 provides an efficiency comparison between different computation methods via various examples of multi-asset instruments. Section 5.5 discusses the effect of wrong way risk on CVA of multi-asset options. Section 5.6 gives conclusions.

5.2 Modeling Assumptions

We need to specify the multi-dimensional models of the underlying asset price processes of the derivative transaction. Different from the model assumptions in chapter 3, in this chapter, the modeling of the counterparty's default risk is required for CVA computation.

5.2.1 Multi-dimensional Models

For a derivatives transaction with multiple underlying assets $\mathbf{S}_t = \left(S_t^1, ..., S_t^d\right)$, and the counterparty's stock price S_t^c, we assume that each asset price is driven by a geometric Brownian motion,

$$\frac{\mathrm{d}S_t^i}{S_t^i} = (r - q_i)\mathrm{d}t + \sigma_i \mathrm{d}W^i(t), \quad i = 1, ..., d,$$
$$\frac{\mathrm{d}S_t^c}{S_t^c} = (r - q_c)\mathrm{d}t + \sigma_c \mathrm{d}W^{d+1}(t),$$

where each asset pays a dividend at a continuous rate of q_i or q_c, r is the risk free interest rate, and σ_i and σ_c are the volatility coefficients. The multi-dimensional process $\big(W^1(t), ..., W^d(t), W^{d+1}(t)\big)$ is $d+1$-dimensional Brownian motion under measure $\mathbb{Q}$. The instantaneous correlation coefficients between the increments of W^i and W^j are $\rho_{i,j}$, $i, j = 1, ..., d, d+1$. The increment of this process for time interval Δt is joint normally distributed,

$$\big(W^1(\Delta t), ..., W^d(\Delta t), W^{d+1}(\Delta t)\big) = L\big(Z^1, ..., Z^d, Z^{d+1}\big)$$

where $Z^1, ..., Z^d, Z^{d+1}$ are independent standard normal random variables. $LL^\top = \Sigma$ is the Cholesky decomposition of the symmetric positive definite $(d+1) \times (d+1)$ matrix Σ, with $\Sigma_{i,j} = \rho_{i,j}\Delta t$, $i, j = 1, ..., d, d+1$. For simplification, we assume that $\rho_{d+1,i} = \rho_c$, for $i = 1, ..., d$, which means the correlation coefficients between the counterparty's stock price and each underlying asset price are the same.

The credit exposure of the multi-asset instruments depends on the multiple underlying asset processes $\mathbf{S}_t = \big(S_t^1, ..., S_t^d\big)$. In chapter 3, we had a detailed discussion about the conditional expectations (or moments) calculation of functions of the underlying assets S_t^i, $i = 1, ..., d$. These results were found in table 3.1 of chapter 3 and will be used in CVA computation.

5.2.2 Hazard Rate Model

Recalling from chapter 4, section 4.3.2, we use the concept of a hazard rate process λ_t to represent the survival function and default probability of a counterparty. To take into account the dependence between the credit exposure and the counterparty's default risk, based on the technique of John Hull and Alan White (2012) [37], we need to specify the functional form of λ_t. We also have introduced two different approaches, EAA and PVA, to specify λ_t. We choose EAA and assume the functional form of the hazard rate as follows [26],

$$\lambda_t = \lambda(S_t^c) = A{S_t^c}^B,$$

where A and B are constant parameters, and S_t^c is the counterparty's equity price. This negative power functional form has been used by many authors to model the hazard rate, see a detailed explanation in section 4.4.2. Note that by specifying the hazard rate as a function the counterparty's stock price, because in the model setup S^c is correlated with the underlying asset prices of the derivative transaction, the hazard rate is correlated with the credit exposure which depends on the underlying asset prices. The calibration issue has been described briefly in chapter 4.

We follow the practical example given in chapter 4 and specify the hazard rate function as follows,

$$\widehat{\lambda}(S_t^c) = 230 S_t^{c-2.3}.$$

5.3 Computation Method

To calculate the exposure on time interval $[0, T]$, we first set up the vector of *observation dates* as $\mathcal{T} = \{t_1, ..., t_M\}$, with $0 = t_0 \leq t_1$ and $t_M = T$, which are assumed to be equally spaced, $t_m - t_{m-1} = \Delta t, m = 1, ...M$. For an accurate computation of CVA, the observation dates should be dense enough (such as monthly or weekly).

Following the discussion of chapter 4, the computation of CVA requires an calculation of the expected exposure conditional on default in time interval (t_{m-1}, t_m), i.e., $EE^*_{t_{m-1},t_m}$. The approximation of $EE^*_{t_{m-1},t_m}$ in the case of multi-asset underlying assets can be written as follows,

$$EE^*_{t_{m-1},t_m} \approx \frac{\sum_{p=1}^{P} E_{t_{m-1}}(\mathbf{s}_{t_{m-1}}(p)) \exp\big(-\sum_{i=1}^{m-1} \lambda(s^c_{t_i}(p))\Delta t\big) \lambda(s^c_{t_{m-1}}(p))}{\sum_{p=1}^{P} \exp\big(-\sum_{i=1}^{m-1} \lambda(s^c_{t_i}(p))\Delta t\big) \lambda(s^c_{t_{m-1}}(p))},$$

or the simplified version,

$$EE^*_{t_{m-1},t_m} \approx \sum_{p=1}^{P} E_{t_{m-1}}\big(\mathbf{s}_{t_{m-1}}(p)\big) \frac{\lambda\big(s^c_{t_{m-1}}(p)\big)}{\sum_{p=1}^{P} \lambda\big(s^c_{t_{m-1}}(p)\big)}. \tag{5.1}$$

5.3.1 Algorithm

Generally, the following algorithm can be used for the CVA computation under the multi-dimensional model assumptions:

1. Under the risk-neutral measure $\mathbb{Q}$, simulate the underlying asset price processes $\mathbf{S}_t$ and the counterparty's stock price process S_t^c in the multi-dimensional models.

2. Use an efficient computation method to get the sample results of exposure $E_{t_{m-1}}(\mathbf{s}_{t_{m-1}}(p))$ on each simulated grid point $(t_{m-1}, \mathbf{s}_{t_{m-1}}(p))$, $m = 1, ...M$.

3. Calculate the expected exposure conditional on default and the default probability in each time interval (t_{m-1}, t_m), by using the hazard rate of the counterparty $\lambda\big(s^c_{t_{m-1}}(p)\big)$;
4. Calculate CVA_W.

In chapter 3, we have introduced the *Stochastic Grid Bundling Method* (SGBM) [39] for an efficient computation of exposures of different multi-asset instruments. We found that in the case of high-dimensional underlying asset processes, by using a bundling technique, the accuracy of exposure profiles is improved significantly, and the computation speed is reasonably fast. Via various numerical examples, we showed the advantages of SGBM as follows: assuming that closed-form formulas or analytical approximations exist for the conditional expectations of the basis functions, then

- Compared with the *Standard Regression Bundling Method* (SRBM), when the same number of simulation paths, basis functions and bundles are used, the discontinuity of the conditional expectations at the boundaries of bundles in SGBM is generally smaller. And this discontinuity in SGBM can become very small by increasing the number of simulation paths and bundles appropriately.
- Compared with the *Standard Regression Method* (SRM) and SRBM, the numerical examples showed that SGBM has the advantage of smaller standard deviation for the direct estimates of option prices. This result is consistent with the conclusion of Glasserman and Yu (2004) [32], in which they theoretically prove the advantage of 'regression later' (used in SGBM) compared with 'regression now' (used in SRBM and SRM) under some conditions (such as *martingale basis functions*, etc.). Generally, the estimates of option prices of SGBM are closer to the reference results than SRM and SRBM. Even though the computation speed of SGBM is slower than SRBM and SRM, it is still efficient in practice.

In addition, we also show that for discontinuous payoffs, such as digital options, by using the bundling technique appropriately, SGBM can get accurate and stable results of option prices and exposure profiles.

In the following sections, we concentrate on the efficient computation of CVA for multi-asset Bermudan options and provide a comparison study of SGBM, SRBM, and SRM for this purpose. Technical details of these methods can be found in chapter 3.

5.3.2 Example of Single-asset Bermudan Options

To provide an efficiency comparison between SGBM and SRM, in this section, we consider a simple example where the derivative transaction is based on a

$s_0 = s_0^c = 40$	$K = 40$	$r = 0.06$	$q = q_c = 0$	$\sigma = \sigma_c = 0.2$
$\rho_c = 0.25$	$T = 1$	$M = 12$	observation dates $= 24$	

Table 5.1

single-asset Bermudan put option. Given the following model assumption,

$$\frac{\mathrm{d}S_t}{S_t} = (r - q)\mathrm{d}t + \sigma \mathrm{d}W^1(t),$$
$$\frac{\mathrm{d}S_t^c}{S_t^c} = (r - q_c)\mathrm{d}t + \sigma_c \mathrm{d}W^2(t),$$

where S_t represents the one-dimensional underlying asset of the Bermudan option, and S_t^c is the counterparty's stock price, we specify the parameters in table 5.1.

To obtain the value of CVA (including CVA$_W$ and CVA$_I$) and the direct estimator of the option price, we use 60000 simulation paths in both SGBM and SRM; and for the path estimators, 120000 simulation paths are generated. The standard deviations of the estimates (the numbers in the parentheses) are based on 30 independent simulation trials. For the regression approximation at time step t_m, basis functions $f_k(\mathbf{S}_{t_m}) = \mathbf{S}_{t_m}^{k-1}$, $k = 1, ..., 4$, are used in SGBM, while basis functions $\widetilde{f}_k(\mathbf{S}_{t_{m-1}}) = \mathbf{S}_{t_{m-1}}^{k-1}$, $k = 1, ..., 4$, are used in SRM. The analytical formulas of $\mathbb{E}^{\mathbb{Q}}[f_k(\mathbf{S}_{t_m}) \mid \mathbf{S}_{t_{m-1}} = \mathbf{s}_{t_{m-1}}(p)]$, which are used for the continuation value computation in SGBM, can be found in table 3.1. The reference results of CVA and option price are provided by the Fourier COS method combined with Monte Carlo simulation (20000 simulation paths) [28, 58].

As illustrated in table 5.2, by using the results of the COS method as a benchmark, the estimates of CVA (CVA$_W$ and CVA$_I$) and option prices (direct estimator and path estimator) from SGBM are better than SRM, and the standard deviations of the estimates of CVA and direct estimator are also smaller. Even though the computation speed of SGBM is a bit slower than SRM, it is reasonably fast. The smaller standard deviation of the estimates in SGBM is because of the moment computation in each bundle, which on the other hand makes the computation speed of SGBM somewhat slower than SRM.

The differences of the CVA computations in SGBM and SRM can be seen more explicitly from figure 5.1a, in which the expected exposures EE_{t_m} and PFE are plotted as functions of time (i.e., risk profiles). Compared with SRM,

Method	CVA_W	CVA_I	CPU time (secs)	Direct est.	Path est.
SGBM	0.0389 (0.0000559)	0.0379 (0.0000460)	2.1318	2.2972 (0.000146)	2.2979 (0.0055)
SRM	0.0437 (0.000404)	0.0430 (0.000365)	1.1319	2.3869 (0.0061)	2.2922 (0.0053)
COS	0.0389 (0.000105)	0.0379 (0.0000713)	4.2729	2.2973 (1.8616×10^{-14})	$-$

Table 5.2: CVA of single asset Bermudan options. Four basis functions are used in SGBM and SRM. The results from Monte Carlo-COS method [28, 58] (with 20000 simulation paths) are used as the reference numbers. CPU time represents the computation time of CVA (including CVA_W and CVA_I). The number in the parentheses is the standard deviation of the estimates.

the profiles generated by SGBM (o) are closer to the benchmark results by the COS method (*). This result gives evidence that a bundling technique can improve the accuracy of exposure profiles significantly.

Figure 5.1b shows that when more bundles are used, the CPU time for the CVA computation increases [1]. Figure 5.1c plots CVA_W as a function of the bundles, from which one can observe that CVA_W changes as the number of bundles increases from one to 32. With no more than 16 bundles, the value of CVA_W is reasonably close to the reference result.

Figure 5.1d provides a comparison of $EE^*_{t_{m-1},t_m}$ and $EE_{t_{m-1}}$. The volatility of the underlying stock price is $\sigma = 0.9$, while the volatility of the counterparty's stock price is $\sigma_c = 0.8$.

At the beginning of the time period, with a positive correlation, $\rho_c = 0.6$, the value of $EE^*_{t_{m-1},t_m}$ is greater than $EE_{t_{m-1}}$. This is because of the positive dependence between the exposure and counterparty's default risk (i.e., wrong way risk). As illustrated in formula (5.1), a higher probability weight (because of higher hazard rate) will be given to the higher exposure, which leads to a higher average value.

Then the value of $EE^*_{t_{m-1},t_m}$ becomes smaller than $EE_{t_{m-1}}$, which is caused by the early exercise feature of the Bermudan options. As more paths have been exercised and the exposures on these exercised paths become zero, the expected exposure $EE_{t_{m-1}}$ decreases. The same holds for $EE^*_{t_{m-1},t_m}$, which may decrease even faster because of the probability weight in formula (5.1).

The relationship between the correlation ρ_c and the value of CVA is shown in figure 5.2a and figure 5.2b. With low volatility coefficients $\sigma = 0.2, \sigma_c = 0.2$, the condition $\rho_c < 0$ implies right way risk, i.e., $\text{CVA}_W < \text{CVA}_I$, while the

[1] This will be different on a parallel computer, however, where computations in different bundles can be performed in parallel.

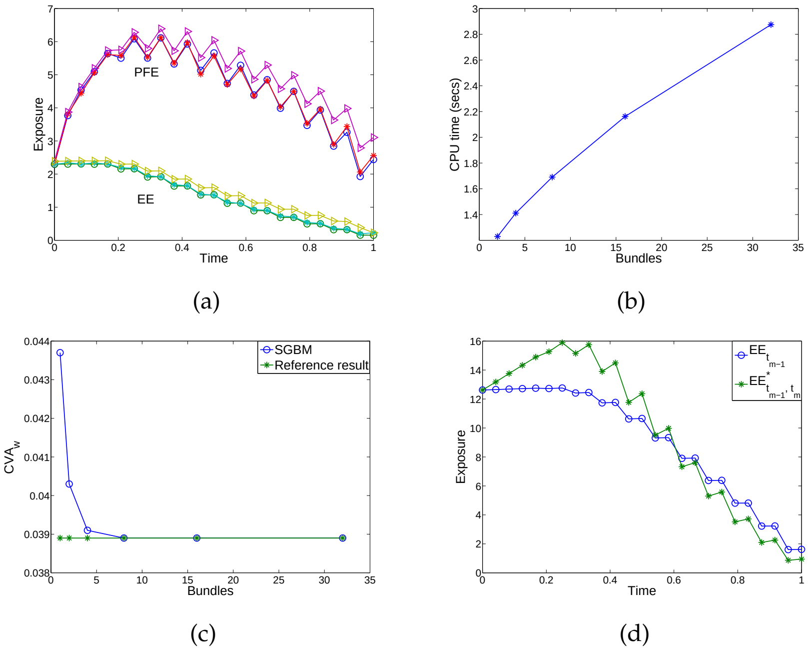

Figure 5.1: Single asset Bermudan options. (A) Comparison of SGBM with 16 bundles (o), COS (*), and SRM (△). Four basis functions are used in SGBM and SRM. High profile: 97.5% PFE. Low profile: EE. (B) SGBM: CPU time scale of CVA computation in number of bundles. (C) The value of CVA_W as a function of bundles. (D) Comparison of expected exposure conditional on default $EE^*_{t_{m-1},t_m}$ and $EE_{t_{m-1}}$, with volatility coefficients $\sigma = 0.9, \sigma_c = 0.8$, and the correlation coefficient $\rho_c = 0.6$.

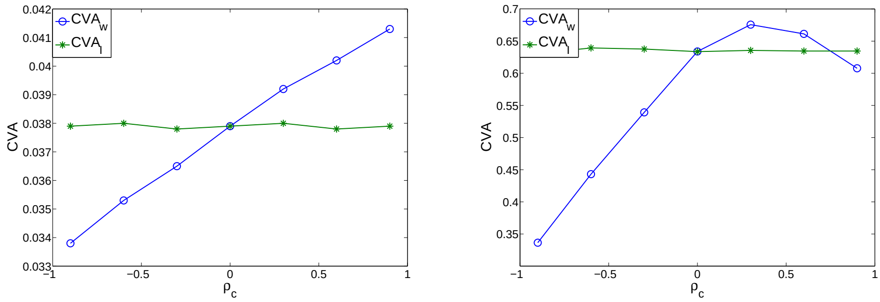

Figure 5.2: CVA of single-asset Bermudan put option as a function of the correlation ρ_c. The volatility coefficients of underlying asset and counterparty's equity price are (A) $\sigma = 0.2, \sigma_c = 0.2$ and (B) $\sigma = 0.9, \sigma_c = 0.8$.

condition $\rho_c > 0$ implies wrong way risk, i.e., $\text{CVA}_W > \text{CVA}_I$. However, with high volatility coefficients $\sigma = 0.9, \sigma_c = 0.8$, when ρ_c is positive and high enough, CVA_W can be smaller than CVA_I. This is because of the early exercise feature which can reduce the wrong way risk effect when the volatilities are high.

5.4 Results and Discussion for Multi-asset Instruments

Following the efficiency comparison of different computation methods for exposure profiles in chapter 3, in this section, we concentrate on the performances of SGBM, SRBM and SRM for CVA of multi-asset options. In the examples of geometric and arithmetic basket options, instead of 2 stocks in chapter 3, 10 stocks are used for the underlying assets. And in the examples of max options, we keep using 5 stocks as the underlying assets. As explained in chapter 3, in the high-dimensional case, the bundling technique is applied on a *dimensionally reduced state space* [39]. To obtain the value of CVA (including CVA_W and CVA_I) and the direct estimator of the option price, we use 60000 simulation paths in SGBM, SRBM and SRM; and for the path estimators, 240000 simulation paths are generated. The standard deviations of the estimates (the numbers in the parentheses) are based on 30 independent simulation trials.

$s_0^i = s_0^c = 40$	$K = 40, d = 10$	$r = 0.06$
$\sigma_i = \sigma_c = 0.2, i = 1, ..., d$	$T = 1, M = 10$	observation dates $= 20$
$q = q_c = 0$	$\rho_{i,j} = 0.25, i \neq j, i, j = 1, ..., d$	$\rho_c = 0.5$

Table 5.3

5.4.1 Geometric Basket Options

The exercise value of a d-asset geometric basket Bermudan option is given by,

$$h(\mathbf{S}_{t_m}) = \big(K - \big(\prod_{i=1}^{d} S_{t_m}^i\big)^{\frac{1}{d}}\big)^+,$$

Under the model assumptions of multi-dimensional geometric Brownian motion, the parameters used are given in table 5.3.

For the regression approximation at time step t_m, basis functions,

$$f_k(\mathbf{S}_{t_m}) = \big((\prod_{i=1}^{d} S_{t_m}^i)^{\frac{1}{d}}\big)^{k-1}, k = 1, ..., 5,$$

are used in SGBM as in [39], while basis functions,

$$\widetilde{f}_k(\mathbf{S}_{t_{m-1}}) = \big((\prod_{i=1}^{d} S_{t_{m-1}}^i)^{\frac{1}{d}}\big)^{k-1}, k = 1, ..., 5,$$

are used in SRBM and SRM. The analytical formulas of $\mathbb{E}^{\mathbb{Q}}[f_k(\mathbf{S}_{t_m}) \mid \mathbf{S}_{t_{m-1}} = \mathbf{s}_{t_{m-1}}(p)]$, which are used for the continuation value computations in SGBM, can be found in table 3.1 of chapter 3.

As shown in table 5.4, the results of CVA generated by SGBM are quite close to the results of SRBM, and the results of CVA from SRM are higher than SGBM and SRBM. The standard deviation of the estimates from SGBM is smaller than that from SRBM and SRM, because of the moment calculation for each bundle in SGBM, which on the other hand makes the computation of SGBM more expensive. The CPU time scale shows us that SRM is the fastest method, and SRBM the second fastest. Compared with the reference results for the option prices, we see that SGBM gets accurate results, particularly, for the direct estimator, it has the lowest standard deviation of the estimates.

Method	CVA_W	CVA_I	CPU time (secs)	Direct est.	Path est.
SGBM	0.0180 (0.0000324)	0.0181 (0.0000334)	5.2728	1.1779 (0.000117)	1.1781 (0.0022)
SRBM	0.0180 (0.000215)	0.0182 (0.000211)	3.8427	1.1789 (0.0033)	1.1778 (0.0020)
SRM	0.0198 (0.000153)	0.0204 (0.000161)	1.9457	1.2075 (0.0031)	1.1732 (0.0029)

Table 5.4: Geometric basket Bermudan option with 10 stocks. The direct estimator and path estimator represent the different estimates of the option prices. CPU time represents the computation time of CVA (including CVA_W and CVA_I). The literature reference of the option price is 1.1779 [5].

The effect of the bundling technique on the exposure computation can be seen in figure 5.3a. For both PFE and EE, the results of SGBM are close to the results of SRBM. The computation time of SGBM and SRBM with different numbers of bundles is shown in figure 5.3b. Compared with SRBM, even though the increase of SGBM's CPU time with respect to bundles is somewhat higher, the computation speed of SGBM is reasonably fast. In figure 5.3c, we also show the CPU time scale of SGBM, SRBM, and SRM with respect to different numbers of simulation paths. The convergence of the CVA value with respect to the number of bundles can be seen in figure 5.3d. When the number of bundles increases, the value of CVA from SGBM and SRBM decreases and becomes stable.

5.4.2 Arithmetic Basket Options

The exercise value of a d-asset arithmetic basket Bermudan option reads

$$h(\mathbf{S}_{t_m}) = \big(K - \frac{1}{d}\big(\sum_{i=1}^{d} S^i_{t_m}\big)\big)^+.$$

Under the model assumptions of the underlying assets and the counterparty's stock price, the parameters in table 5.3 are used for the numerical examples. For the regression approximation at time step t_m, basis functions,

$$f_k(\mathbf{S}_{t_m}) = \big(\frac{1}{d}\sum_{i=1}^{d} S^i_{t_m}\big)^{k-1}, k = 1, ..., 4,$$

are used in SGBM as in [39], while basis functions,

$$\widetilde{f}_k(\mathbf{S}_{t_{m-1}}) = \big(\frac{1}{d}\sum_{i=1}^{d} S^i_{t_{m-1}}\big)^{k-1}, k = 1, ..., 4,$$

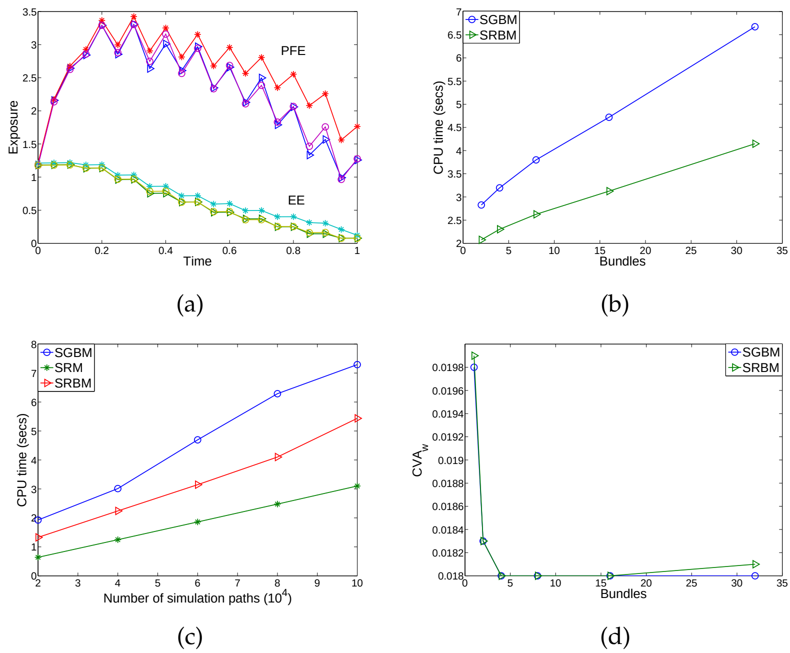

Figure 5.3: Geometric basket Bermudan option with 10 stocks. (A) Comparison of SGBM with 16 bundles (o), SRM (*), and SRBM ($\triangle$) with 16 bundles. High profile: 97.5% PFE. Low profile: EE. (B) CPU time scale of CVA computation in number of bundles. (C) CPU time scale of CVA computation in number of simulation paths. (D) The value of CVA_W as a function of bundles.

Method	CVA_W	CVA_I	CPU time (secs)	Direct est.	Path est.
SGBM	0.0149 (0.000027)	0.0151 (0.000027)	9.3446	1.0625 (0.000146)	1.0621 (0.0029)
SRBM	0.0150 (0.000134)	0.0151 (0.000133)	3.7306	1.0630 (0.0027)	1.0616 (0.0020)
SRM	0.0166 (0.000158)	0.0171 (0.000164)	1.8510	1.0895 (0.0033)	1.0586 (0.0022)

Table 5.5: CVA of arithmetic basket Bermudan options with 10 stocks. Four basis functions are used in SGBM, SRBM and SRM. CPU time represents the computation time of CVA (including CVA_W and CVA_I). The number in the parentheses is the standard deviation of the estimates. The estimate of the option price by LSM is $1.0607(0.0021)$.

are used in SRBM and SRM. The analytical formulas of $\mathbb{E}^{\mathbb{Q}}[f_k(\mathbf{S}_{t_m}) \mid \mathbf{S}_{t_{m-1}} = \mathbf{s}_{t_{m-1}}(p)]$ that are used for the continuation value computations in SGBM, can be found in table 3.1 of chapter 3.

According to the results reported in table 5.5, the values of CVA generated by SGBM are close to the results of SRBM, and the results of CVA from SRM are higher than both SGBM and SRBM. The standard deviation of CVA estimates from SGBM is smaller than SRBM and SRM. For the direct estimates of the option price, SGBM has the lowest standard deviation of estimation.

Similar as for the geometric basket options, the application of the bundling technique can significantly improve the accuracy of PFE and EE, which can be seen from figure 5.4a. For both PFE and EE, the results of SGBM are close to the results of SRBM. The computation time of SGBM and SRBM with different numbers of bundles is shown in figure 5.4b. Compared with the geometric basket options, since the basis functions used for arithmetic basket options have a more involved moment formula, the corresponding CPU time of SGBM is now higher.

In figure 5.4c, we show the CPU time of SGBM, SRBM, and SRM with respect to different numbers of simulation paths. The convergence of the CVA value with respect to the number of bundles can be seen in figure 5.4d. We see the same behavior as for the geometric basket options above.

5.4.3 Max Options

The exercise value of a d-asset Bermudan max option is given by,

$$h(\mathbf{S}_{t_m}) = \left(\max(S^1_{t_m}, ..., S^d_{t_m}) - K\right)^+.$$

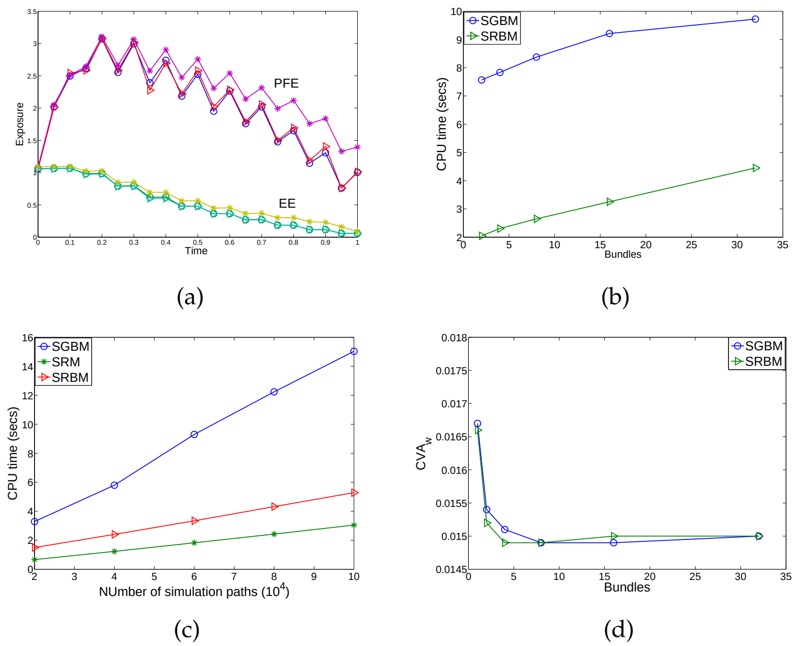

Figure 5.4: Arithmetic basket Bermudan option with 10 stocks. (A) Comparison of SGBM with 16 bundles (o), SRM (*), and SRBM ($\triangle$) with 16 bundles. High profile: 97.5% PFE. Low profile: EE. (B) CPU time scale of CVA computation in the number of bundles. (C) CPU time scale of CVA computation in the number of simulation paths, with 16 bundles in each method. (D) The value of CVA_W as a function of bundles.

$s_0^i = s_0^c = 100$	$K = 100, d = 5$	$r = 0.05$
$\sigma_i = \sigma_c = 0.2, i = 1, ..., d$	$T = 3, M = 9$	observation dates $= 36$
$q = q_c = 0.1$	$\rho_{i,j} = 0, i \neq j, i, j = 1, ..., d$	$\rho_c = 0.3$

Table 5.6

For the multi-dimensional geometric Brownian motion, the parameters are given in table 5.6.

For the regression approximation at time step t_m, basis functions,

$$f_k(\mathbf{S}_{t_m}) = \big(\log(\max(S^1_{t_m}, ..., S^d_{t_m}))\big)^{k-1}, k = 1, ..., 5,$$

$$f_6(\mathbf{S}_{t_m}) = \big(\prod_{i=1}^{d} S^i_{t_m}\big)^{\frac{1}{d}},$$

$$f_{6+i}(\mathbf{S}_{t_m}) = S^i_{t_m}, i = 1, ..., d,$$

are used in SGBM as in [39], while basis functions,

$$\widetilde{f}_k(\mathbf{S}_{t_{m-1}}) = \big(\log(\max(S^1_{t_{m-1}}, ..., S^d_{t_{m-1}}))\big)^{k-1}, k = 1, ..., 5,$$

$$\widetilde{f}_6(\mathbf{S}_{t_{m-1}}) = \big(\prod_{i=1}^{d} S^i_{t_{m-1}}\big)^{\frac{1}{d}},$$

$$\widetilde{f}_{6+i}(\mathbf{S}_{t_{m-1}}) = S^i_{t_{m-1}}, i = 1, ..., d,$$

are used in SRBM and SRM. Since the analytical formulas of $\mathbb{E}^{\mathbb{Q}}[f_k(\mathbf{S}_{t_m}) \mid \mathbf{S}_{t_{m-1}} = \mathbf{s}_{t_{m-1}}(p)]$ only exist for $d = 2$, an approximation formula by the Clark's algorithm will be applied in the case of more than two assets ($d > 2$) [23, 39].

From table 5.7, we can see that the values of CVA generated by SGBM are close to the results of SRBM, and the results of CVA from SRM are higher than both SGBM and SRBM. The standard deviation of the CVA estimates from SGBM is smaller than SRBM and SRM. For the direct estimation of option price, SGBM has the smallest standard deviation of estimates. For the standard deviation of the path estimator, all three methods are similar. SGBM seems to provide the best estimates of the option prices among theses three methods.

Method	CVA_W	CVA_I	CPU time (secs)	Direct est.	Path est.
SGBM	0.2871 (0.0011)	0.2870 (0.0011)	18.5511	26.1673 (0.0127)	26.0871 (0.0320)
SRBM	0.2891 (0.0023)	0.2893 (0.0022)	8.4731	26.3164 (0.0607)	26.0474 (0.0335)
SRM	0.3038 (0.0022)	0.3014 (0.0020)	2.9839	26.4223 (0.0413)	26.0049 (0.0361)

Table 5.7: CVA of max options with 5 stocks. 16 bundles are used in SGBM and SRBM. The direct estimator and path estimator represent the different estimates of option prices. CPU time represents the computation time of both CVA_W and CVA_I. The literature reference of the option price is $[26.115, 26.164]$, with 95% CI.

Similar as for the geometric and arithmetic basket options, the application of the bundling technique can improve the accuracy of PFE and EE, which can be observed from figure 5.5a. The computation time of SGBM and SRBM with different numbers of bundles is shown in figure 5.5b. Compared with the geometric and arithmetic basket options, since more basis functions are used for max options (11 basis functions for five assets), and the conditional expectations of the basis functions have more involved formulas, the corresponding CPU time of SGBM is higher.

In figure 5.5c, we also show the CPU time scale of SGBM, SRBM, and SRM with respect to different numbers of simulation paths. The convergence of CVA w.r.t. the number of bundles can be seen in figure 5.5d. When the number of bundles increases, the value of CVA from SGBM and SRBM decreases and becomes stable.

5.5 Effect of Wrong Way Risk

To show the effect of wrong way risk (WWR) on the CVA of multi-asset options, we take the example of the geometric basket Bermudan put option discussed in section 5.4.1. This example allows for an easy exposition, because the computation of these options can be reduced to a one-dimensional problem. By using Itô's lemma, the process $Y_t = \log\left(\prod_{i=1}^{d} S_{t_m}^i\right)^{\frac{1}{d}}$ follows the risk-neutral process [5]

$$\mathrm{d}Y_t = \widehat{\mu}\mathrm{d}t + \widehat{\sigma}\mathrm{d}W(t), \tag{5.2}$$

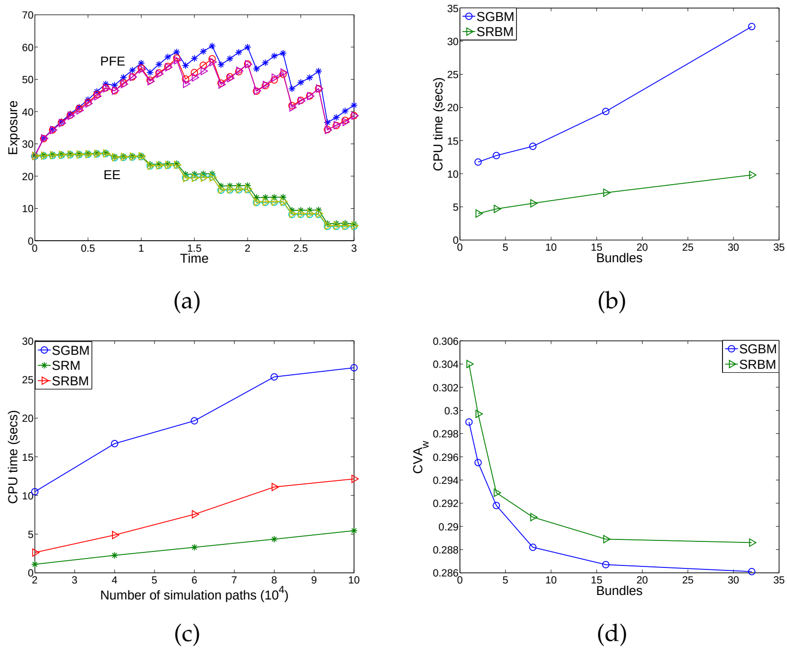

Figure 5.5: Max Bermudan option with 5 stocks. (A) Comparison of SGBM with 16 bundles (o), SRM (*), and SRBM (△) with 16 bundles. High profile: 97.5% PFE. Low profile: EE. (B) CPU time scale of CVA computation in the number of bundles. (C) CPU time scale of CVA computation in the number of simulation paths, with 16 bundles in SGBM and SRBM. (D) Value of CVA_W as a function of bundles.

where

$$\widehat{\mu} = r - \frac{1}{d}\sum_{i=1}^{d} q_i - \frac{1}{2d}\sum_{i=1}^{d}\sigma_i^2, \tag{5.3}$$

and

$$\widehat{\sigma} = \sqrt{\frac{1}{d^2}\sum_{j=1}^{d}\sum_{k=1}^{d}\rho_{j,k}\sigma_j\sigma_k}. \tag{5.4}$$

The geometric basket option is then equivalent to a single-asset option with strike price K, for which the underlying asset price process, $S_t^* = \left(\prod_{i=1}^{d} S_{t_m}^i\right)^{\frac{1}{d}}$, is given as follows,

$$\frac{\mathrm{d}S_t^*}{S_t^*} = (r - q^*)\mathrm{d}t + \widehat{\sigma}\mathrm{d}W(t), \tag{5.5}$$

with r the risk free interest rate, $q^* = \frac{1}{d}\sum_{i=1}^{d} q_i + \frac{1}{2d}\sum_{i=1}^{d}\sigma_i^2 - \frac{1}{2}\widehat{\sigma}^2$ the continuous dividend stream, and $S_0^* = \exp(Y_0)$ the initial value of S_t^*.

To simplify the analysis, we assume that $\sigma_i = \sigma$, $q_i = 0$ for all i, and the correlations $\rho_{i,j} = \rho$, $i \neq j$. Then the process S_t^* reads,

$$\frac{\mathrm{d}S_t^*}{S_t^*} = \left(r - \frac{\sigma^2(1-\rho)(1-\frac{1}{d})}{2}\right)\mathrm{d}t + \sigma\sqrt{\rho(1-\frac{1}{d}) + \frac{1}{d}}\mathrm{d}W(t). \tag{5.6}$$

To investigate the effect of WWR on CVA, we assume that the counterparty's stock price process S_t^c is positively correlated with each underlying asset of the geometric basket options, i.e., $\rho_c > 0$. Particularly, in the following numerical examples, we use a constant value of $\rho_c = 0.5$. We also assume that the volatility of S_t^c is constant, i.e., $\sigma_c = 0.6$. The initial stock price is $s_0^c = 40$.

From equation (5.6), we see that the variation of σ and ρ will change the dynamics of S_t^* and then influence the early exercise features of the Bermudan options. Other factors that will affect the early exercise features include the strike price K and the number of possible early exercise dates M. Recalling the discussion in chapter 4, the change of early exercise features will influence the expected exposure profiles and CVA of single-asset Bermudan options. Using a similar methodology, in the following examples, we show the effect of WWR on CVA of geometric basket options by changing its early exercise features (i.e., changing the value of σ, ρ, K, and M). All of the results are generated by SGBM, although SRBM can also produce good results, as shown in the comparison study of different methods.

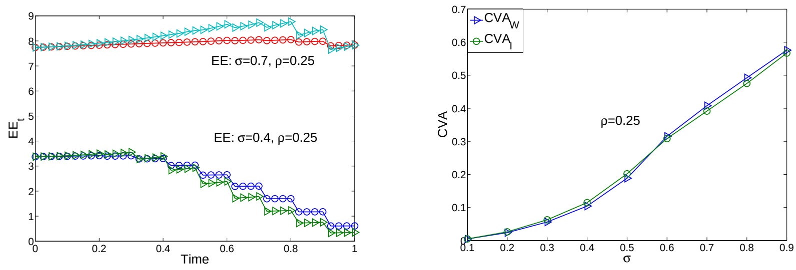

(a) (b)

Figure 5.6: (a), EE with WWR ('△') and EE without WWR ('o'). (b), CVA w.r.t. σ. Parameter setting: $M = 10$, observation dates=40, $K = 40$, $s_0^i = 40$, $i = 1, ..., d$.

5.5.1 Volatilities of Underlying Asset Prices σ

Given the correlations of the underlying asset price processes ($\rho = 0.25$), results of EE and CVA with respect to different values of volatility σ are illustrated in figures 5.6a and 5.6b. From figure 5.6a, we can see that with a relatively low volatility (such as $\sigma = 0.4$ in the example), because of the early exercise features, results of EE are decreasing w.r.t time t. Furthermore, the decrease of EE with WWR is faster than EE without WWR, which leads to CVA$_W$ < CVA$_I$ (see figure 5.6b).

In the case of relatively high volatility (such as $\sigma = 0.7$), however, EE becomes a straight line (see figure 5.6a). This is because the exercise intensity (see the explanation in chapter 4, section 4.6.) with $\sigma = 0.7$ becomes lower than in the case of $\sigma = 0.4$, which is caused by the change of the dynamics of the underlying asset prices. More precisely, from the dynamics of S_t^* in equation (5.6), we find that the drift coefficient $r - \frac{\sigma^2(1-\rho)(1-\frac{1}{d})}{2}$ is positive when $\sigma = 0.4$, however, it becomes negative when $\sigma = 0.7$. In the case of $\sigma = 0.7$, most of the time, EE with WWR is greater than EE without WWR (see figure 5.6a), which leads to CVA$_W$ > CVA$_I$ (see figure 5.6b). The feature has a similar effect as a large continuous proportional dividend payment for the S_t^* process.

Figure 5.6b also shows that CVA$_W$ and CVA$_I$ are increasing functions of σ.

5.5.2 Correlations of Underlying Asset Prices ρ

From equation (5.6), we can see that variation of ρ will also change the dynamics of S_t^* and then influences the results of CVA.

When the volatility σ is relatively low ($\sigma = 0.2$ used in the example), the

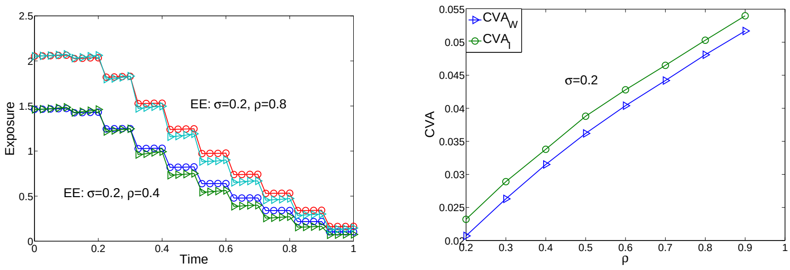

(a) (b)

Figure 5.7: (a), EE with WWR ('△') and EE without WWR ('o'). (b), CVA w.r.t. ρ. Parameter setting: $M = 10$, observation dates=40, $K = 40$, $s_0^i = 40$, $i = 1, ..., d$.

drift coefficient of the dynamics of S_t^*, $r - \frac{\sigma^2(1-\rho)(1-\frac{1}{d})}{2}$, is positive. Figure 5.7b shows that CVA_W and CVA_I are increasing functions of ρ. This is because with a higher correlation, the value of EE becomes higher in general (see figure 5.7a). The effect of WWR on CVA is shown in figure 5.7b, i.e., with the early exercise features, EE with WWR decreases faster than EE without WWR, which leads to $\text{CVA}_W < \text{CVA}_I$.

However, if we use a relatively high volatility ($\sigma = 0.8$ used in the example), the drift coefficient of the dynamics of S_t^* will be negative. In this case, CVA_W and CVA_I will become decreasing functions of ρ, as shown in figure 5.8b. Figure 5.8a shows that compared with the case of $\rho = 0.4$, EE with $\rho = 0.8$ can be much lower which affects the value of CVA. Figure 5.8b illustrates the effect of WWR on CVA. When ρ is low, we have $\text{CVA}_W > \text{CVA}_I$, and a higher ρ leads to a more active early exercise policy and $\text{CVA}_W < \text{CVA}_I$.

5.5.3 Strike Price K and Early Exercise Rights M

The variation of strike price K can also affect EE and CVA. Generally, increasing K will increase EE and the CVA of put options, as shown in figure 5.9a. With relatively low strike prices (such as $K < 35$ in this example), we have $\text{CVA}_W > \text{CVA}_I$. With relatively high strike prices (such as $K > 35$), we will have $\text{CVA}_W < \text{CVA}_I$.

Regarding the number of possible exercise dates M, although increasing M will increase the option price, EE will decrease because of the early exercise features. CVA_W and CVA_I are decreasing functions of M, see figure 5.9b. The effect of WWR on CVA can be seen from the comparison of CVA_W and CVA_I.

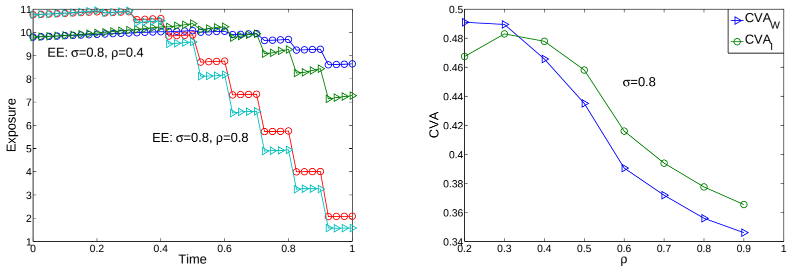

(a) (b)

Figure 5.8: (a), EE with WWR ('△') and EE without WWR ('o'). (b), CVA w.r.t. ρ. Parameter setting: $M = 10$, observation dates=40, $K = 40$, $s_0^i = 40$, $i = 1, ..., d$.

With a low value of M ($M < 5$ in this example), we have $\text{CVA}_W > \text{CVA}_I$, and if M is high, the value of CVA_W can be smaller than CVA_I.

5.6 Conclusion

For an efficient computation of CVA of multi-asset options, we concentrated on an efficiency comparison of SGBM, SRM and SRBM. For the accurate computation of CVA, exposure profiles and option prices, by using the bundling technique, both SRBM and SGBM are better than SRM. Compared with SRBM, one of the advantages of SGBM is that the standard deviation of the CVA estimates and the option price direct estimates is smaller. While the results of CVA, exposure profiles and option prices are similar for SGBM and SRBM, the computation speed of SGBM is slower than SRBM. The effect of wrong way risk on exposure profiles and CVA for multi-asset options can be significant. Because of the early exercise features of Bermudan options, the value of CVA with WWR can be smaller than of CVA without WWR. The geometric basket option offers useful insight in the effect of wrong way risk because of its analytical properties.

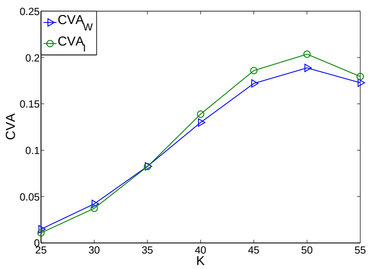

(a) CVA w.r.t. strike price K.

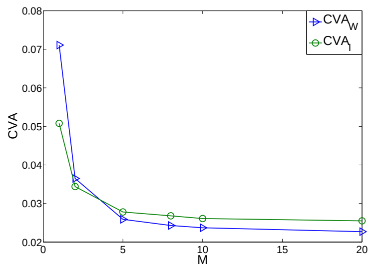

(b) CVA w.r.t possible exercise dates M.

Figure 5.9: (a), parameter setting: $M = 10$, observation dates=40, $\sigma = 0.4$, $\rho = 0.6$, $s_0^i = 40$, $i = 1, ..., d$. (b), parameter setting: $K = 40$, observation dates=40, $\sigma = 0.2$, $\rho = 0.25$, $s_0^i = 40$, $i = 1, ..., d$.

Chapter 6

Conclusions and Outlook

6.1 Conclusions

In this thesis we have presented efficient computation methods for the quantification of counterparty credit risk of multi-asset options.

We have described a new procedure to embed the Fourier cosine expansions as a useful tool in counterparty credit exposure modeling of European and Bermudan single-asset options. The Fourier cosine expansions are directly connected to the characteristic function of the underlying asset process to produce accurate results of option prices. Combined with a Monte Carlo simulation approach, we are able to obtain the risk profiles, such as PFE and EE. Our approach is applicable for a Lévy process which can be simulated accurately. We have also illustrated that the approach is different from regression-based simulation approaches, such as the Longstaff-Schwartz Method (LSM), in which a conditional expectation is approximated by using a least squares regression method. And the results generated by our Fourier-based approach can serve as a benchmark for analysing the error in American Monte Carlo methods (LSM). We have shown the difference of risk profiles under different measures ($\mathbb{P}$ and $\mathbb{Q}$). We further point out that the results of EE form the basis of CVA computations.

For the calculation of risk profiles in multi-dimensional models, we have proposed algorithms based on a simulation approach, named the Stochastic Grid Bundling Method (SGBM) [39]. To investigate the efficiency of SGBM, we have examined different simulation approaches, including the Standard Regression Method (SRM) and the Standard Regression Bundling Method (SRBM). Although all of these methods can produce risk profiles, the results are different in accuracy, computation speed and standard deviation of option price estimates. We find that compared with SRBM, when the same number of simulation paths, basis functions and bundles are used, the discontinuity of the conditional expectations at the boundaries of bundles in SGBM is generally smaller. And this discontinuity in SGBM can become very small by increasing the number of simulation paths and bundles appropriately. In this case, the effect of this discontinuity on the results of risk profiles is limited. Compared with SRM and SRBM, the numerical examples show that SGBM has the advantage of the smallest standard deviation for the direct estimates of the option prices. This result is consistent with the conclusion of [32], in which the authors theoretically prove the advantage of 'regression later' (used in SGBM) compared with 'regression now' (used in SRBM and SRM) under some conditions. Generally, the estimates of option prices of SGBM are closer to reference results than SRM or SRBM. We also show that for discontinuous payoffs, such as digital options, by using the bundling technique appropriately, SGBM can get accurate and stable results of option prices and exposure profiles. We conclude that in the case of high-dimensional underlying asset processes, by using a bundling technique, the accuracy of exposure profiles is improved significantly, and the computation speed is kept reasonably high. We also point out that SGBM can be further applied as an efficient computation method for CVA of multi-asset portfolios.

We then switch to quantify the counterparty credit risk by using the risk-neutral pricing technique, i.e., the computation of credit value adjustment (CVA). Based on Monte Carlo simulation and the Fourier inverse option pricing method introduced in chapter 2, an efficient calculation method for Bermudan options' CVA is proposed. The method is applicable when the underlying stock price follows a Lévy process which can be simulated accurately. By using the concept of stochastic hazard rate, we derive an analytical approximation of the expected exposure conditional on default, which is applicable for the calculation of expected exposure and CVA with wrong way risk. To model the wrong way risk, we compare the empirical analysis approach (EAA) and the portfolio value approach (PVA), and prefer EAA in our problem setting. The numerical results show that the wrong way risk has significant effect on the expected exposure (EE) and CVA of Bermudan options, however, this effect depends on the Bermudan option's early exercise features. More precisely, a high exercise intensity (i.e., high volatility, high strike price, or high number of possible early exercise dates) may lead to $\text{CVA}_W < \text{CVA}_I$, which is different from the conclusion if one uses the α multiplier approach with $\alpha > 1$.

Finally, the efficient computation of CVA for multi-asset options is illustrated in chapter 5. When the underlying asset of the derivative transaction is one-dimensional, we show that this is an extension of the one-dimensional problem described in chapter 4. In the case of multi-asset instruments, an efficiency comparison of SGBM, SRM and SRBM is given. By using the bundling technique, the accuracy of CVA produced by SGBM can be improved significantly, while the computation speed is kept reasonably fast. Compared with SRBM, the standard deviation of CVA estimates in SGBM is smaller. We have also discussed the effect of correlation between exposure and default risk on CVA for multi-asset options.

6.2 Outlook

In the problem formulation for the CVA computation, we have only considered the so-called one-sided default risk (unilateral), i.e., one counterparty is defaultable and the other one is assumed to be default-free. A more realistic version is the two-sided default risk (bilateral), i.e., both counterparties are defaultable. Related references such as Duffie and Singleton (2003) [26], have provided a general Monte Carlo valuation approach for CVA under these conditions. Based on the methods we have introduced in the case of one-sided default risk, it is interesting to explore efficient computation methods in the situation of two-sided default risk. Important applications of such methods include the quantification of counterparty risk of interest rate instruments (swaps, Bermudan swaptions, etc.) and credit derivatives (CDS, etc.). In addition, related probability problems such as simultaneous defaults are also interesting for consideration.

Another interesting direction for further research is in the further modeling of wrong way risk (WWR), which describes the dependence between exposure to a counterparty and its default risk. In chapter 4, we have discussed different approaches for a general WWR modeling. An extension is to take into account the impact of systemically important counterparties (SICs), such as large financial institutions and sovereigns, see Pykhtin and Sokol (2013) [50]. An SIC is defined as a counterparty whose default is likely to have a significant impact on the whole financial market. The impact of an SIC's default on risk factors and, through them, on exposure is referred as systemic WWR. For the general WWR, it arises when a counterparty's credit spread and exposure share the same risk factors. For systemic WWR, however, it arises from the default of SICs.

A term closely related to the default risk is collateral. For ease of discussion, in the examples given in the thesis, we assumed that no collateral was posted. In practice, it is nowadays common to include a credit support annex (CSA) in the transactions which are cleared bilaterally. The CSA typically provides formulas governing the amount of collateral that is required by each side at any given time. And the collateral posted for derivatives positions is usually in the form of cash or liquidity securities. A detailed discussion of the impact of collateral agreements on the price of derivative transaction can be found in Hull and White (2014) [38].

The work in chapter 4 is closely related to the pricing of defaultable options. It should be interesting to give a more general approach of equity-credit modeling (see Carr and Wu (2010) [20]), for example, the GBM process of the underlying asset can be extended into an affine jump diffusion process, etc. The default process can be modeled by the reduced form or the structure form framework. Under this model, we can consider the efficient valuation of credit-sensitive derivatives such as defaultable European and Bermudan options, or even credit default swaps (CDS), while the correlation between default risk and underlying risk factors can also be taken into account.

Bibliography

[1] A. Antonov, S. Issakov, and S. Mechkov. Algorithmic exposure and CVA for exotic derivatives. *Available at SSRN, http://ssrn.com/abstract=1960773*, 2011.

[2] G. Bakshi, D. Madan, and F. Zhang. Investigating the role of systematic and firm-specific factors in default risk: Lessons from empirical evaluating credit risk models. *Journal of Business*, 79:1955–1987, 2006.

[3] J. Barraquand and D. Martineau. Numerical valuation of high dimensional multivariate American securities. *Journal of Financial and Quantitative Analysis*, 30:383–405, 1995.

[4] G. Bekaert and G. Wu. Asymmetric volatilities and risk in equity markets. *Review of Financial Studies*, 13:1–42, 2000.

[5] S. J. Berridge and J. M. Schumacher. Pricing high-dimensional American options using local consistency conditions. In J. Appleby J. Miller, D. Edelman, editor, *Numerical Methods for Finance*. Chapman & Hall/CRC, London, 2007.

[6] F. Black. The pricing of commodity contracts. *Journal of Financial Economics*, 3:167–179, 1976.

[7] F. Black and M. Scholes. The pricing of options and corporate liabilities. *Journal of Political Economy*, 81(3):637–654, 1973.

[8] D. Brigo, C. Buescu, and M. Morini. Counterparty risk pricing: Impact of closeout and first-to-default times. *International Journal of Theoretical and Applied Finance*, 15(06):1250039, 2012.

[9] D. Brigo and M. Masetti. Risk neutral pricing of counterparty risk. In M. Pykhtin, editor, *Counterparty credit risk modeling: risk management, pricing and regulation*. Risk Books, London, 2005.

[10] D. Brigo and A. Pallavicini. Counterparty risk and CCDSs under correlation. *Risk February*, pages 84–88, 2008.

[11] M. Broadie and M. Cao. Improved lower and upper bound algorithms for pricing American options by simulation. *Quantitative Finance*, 8(8):845–861, 2008.

[12] M. Broadie and P. Glasserman. A stochastic mesh method for pricing high-dimensional American options. *The Journal of Computational Finance*, **7**(4):35–72, 2004.

[13] M. Broadie, P. Glasserman, and Z. Ha. Pricing American options by simulation using a stochastic mesh with optimized weights. *(S. Uryasev, ed.) Probabilistic Constrained Optimization: Methodology and Application, Kluwer Publishers, Norwell, Mass*, 2000.

[14] J. Y. Campbell and L. Hentschel. No news is good news: An asymmetric model of changing volatility in stock return. *Review of Economic Studies*, 31:281–318, 1992.

[15] J. Y. Campbell and A. S. Kyle. Smart money, noise trading and stock price behavior. *Review of Economic Studies*, 60:1–34, 1993.

[16] J. Y. Campbell and G. B. Taksler. Equity volatility and corporate bond yields. *Journal of Finance*, 63:2321–2349, 2003.

[17] E. Canabarro and D. Duffie. Measuring and marking counterparty risk. In L. Tilman, editor, *Asset/Liability Management for Financial Institutions*. Institutional Investor Books, 2003.

[18] P. Carr and V. Linetsky. A jump to default extended CEV model, An application of Bessel process. *Finance Stoch.*, 10:303–330, 2006.

[19] P. Carr and D. B. Madan. Local volatility enhanced by a jump to default. *SIAM J. Financial Math*, 1:2–15, 2010.

[20] P. Carr and L. Wu. Stock options and credit default swaps: A joint framework for valuation and estimation. *Journal of Financial Econometrics*, 8(4):409–449, 2010.

[21] P. Carr and L. Wu. Leverage effect, volatility feedback, and self-exciting market disruptions: Disentangling the multi-dimensional variations in S&P 500 index options. *Bloomberg Portfolio Research Paper*, 2011.

[22] G. Cesari, J. Aquilina, N. Charpillon, Z. Filipovic, G. Lee, and I. Manda. *Modeling, pricing, and hedging counterparty credit exposure: a technical guide*. Springer Finance, Berlin, 2010.

[23] C. E. Clark. The greatest of a finite set of random variables. *Operations Research*, 9:145–162, 1961. 2.

[24] P. Collin-Dufresne, R. S. Goldstein, and J. S. Martin. The determinants of credit spread changes. *Journal of Finance*, 56:2177–2207, 2001.

[25] R. Cont and T. Kokholm. Central clearing of OTC derivatives: bilateral vs multilateral netting. *Statistics and Risk Modeling*, 31(1):3–22, 2014.

[26] D. Duffie and K. J. Singleton. *Credit risk: pricing, measurement, and management*. Princeton University Press, 2003.

[27] F. Fang and C. W. Oosterlee. A novel pricing method for European options based on Fourier-Cosine series expansions. *SIAM J. Sci. Comput*, 31:826–848, 2008.

[28] F. Fang and C. W. Oosterlee. Pricing early-exercise and discrete barrier options by Fourier-cosine series expansions. *Numerische Mathematik*, 114(1):27–62, 2009.

[29] N.P. Firth. *High dimensional American options*. PhD thesis, Oxford University, Oxford, 2005.

[30] C. Fries. *Mathematical Finance: Theory, Modeling, Implementation*. John Wiley & Sons, 2007.

[31] P. Glasserman. *Monte carlo methods in financial engineering*. Chapman and Hall, Boca Raton, FL, 2003.

[32] P. Glasserman and B. Yu. Pricing American options by simulation: Regression now or regression later? *Monte Carlo and Quasi-Monte Carlo Methods in Scientific Computing 2002, (H. Niederreiter, ed.)*, pages 213–226, 2004.

[33] J. Gregory. *Counterparty credit risk*. John Wiley & Sons, 2010.

[34] R. A. Haugen, E. Talmor, and W. N. Torous. The effect of volatility changes on the level of stock prices and subsequent expected returns. *Journal of Finance*, 46(3):985–1007, 1991.

[35] P. Henry-Labordère. Cutting CVA's complexity. *Risk*, 25(7):67–74, 2012.

[36] J. Hull and A. White. The impact of default risk on the prices of options and other derivative securities. *Journal of Banking & Finance*, 19(2):299–322, 1995.

[37] J. Hull and A. White. CVA and wrong way risk. *Financial Analysts Journal*, 68(5):58–69, 2012.

[38] J. Hull and A. White. Collateral and credit issues in derivatives pricing. *working paper*, 2014.

[39] S. Jain and C. W. Oosterlee. The stochastic grid bundling methods: efficient pricing of multidimensional Bermudan options and the Greeks. *Available at SSRN, http://ssrn.com/abstract=2293942*, 2013.

[40] R. A. Jarrow and S. M. Turnbull. Pricing derivatives on financial securities subjets to credit risk. *The Journal of Finance*, L(1):53–85, 1995.

[41] X. Jin, H.H. Tana, and J. Sun. A state-space partitioning method for pricing high-dimensional American-style options. *Mathematical Finance*, 17:399–426, 2007.

[42] H. Johnson and R. Stulz. The pricing of options with default risk. *The Journal of Finance*, XLII(2):267–280, 1987.

[43] V. Linetsky. Pricing equity derivatives subject to bankrupcy. *Mathematical Finance*, 16(2):255–282, 2006.

[44] D. Lomibao and S. Zhu. A conditional valuation approach for path-dependent instruments. In M. Pykhtin, editor, *In Counterparty Credit Risk Modeling: Risk Management Pricing and Regulation*. Risk Books, London, 2005.

[45] F. A. Longstaff and E. S. Schwartz. Valuing American options by simulation: A simple Least-Square approach. *Review of Financial Studies*, 3:113–147, 2001.

[46] R. Merton. Theory of rational option pricing. *Bell Journal of Economics and Management Science*, Spring(4):141–183, 1973.

[47] L. Ng, D. Peterson, and A. E. Rodriquez. Potential future exposure calculations of multi-asset exotic products using the stochastic mesh method. *The Journal of Computational Finance*, 14(2):119–153, 2010.

[48] M. Pykhtin. Counterparty credit risk: Modeling counterparty credit exposure. *The International Association of Financial Engineers, workshop, New York*, 2011.

[49] M. Pykhtin. Counterparty risk management and valuation. In T.R. Bielecki, D. Brigo, and F. Patras, editors, *Credit risk frontiers, chapter 16*. John Wiley & Sons, Hoboken, 2011.

[50] M. Pykhtin and A. Sokol. Exposure under systemic impact. *Risk*, 26(9):100–105, 2013.

[51] M. Pykhtin and S. Zhu. Measuring counterparty credit risk for trading products under Basel ii. In M. K. Ong, editor, *The Basel II Handbook 2nd edn*. Risk Books, London, 2006.

[52] M. Pykhtin and S. Zhu. A guide to modeling counterparty credit risk. *GARP. Risk Review*, 37:16–22, 2007.

[53] D. Rosen and D. Saunders. CVA the wrong way risk. *Journal of Risk Management in Financial Institutions*, 5:152–272, 2012.

[54] M. Ruijter and C. W. Oosterlee. Two-dimensional Fourier cosine series expansion method for pricing financial options. *SIAM J. Sci. Comput*, 34(5):642–671, 2012.

[55] I. Ruiz, R. Pachón, and P. del Boca. Optimal right and wrong way risk: a methodology review, empirical study and impact analysis from a practitioner standpoint. *Working paper*, 2013.

[56] R. Schöftner. On the estimation of credit exposures using regression-based Monte Carlo somulation. *The Journal of Credit Risk*, 4:37–62, 2008.

[57] Y. Shen, J.H.M. Anderluh, and J.A.M. van der Weide. Algorithmic Counterparty Credit Exposure of Multi-Asset Bermudan Options. *accepted for publication in International Journal of Theoretical and Applied Finance*, 2014.

[58] Y. Shen, J.A.M Van Der Weide, and J.H.M Anderluh. A benchmark approach for the counterparty credit exposure of Bermudan options under Lévy process: The Monte Carlo-COS method. *Procedia Computer Science*, 18:1163–1171, 2013.

[59] S. E. Shreve. *Stochastic calculus for finance II: continuous-time models*. Springer, 2004.

[60] J. A. Tilley. Valuing American options in a path simulation model. *Transactions of the Society of Actuaries*, 45:83–104, 1993.

[61] H. Zhu, Y. Zhang, and H. Zhou. Equity volatility of individual firms and credit spreads. *Working paper, Bank for International Settlements*, 2005.

Curriculum Vitae

Yanbin Shen was born in Huzhou, Zhejiang, China, on October 21, 1984. After he finished his high school in July 2003, he went to Sichuan University to study Applied Mathematics, where he obtained his Bachelor of Science degree in July 2007. After graduation, he went to Nankai University to pursue graduate studies in the department of Finance. In July 2009, he received his Master of Economics diploma, with a specialty of Finance.

In October 2009, the China Scholarship Council (CSC) granted him a scholarship to support his Ph.D research abroad. Then, he moved to the Netherlands, where he studied Financial Mathematics as a Ph.D student in Delft University of Technology under the supervision of Dr. J. A. M. van der Weide. His research project concentrates on the efficient quantification of counterparty credit risk. He has presented his work at the Bachelier Finance Society 7th World Congress 2012 in Sydney, the International Conference on Computational Science (ICCS) 2013 in Barcelona, and the 13th Winter school on Mathematical Finance 2014 in Lunteren.

120

List of Publications and Presentations

1. Y. Shen, J. A. M. van der Weide, and J. H. M. Anderluh. 'A benchmark approach for the counterparty credit exposure of Bermudan options under Lévy process: the Monte Carlo-COS method', Procedia Computer Science, 18: $1163 - 1171$, 2013
2. Y. Shen, J. H. M. Anderluh, and J. A. M. van der Weide. 'Algorithmic Counterparty Credit Exposure for Multi-Asset Bermudan Options', accepted for publication in Int. J. of Theoretical and Applied Finance, 2014.
3. Y. Shen, J. A. M. van der Weide, 'Credit Value Adjustment with Wrong Way Risk for Bermudan and Multi-asset Options', submitted, 2014.

Presentations:

1. Bachelier Finance Society 7th World Congress, June $19-22$, 2012, Sydney, Australia.
2. The International Conference on Computational Science (ICCS), June $5-7$, 2013, specified in the workshop of computational finance, Barcelona, Spain.
3. 13th Winter school on Mathematical Finance, January $20-22$, 2014, Lunteren, Netherlands.

Other conferences:

1. Interest Rate Modelling and Applications in Practice, May $12-13$, 2011, University College London, London, UK.
2. Quantitative Methods in Finance Conference (QMF), June $26-30$, 2012, Cairns, Australia.
3. Princeton RTG Summer School in Financial Mathematics, June $17-28$, 2013, Princeton university, US.